8-1-2002

Fiber reinforced composites of a novel pendent polyimide: Optimum processing and mechanical properties

Akshay Kamdar

Fiber Reinforced Composites of a Novel Pendent Polyimide: Optimum Processing and Mechanical Properties

A Thesis

Presented to

The Graduate Faculty of Rochester Institute of Technology

In partial fulfillment

Of the requirements for the Degree of

Master of Science in Materials Science and Engineering

Akshay R Kamdar

August 2002

Fiber Reinforced Composites of a Novel Pendent Polyimide: Optimum Processing and Mechanical Properties

Akshay R Kamdar

Approved:

Dr. Marvin L. Illingsworth (Advisor)

Dept. of Chemistry

Accepted:

Dr. K.S.V. Santhanam

Interim Department Chair

Material Science and Engineering

Copyright Release Form

Fiber Reinforced Composites of a Novel Pendent Polyimide: Optimum Processing and Mechanical Properties

Date: 8-02-02

Signature: _____

ABSTRACT

A 2-component polyimide [3,4'-ODA + 4,4'-ODPA], a 3-component "parent" polyimide [3,4'-ODA + 4,4'-ODPA + 10 mol % Mellitic acid dianhydride (MADA)] and a 4-component "pendent" polyimide [3,4'-ODA + 4,4'-ODPA + 10 mol % MADA + 10 mol % Zr] were synthesized and characterized using fourier transform infrared spectroscopy (FTIR), differential scanning calorimetry (DSC) and thermogravimetric analysis (TGA) techniques. Since temperature and time are critical factors influencing the thermal and mechanical properties of the final polyimide, it is important to have detailed information on the best time-temperature conditions for imidization and cure in order to optimize the processing and properties of this polyimide. The present investigation focused on developing these conditions for the polymer. The processing condition of heating the poly(amic acid) at 310 °C for 15 minutes was chosen as an optimum processing condition for the Zr-pendent polyimide. The sample showed complete imidization without any decomposition at the given processing temperature.

The polyimide resins were also investigated as a matrix for high performance composites. Prepregs were fabricated using the conventional hand lay-up technique. Carbon and/or glass fiber reinforced composite laminates were fabricated in an autoclave to obtain a 60:40 fiber to resin by weight ratio. Tensile, flexural, Izod impact and dynamic mechanical analysis tests were carried out on the composite laminates. Mechanical properties of the pendent polymer were compared with those of the parent (without pendent groups) polyimide. Failure mechanisms were studied through the use of optical and scanning electron microscopy. The Zr-pendent polyimide composites showed lower moduli for the mechanical tests performed as compared to the 2-component and parent polyimide composites. Comparisons of mechanical data with laminates fabricated using a different molding cycle are also included.

ACKNOWLEDGEMENTS

"*If an experiment works, something has gone* wrong"—Finagle's First Law. Dr. Illingsworth certainly helped me prove him wrong through his valuable suggestions, continuous encouragement and extreme patience, especially when the research struggled.

This thesis would not have been a success without the constant support and valuable insights of my committee members, Dr. Langner, Dr. Angela at Xerox Corporation and Dr. Carle from the Mechanical Engineering Technology Department. Special thanks to Dr. Kim for helping me during the initial phases of my thesis.

I would like to thank Owens Corning and Mr. John Alexion at Composites One for the supply of glass and carbon fibers. I appreciate the efforts of the staff at the Center for Composite Materials at the University of Delaware for fabricating the composite samples and that of Die Max of Rochester for cutting them. I also thank Tom Locke at the Center for Integrated Manufacturing Studies (CIMS) for his help in making notches in the composite samples. Sincere thanks to Dr. Michael Jackson and Peter Terrana for their help with the SEM at the microelectronics department.

I am grateful to the Material Sciences and Engineering department and the Chemistry department for awarding me with a Teaching Assistantship. To Tom Allston and the stock room staff, your constant support made all the hurdles so easy to jump. I would like to say a special "thank you" to Brenda Mastrangelo for always cheering me up.

To my lab co-workers, Wei Cheng and Sangeeta for their help, and to my friends, Prakash, Vivek, Eugene, Abhishek, Ashish, Mayank, Suruchi, Hrishikesh and Rajiv, this thesis would not have been so much fun without your help and witty comments.

Writing this thesis would not have been so interesting without listening to the tunes of Dire Straits and Pink Floyd.

And last but never the least, to my parents and family for loving me so much and giving me the opportunity to prove myself.

TABLE OF CONTENTS

LIST OF TABLES

LIST OF FIGURES

CHAPTER I

INTRODUCTION & BACKGROUND

1.1 Introduction

Fiber reinforced polymer composites are considered to be an important class of engineering materials offering unique flexibility in design capabilities. The advantages are high specific strengths and moduli, strength to weight ratio and fatigue strength. They are used in many diverse applications in the aerospace, electronics and automotive industries.

Currently, a majority of aerospace applications rely upon composites having epoxy, bismaleimide or polyimide polymer matrices reinforced with one of a number of high performance carbon or aramid fibers. The choice of polymer matrix depends primarily on its long-term use temperature and the service environment in which it will be used. In low earth orbit (LEO), atomic oxygen (AO) is the most dominant species at altitudes between 200 and 700 km. As spacecraft orbit the earth at these altitudes, they collide with atomic oxygen and due to their high orbital velocity, these collisions are energetic enough to break chemical bonds and oxidize materials. This degradation results not only in mass loss but also a reduction in mechanical and thermal properties.

A DuPont polyimide, Kapton®, has been chosen for a variety of applications aboard spacecraft in low earth orbit (LEO), such as the International Space Station (ISS). Its characteristic features are its low density, high flexibility and good thermal stability.

Figure 1.1. Kapton® cover on solar panel in the spaceship "Discovery"[1]

However, the oxidation rate of Kapton® in LEO atomic oxygen environment is great enough that structural failure of the part occurs in much less time than the operating life of the spacecraft. The novel polymer under investigation is a zirconium pendent polyimide based on 3,4'-oxydianiline (3,4'-ODA) and 4,4'-oxydiphthalic anhydride (4,4'-ODPA). Films have demonstrated excellent resistance to atomic oxygen (AO) by forming ZrO_2, a white powder that acts a protective layer [2]. A schematic diagram representing the process of ZrO_2 formation has been shown in Figure 1.2.

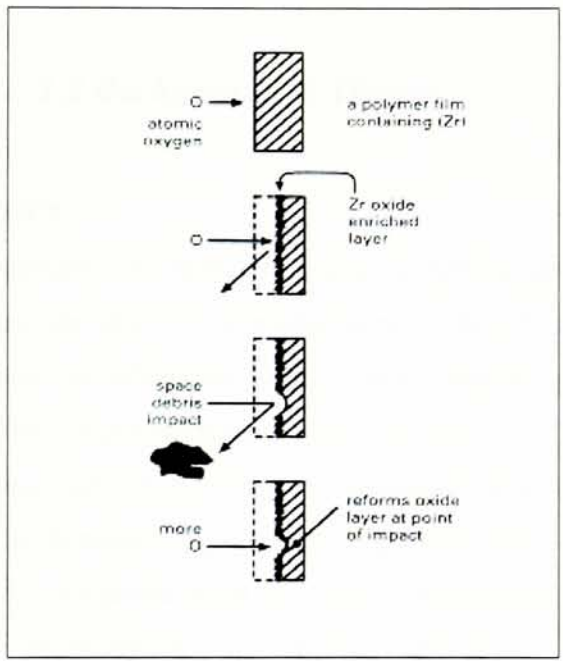

Figure 1.2. Atomic oxygen resistance exhibited by polyimides with zirconium components

The onset of imidization for this polymer occurs at ~166° C, the glass transition temperature is ~296 °C and the thermo-oxidative decomposition temperature of this polymer in air is ~551 °C [3]. The high glass transition and decomposition temperatures, coupled with its improved AO resistance, make this novel polymer a strong candidate for use as a structural material aboard the ISS. However, the properties of this novel polymer as a composite material for structural applications have not yet been investigated.

When polyimides are thermally imidized and cured for use either as composite matrix resins or as photoresists and dielectrics in electronic integrated circuits, temperature and time become critical factors that influence the thermal and mechanical properties of the final polyimide. Therefore, it is important to have detailed information

on the best time-temperature conditions for imidization and cure in order to optimize the processing and properties of this polyimide. It is critical to develop an understanding of the role of thermal parameters such as imidization temperature, glass transition temperature and cure temperature at the partially or fully imidized and cured stages and their effect on the final mechanical properties and adhesion [4]. Since the optimized processing conditions for this novel polymer is not known, the present investigation will focus on developing these conditions for the polymer.

1.2 Background & Theory

1.2.1 Polyimides Overview

Polyimides are a sophisticated family of materials having applications in highly technical end use fields from aerospace to microelectronics. Their diversity is such that it leads them into applications as adhesives, films, foams, plastic moldings and resin matrices for composites. Their major advantage, a high resistance to heat, places them in a niche other polymers cannot enter [5, 6]. They are considered specialty plastics because of their outstanding high performance engineering properties. As such, they are priced well above the commodity polymers such as polyethylene and polystyrene. Many monomers used to prepare polyimides are also specialty chemicals. Therefore, the price of commercial polyimides covers a wide range, $ 8.80 – $ 111.00 per kg [7].

Synthesis of Polyimides

Polyimides, prepared from a variety of dianhydride and diamine monomers, are characterized by repeating imide structural units in the polymer backbone as seen in Figure 1.3. This structure contributes to the exceptional thermal and oxidative stability of polyimides.

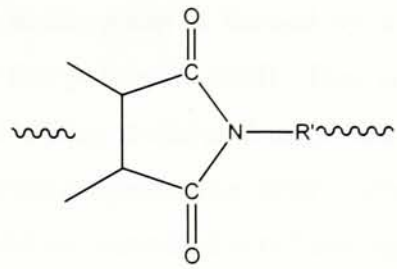

Figure 1.3 Chemical structure of an imide group

1.2.1.1 Linear Condensation Polyimides

There are three main types of polyimides: (1) Linear condensation polyimides, (2) Thermoplastic polyimides, and (3) Addition polyimides [12]. Linear condensation polyimides are prepared from a two-step method. In the first step, an aromatic dianhydride combines with an aromatic diamine in the presence of a polar solvent to form a poly(amic acid). An example is presented in Figure 1.4.

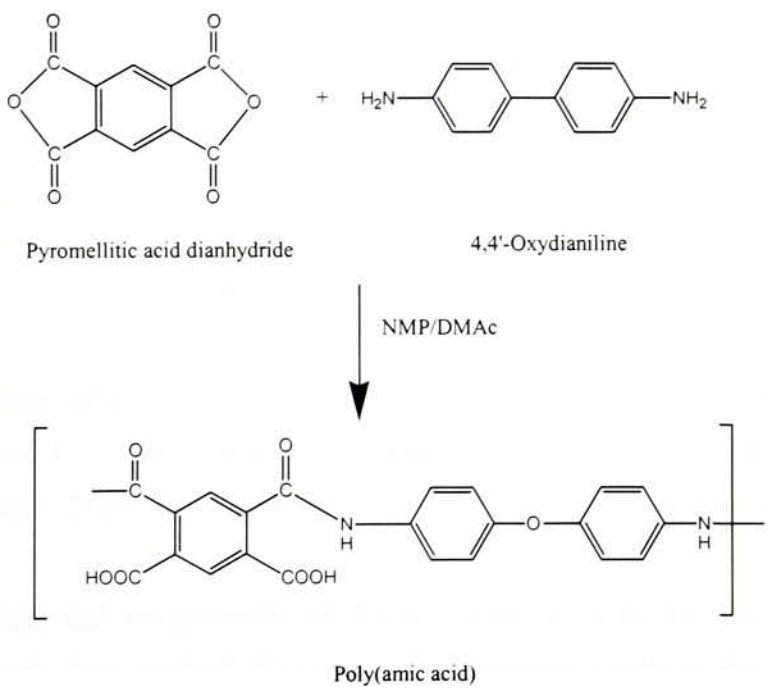

Figure 1.4. Formation of poly(amic acid)

As the poly(amic acid)s have high viscocity, this solution is usually used to impregnate fiber reinforcements to produce prepregs.

In the second step, the imide group is formed by a ring closing mechanism involving cyclodehydration of the poly(amic acid). This is achieved by a thermal imidization process by extended heating at elevated temperatures of 250 - 400 °C or by treatment with chemical dehydrating agents. The latter method is generally not used commercially because of the problems associated with handling the reagents. Imidization involves the release of by-products such as water and the loss of residual solvents or volatiles. The thermal imidization step is usually preceded by a processing operation, whereby a poly(amic acid) solution is used to cast a film, coating or spin a fiber. The polymer in its different forms is dried and then subjected to specific heating cycles.

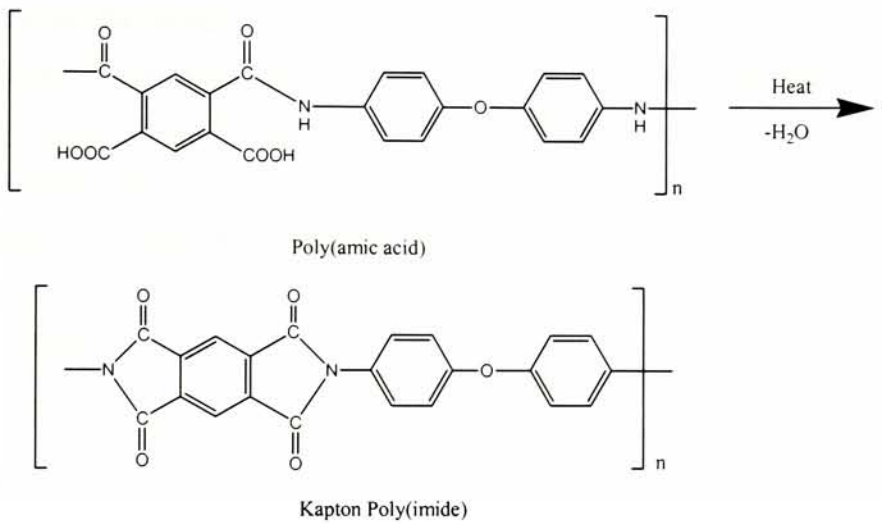

Figure 1.5. Conversion from poly(amic acid) to polyimide

Polyimides synthesized for this research work follow the condensation technique described above. Commercially available Kapton® (DuPont) and LARC-IA (Langley Research Center – Improved Adhesive) made by NASA are examples of condensation polyimides.

Polyimides that are generally soluble in organic solvents are often prepared by a one-step or single-stage method. This method is especially useful in the polymerization of unreactive dianhydrides and diamines and can yield a material with a higher degree of crystallinity than can be obtained from the two-step method.

1.2.1.2 Thermoplastic polyimides

Thermoplastic polyimides are obtained by introducing large cyclic side groups into the polymer chain, by tailoring random sequences into the chain, or by the interposition of flexible, aliphatic linking groups between the aromatic and heterocyclic moieties. One general drawback of thermoplastic polyimides is that for use at elevated temperatures, their glass transition temperatures must be high (> 200 °C) and hence their processing temperatures must be even higher. Ultem®, produced by General Electric, is an example of a commercially available thermoplastic polyimide.

1.2.1.3 Addition Polyimides

Addition polyimides usually consist of short chain preimidized oligomers with reactive end groups that can react by addition polymerization. The end groups used have been norbornene, maleimide, acetylenic, allynadic and benzocyclobutene. PMR-15 (Polymerization of Monomer Reactants), developed by NASA Langley is the most widely used polyimide made by this technique. Other resins include the bismaleimides, V-CAP [8], PMR-11, LARC-13 and LARC-160 systems.

*Table 1.1. Chemical structures of addition polyimides**

Trade Name	Chemical Structure
PMR-15	BTDE/NE/DDM [diester of benzophenone tetracarboxylic acid + monoester of nadic acid + 4,4'-diaminodiphenylmethane]
LARC-13	BTDA/NA/3,3'-DDM [benzophenone tetracarboxylic dinahydride + nadic anhydride + 3,3'-diaminodiphenylmethane]
PMR-11	HFDE/NE/PPD [hexafluoropropene dianhydride + monoester of nadic acid + p-phenylenediamine
LARC-160	BTDE/NE/AP22 [diester of benzophenone tetracarboxylic acid + Monoester of nadic acid + Jeff amine 22]

* For more information, refer to Winters, W.; Cavano, P.J.,*10th Nat. SAMPE Tech. Conf.*, 10 (1978) 661; T.L. St. Clair; Progar, D.J., *24th Nat. SAMPE Symp., 24 (1979) 1081* and T.L. St. Clair; Jewell, R.A., *23rd Nat. SAMPE Symp.* 23(1978) 520.

Characterization of polyimides

Polyimides can be characterized using several techniques including analytical, thermal, rheological and mechanical. Analytical techniques such as gel permeation chromatography (GPC) and dilute solution viscometry have been used to determine the molecular weight of poly(amic acid)s. Verification of the polymer structure and monitoring of the polyimide formation during cure can be accomplished using Fourier Transform Infrared (FTIR) Spectroscopy. Thermal techniques involving thermogravimetric analysis (TGA), thermal mechanical analysis (TMA) and differential scanning calorimetry (DSC) allow measurement of thermal decompositions and glass transition temperatures. Rheological properties provide information regarding the flow characteristics of the resin and help to define processing windows for fabricating fiber reinforced composites. Mechanical and electrical properties are usually obtained by casting and curing of poly(amic acid) films and performing the desired tests. Tensile, impact and tear strength are some of the common mechanical tests while dielectric constant, dielectric strength and volume resistivity are the common electrical tests performed on polyimide films.

1.2.2 Properties and Applications of Polyimides

The thermal and oxidative stabilities of polyimides are primarily determined by the structural features of the polymer. Polyimides derived from aromatic diamines and aromatic dianhydrides exhibit outstanding thermal stability at elevated temperature. The T_g determines the method of processing and the maximum temperature at which a polymer can be used in any given application. The high glass transition temperatures offered by these polymers are attributed to their stiff molecular backbones, which contain aromatic rings [6, 7]. Polyimides exhibit good solvent resistance to acidic or neutral aqueous environments. However, almost all polyimides undergo hydrolytic degradation in the presence of strong alkaline aqueous solutions. Their outstanding mechanical properties make them excellent candidates in high performance applications. Like most organic polymers, polyimides are good insulators and have low dielectric constants.

Polyimides are widely used in load bearing applications such as struts, chassis and brackets in automotive and aircraft structures. Other applications include brake linings,

bearings, grinding wheels and communicators in electric motors. Polyimide films are used as high temperature insulation materials and passivation layers in integrated circuits [7]. They are also used as resin matrices in advanced composites and as photo resists and inter level dielectrics in integrated circuits in the microelectronic industry.

1.2.3 Fiber Reinforced Polymer Composites

A judicious selection of fiber, matrix and interface conditions can lead to a composite with a combination of strength and modulus comparable to or better than those of many conventional metallic materials. Composites are superior to metals in specific strength and specific stiffness. Table 1.2 shows a comparison between selected conventional and composites materials.

Table 1.2 Properties of selected conventional and composite materials [9]

Material	Density (ρ), g /cm^3	Tensile Modulus (E), GPa	Tensile Strength (σ), MPa	E / ρ 10^6 N.m / kg	σ / ρ 10^3 N.m / kg
Al 6061- T6	2.70	68.90	310.00	25.70	115.00
Ti-6Al-4V	4.43	110.00	1171.00	25.30	26.40
Nylon 6/6	1.14	2.00	70.00	1.75	61.40
Unidirectional high strength carbon fiber/epoxy	1.55	137.80	1550.00	88.90	1000.00
Unidirectional E-glass fiber/epoxy	1.85	39.30	965.00	21.20	522.00
Random glass fiber/epoxy	1.55	8.50	110.00	5.48	71.00

1.2.3.1 Resin Matrices

The role of the resin matrix is primarily to bind the fibers together and hence it determines the thermal stability of the composite. The resin keeps the fiber in a desired location and orientation and acts as a load transfer medium between fibers. It protects the fiber from environmental damage before, during and after composite processing. The chief polymers used in high performance composites are thermosetting resins. These include the unsaturated polyesters, vinyl esters, epoxides, phenolics and polyimides.

The field of thermally stable heteroaromatic polymers is dominated by the polyimides. Most recently their use as resin matrices has attracted the greatest attention. The needs of the defense industry and the high temperature requirements of the electronics industry have promoted the use of polyimide coatings, films and laminates. The most commonly used polyimide resin matrices for composites are condensation polyimides, polymerization of monomer reactants (PMR) and bismaleimides (BMI) [9].

It is the outstanding thermal stability and relative ease of fabrication that have established the reputation of polyimides as viable engineering materials and particularly as resin matrices for advanced composites. Figure 1.7 shows the use temperature for resin matrix composites.

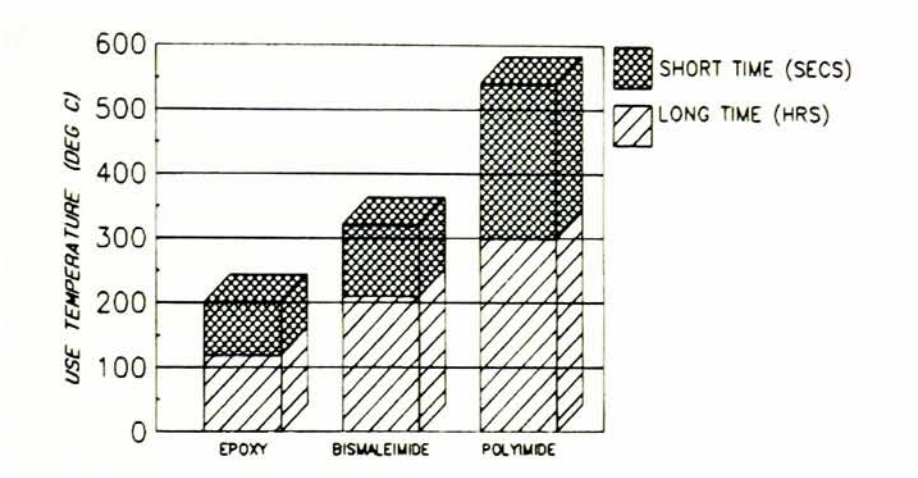

Figure 1.7. Use temperatures for resin matrix composites [10]

Until now, epoxy based composites were the most important matrix materials. However, their long-term use is limited to temperatures up to 130 °C. Bismaleimide (BMI) resins offer a "half way house" in temperature performances between epoxies and polyimides. The reason for the intense interest in BMI systems is their ability to be fabricated using epoxy-like conditions and without the evolution of void-producing volatiles. BMI systems are capable of performing at temperatures up to 230 °C [10]. Service temperatures for polyimides depend on the application requirements. For aerospace applications, where the materials undergo cyclic temperature variations,

polyimides have shown to exhibit good short-term and long-term performance over large temperature ranges.

1.2.3.2 Fiber Reinforcements

Fibers are the principal load bearing members in a composite. They are usually of high strength and modulus and are incorporated into the matrix either in continuous lengths or as chopped fibers. Examples of fiber reinforcements are glass, carbon, aramid, boron, alumina, silicon carbide and polyethylene fibers. Even though these fibers have high tensile moduli, they are usually brittle (have low elongation), with carbon fibers more brittle than aramid or glass fibers.

1.2.4 Fabrication of Composites

The techniques most commonly used for the fabrication of composites are [11]:

1) Manual Lay-Up (Wet Lay-Up and Prepreg Method)
2) Automated Tape Lamination
3) Vacuum Bag Molding
4) Autoclave Curing
5) Filament Winding
6) Pultrusion
7) Matched-Die Molding
8) Resin Transfer Molding (RTM) and
9) Spray-Up Methods

Prepregs for the research work were made using the manual wet lay-up technique and composites were then fabricated by autoclave curing. These techniques have been described below:

1.2.4.1 Prepreg Fabrication

A prepreg is a fiber reinforcement that has been impregnated with resin, slightly cured to increase viscosity to facilitate easy handling and lay-up. The processing of

prepregs to produce laminates depends upon the type of polyimide used for impregnation, the equipment (autoclave or press), and the shape of the item and its thickness [12].

There are two primary varieties of fiber reinforcement, unidirectional fibers (tapes) and woven fabrics. These fiber assemblies are impregnated either via solution coating procedures or by hot melt methods. Recent work has also shown that prepreg can be produced by powder impregnation and by the co-mingling of fibers. In the hot-melt method, resin is rolled into a thin film of desired thickness to provide the correct fiber/resin ratio. The reinforcement and resin film are then joined and passed between heated rollers to saturate the bundles of fibers producing a prepreg. In solvent coating, the fibers (usually a woven fabric) are passed through baths containing a solution of the resin in a solvent. The preimpregnated fabric is then passed through a heated oven to remove most of the solvent. The prepreg is rolled at the end of the line with a release paper interleaf [10].

1.2.4.2 Autoclave Curing

The technique most often used in the lamination of carbon or graphite fiber reinforced composites is the autoclave processing (See Figure 1.8). It is a large pressure vessel equipped with a temperature and pressure control system. The elevated pressures and temperatures, required for processing of the laminate, are commonly achieved by electrically heating a pressurized inert gas such as nitrogen to reduce oxidizing reactions that occur in the resin at elevated temperatures. Pressure applied in the autoclave provides force to consolidate the plies and to compress vapor bubbles to obtain a product with minimum void content.

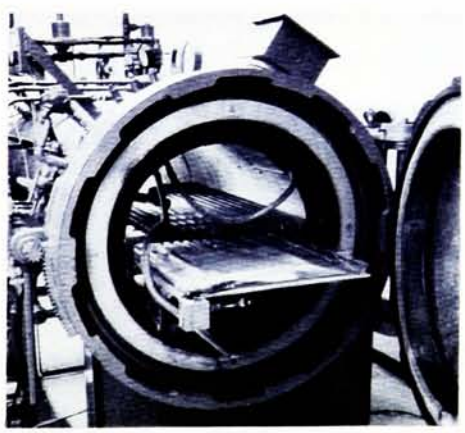

Figure 1.8. Autoclave [13]

The first step involved in this process is the vacuum bagging. The starting material is normally a prepreg, which is then laid up as plies on a mold surface. This is followed by the placement of a porous release film and a bleeder material. The porous release film permits the excess resin to flow through, while the bleeder material absorbs the excess resin. This stack is then covered with a barrier film, a breather material and a heat resistant vacuum bag. The barrier material prevents the resin from clogging the breather and vacuum lines whereas the breather material acts as a distributor for air and escaping volatiles and gases. The entire assembly is then placed inside the autoclave and a vacuum is applied within the bagging film to achieve a uniform pressure and to draw out volatiles created during cure. Figure 1.9 shows a typical vacuum bag assembly [9, 11].

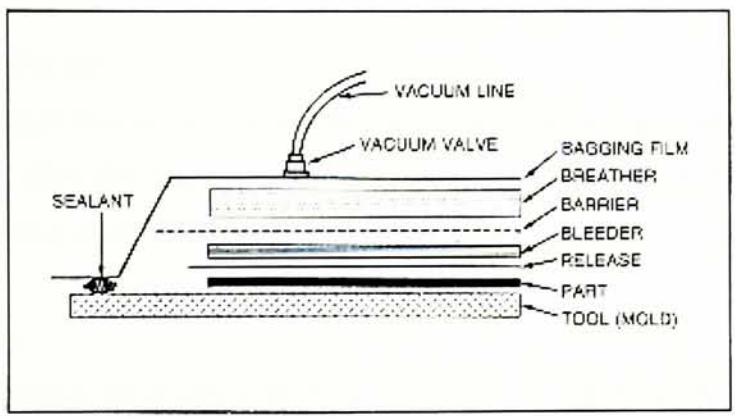

Figure 1.9. Typical vacuum bag assembly [11]

However, the above hand lay-up/autoclave fabrication type of processing is not only costly but also environmentally unfriendly. NASA is currently developing an automated robotic tow placement technology that could overcome these deficiencies [14].

1.2.5 Failure Mechanisms in Composites

Failure behavior of composites is complex due to their anisotropic nature. It is not only the magnitude of the stresses that are important, but also the orientation of the main stresses relative to the axes of the material's anisotropy. Composite polymers can have a number of fiber orientations i.e. continuous, discontinuous or randomly oriented. The orientation of the fibers is an important consideration in the failure modes that it can

undergo. For unidirectional, continuous fiber composites, the direction of the externally applied stress largely determines the failure mode of the composite. However, in laminates, comprised of a number of plies with varying orientations, the failure mode is the result of a complex interaction of factors. The mechanical response to loading is often referred to as being either fiber or matrix dominated. The typical composite failure modes are described below [15]:

1) Debonding

Debonding is due to interfacial failure along the fiber-matrix boundary. This is characterized by the fracture surface showing numerous protruding fibers with little or no resin adhering to them.

2) Inter laminar Failure

Inter laminar failure can occur when the interfacial strength between matrix and fibers is greater than the matrix cohesive strength. Such failure is manifested in the composite exhibiting excessively brittle behavior.

3) Fiber Buckling

Fiber buckling can occur in compression when the matrix has inadequate strength. Micro buckling of fibers is a common form of failure in the case of continuous fiber reinforced composites subjected to compression. This failure has also been found to occur as a result of curing at high temperatures when there is a significant difference between the degree of contraction of the matrix and the fibers.

4) Fiber Pull Out

Fiber pull out arises due to variations in the interfacial bond strength and localized load transfer from the fiber to the matrix. The energy dissipated during fiber pull out from the matrix is largely dependant in the degree of interfacial friction present, which in turn is determined by the shrinkage forces which arise on cooling of the composite.

5) Fiber Breakage

Fiber breakage has been regarded as a significant energy absorbing mechanism in the failure of composite materials.

6) Cracking of Composites

Cracking in composites can be initiated by debonding at the fiber resin interface. This can result in a transverse ply crack that increases in length, and upon reaching a fiber continues along it and then proceeds back into the matrix. This phenomenon, where a propagating crack in the matrix can be deflected a number of times when it impinges on the fiber reinforcement is called crack deflection. This crack deflection phenomenon is an important mechanism in increasing the toughness of the polymer matrix, since the fracture path length is much less readily achieved.

7) Micro cracking

Micro cracking of continuous fiber composites is induced by thermal expansion mismatches between the fiber and the matrix causing considerable stresses and these can result in complete yielding of the matrix. Furthermore, macroscopic thermal mismatches can also occur between cross plies. Cross-ply laminates generate higher residual stresses than unidirectional laminates because of the anisotropy in the thermal expansion of the plies.

1.2.6 Overview of Research Polyimides under Investigation

Three different types of polyimides have been synthesized for this research work by the condensation technique described above:

1) 2-component polyimide based on 3,4'-ODA and 4,4'-ODPA
2) 3-component "parent" polyimide based on 3,4'-ODA, 4,4'-ODPA and 10 mol % Mellitic Acid Dianhydride (MADA) to form a copolymer of (3,4'-ODA + 4,4'-ODPA) & (3,4'-ODA + MADA). MADA acts as a site for pendent group attachment and,
3) 4-component "pendent" polyimide based on 3,4'-ODA, 4,4'-ODPA, 10 mol %

MADA and 10 mol % zirconium pendent group to form a copolymer of (3,4'-ODA + 4,4'-ODPA) & (3,4'-ODA + MADA + Zr). The Zr-pendent group is attached at the site of the MADA.

Figure 1.6 shows comparisons with respect to chemical structures made between the pendent polyimide and commercially available Kapton® and LARC-IA.

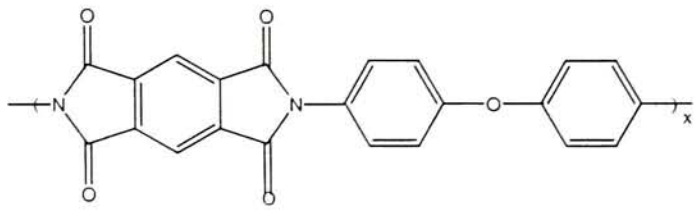

DuPont Kapton ®

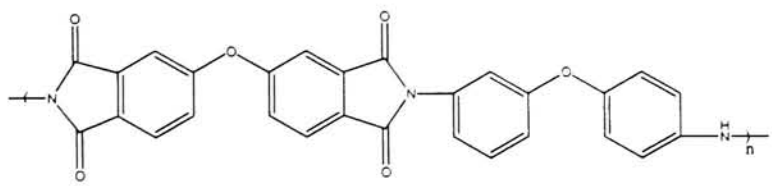

NASA-LARC-IA

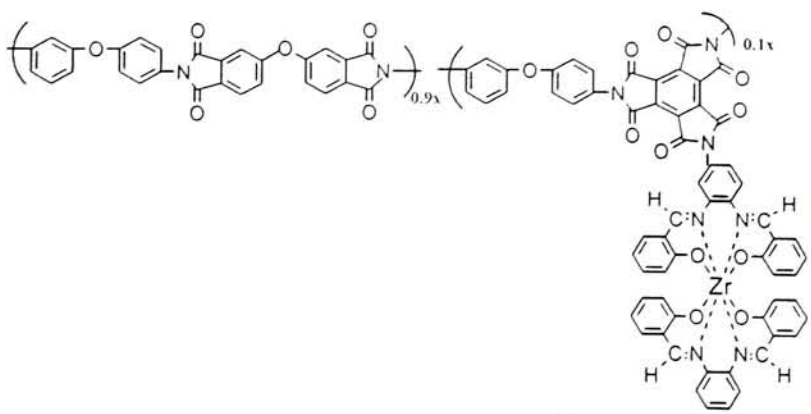

Zirconium-pendent polyimide

Figure 1.6. Chemical structures of different polyimides

As seen from Figure 1.6, Kapton® has one ether linkage while NASA's LARC-IA polymer has two ether linkages along the polymer chain. This imparts a certain degree of mobility to the polymer backbone. The novel research polymer also has two ether linkages in 90 % of its monomer groups (which are identical to LARC-IA), but due to the heavy zirconium pendent group attached in the remaining monomers, its mobility may be somewhat diminished.

The 2-component polyimide synthesized in the present research is very similar to the LARC-IA developed by NASA. LARC-IA is prepared from 3,4'-ODA and 4,4'-ODPA in NMP as a 30 % w/w solids solution and the molecular weight is controlled by end capping groups such as phthalic anhydride (PA) while the 2-component polyimide is prepared from 3,4'-ODA and 4,4'-ODPA in NMP as a 15 % w/w solids solution without any end capping groups.

1.3 Hypothesis

Since the pendent group structure is massive relative to the mass of the repeat units of the polymer chain, mobility of the chain should be hindered, which should make the resin stiffer and more brittle. It is hypothesized that the moduli for a variety of mechanical properties will be lower for composites with pendent polymer as the resin matrix as compared to those with parent (without pendent groups) polymer as the resin matrix.

1.4 Major Objectives of this Study

There are two objectives defined for this present study. In the first objective, the aim is to identify the processing conditions that produce the maximum degree of imidization in the shortest time possible. This would potentially be important to processing industries using polyimides, as there would be optimum product performance and shorter cycle times to manufacture the product leading to higher production rates. To achieve this, optimum processing conditions for the 2-component polyimide (3,4'-ODA + 4,4'-ODPA), 3-component "parent" polyimide (3,4'-ODA + 4,4'-ODPA + 10 mol % MADA, where MADA is mellitic acid dianhydride, the site of pendent group attachment), and the 4-component zirconium pendent polyimide (3,4'-ODA + 4,4'-

ODPA + 10 mol % MADA + 10 mol % zirconium complex) will be established by varying the time and temperature parameters of a programmable oven.

The second objective is to fabricate woven carbon or glass fabric reinforced composites of the 2-, 3- and 4-component polyimide and evaluate their mechanical properties for structural applications. Comparisons of mechanical data with laminates fabricated using a different molding cycle are included.

Chapter II

EXPERIMENTAL

2.1 Chemicals and Materials

3,4'-Oxydianiline (3,4'-ODA) (TCI, Tokyo) and 4,4'-Oxydiphthalic anhydride (4,4'-ODPA) (ChrisKev Company, Inc.) were purified by subliming three times at 84 °C and 254 °C, respectively. These chemicals were then stored in a dessicator containing P_2O_5 to prevent moisture absorption. The 1-methyl-2-pyrollidinone (NMP) (Aldrich Chemical Co.) was dried by distillation over CaH_2 just prior to its use. Benzenehexacarboxylic acid (mellitic acid) was obtained from TCI, Tokyo. The zirconium(IV) n-butoxide [Zr-(O-n-Bu)$_4$] and dicyclohexylcarbodiimide (DCC) were obtained from Aldrich and used as received. IR grade potassium bromide (KBr) for infrared spectroscopic analysis was acquired from Aldrich Chemical Co.

Carbon fabric (Hexcel Style 282) was received from Composites One. Glass fabric (Corning Style WR24-5X4C) was obtained from Owens Corning, Inc. Other relevant properties are presented in Table 2.1.

Table 2.1. Fabric Specifications

E- Glass Fabric, Owens Corning Style WR24-5X4C	
Weave Style:	Plain
Warp Count:	5 ends/inch
Fill Count:	4 ends/inch
Areal Weight:	24 oz./sq.yd.
Avg. Filament Diameter:	17.2 microns
Carbon Fabric, Hexcel Style 282 (3K filaments per bundle)	
Weave Style:	Plain
Warp Count:	12.5 yarns/inch
Fill Count:	12.5 yarns/inch
Areal Weight:	5.8 oz/sq.yd.
Fabric Thickness:	8.7 mils
Avg. Filament Diameter:	7 microns

2.2 Synthesis of 2-, 3- and 4-Component Poly(amic acid)s

2.2.1 Synthesis of 2-component poly(amic acid) based on 3,4'- ODA and 4,4'- ODPA

A 15 weight % solid solution of poly(amic acid) using a 1:1 mole ratio of 3,4'-ODA: 4,4'-ODPA was achieved. Triply sublimed 4,4'-ODPA, 27.3433 g (88.1473 mmol) was added to 106 mL of NMP in a 1000 mL round bottom flask. The reaction flask was capped with a rubber septum and stirred for half an hour and the temperature was maintained at 0° C using an ice-water bath. A steady flow of nitrogen was maintained in the reaction flask. A solution of 17.6506 g (88.1472 mmol) of triply sublimed 3,4'-ODA dissolved in 65 mL of NMP was then added dropwise into the flask using a 10 mL syringe. NMP, 75 mL, was used to rinse the flask and syringe. Upon gradual addition of the 3,4'-ODA, the 4,4'-ODPA dissolved in the solution and ultimately yielded a viscous, homogeneous solution. The poly(amic acid) was then kept in a cold room and the solution was continuously stirred overnight. The structures for this reaction are shown in Figure 2.1.

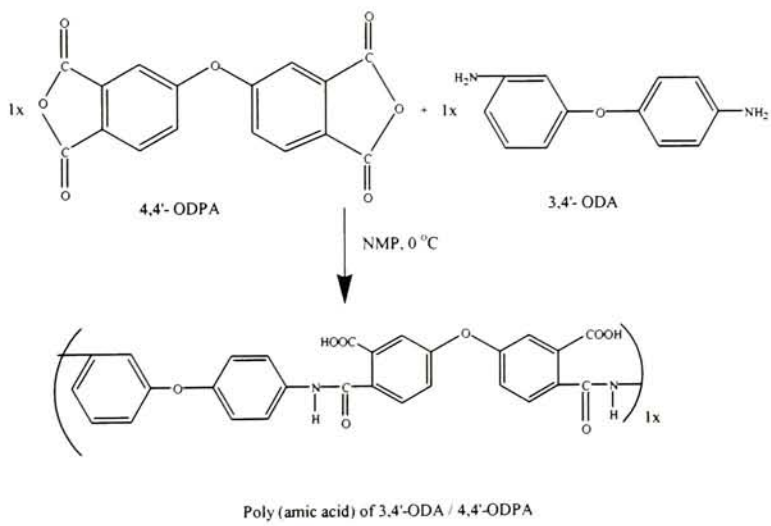

Figure 2.1. Synthesis of Poly(amic acid) of 3,4'- ODA / 4,4'-ODPA

2.2.2 Synthesis of Mellitic Acid Dianhydride (MADA)

Mellitic acid dianhydride (MADA) is a light brown solid prepared from the cyclodehydration of mellitic acid. The mellitic acid was heated in a nitrogen atmosphere at 190°-195° C by using ethylene glycol as a reflux for ~ 108 hours. Well ground mellitic

acid (~ 11 g) was placed in a 20 mL test tube covered with a rubber stopper. The test tube was then laid horizontally in a drying pistol sealed by another rubber stopper. The thermometer, nitrogen inlet and outlet tubes pass through both the inner and outer rubber stoppers. The sample was rotated periodically to achieve uniform heating of the mellitic acid by turning the outer rubber stopper, which in turn rotates the inner stopper and thus ultimately rotating the inner tube. The change in chemical structure which occurs is shown in Figure 2.2.

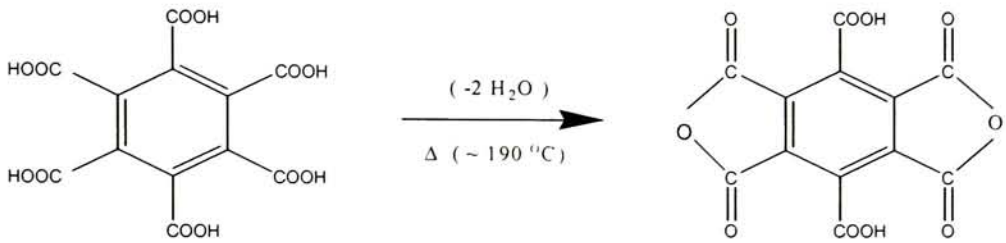

Mellitic Acid

Mellitic Acid Dianhydride

Figure 2.2. Conversion of Mellitic acid to Mellitic Acid Dianhydride

One mole mellitic acid loses 2 moles of water to form MADA. The purity of the MADA has been confirmed by the TGA analysis that shows a one-step weight loss of 5.88 % due to the loss of 1 mole of water per mole MADA forming mellitic acid trianhydride (MATA).

2.2.3 Synthesis of 3-component poly(amic acid) based on 3,4'-ODA, 4,4'-ODPA & 10 mol % MADA

Synthesis of the 3-component poly(amic acid) is similar to the 2-component poly(amic acid) except that in this case, the MADA and 4,4'-ODPA were added together to the reaction flask. A mole ratio of 1.0:0.9:0.1 of 3,4'-ODA: 4,4'-ODPA: MADA with a 15 weight % solid solution was achieved. A total volume of 750 mL solution of poly(amic acid) was prepared for processing evaluation, preparation of prepregs and further reaction. The structures for this reaction are depicted in Figure 2.3.

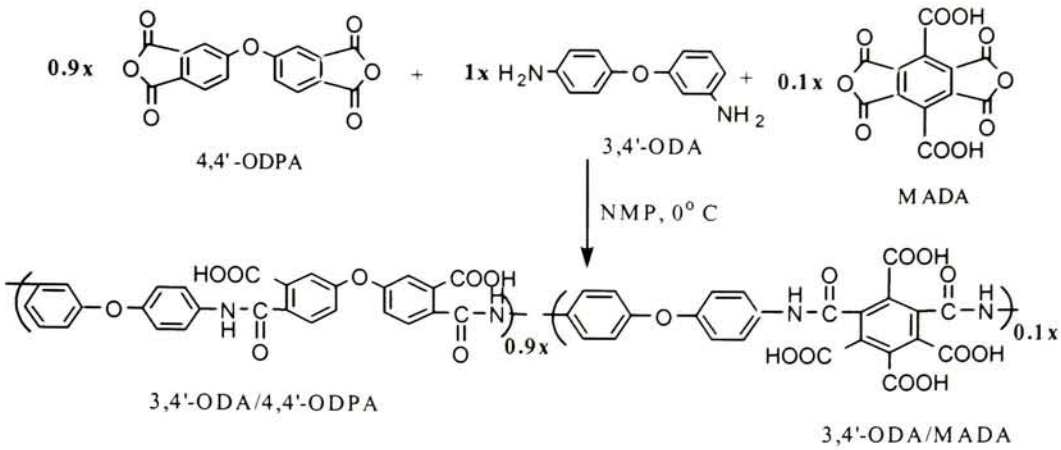

Figure 2.3. Synthesis of Poly(amic acid) of 3,4'-ODA / 4,4'-ODPA / 10 mol % MADA

2.2.4 Synthesis of 4-component poly(amic acid) based on 3,4'-ODA, 4,4'-ODPA, 10 mol % MADA & 10 mol % Zr complex [Zr(adsp)(dsp)]

Some of the 3-component poly(amic acid) solution (160 mL) prepared above was then separated in to two portions. One portion was stored for characterizing and composite fabrication purposes while the other part was used to synthesize the 4-component poly(amic acid). The zirconium complex pendent poly(amic acid) was synthesized by the addition of the mixed ligand complex Zr(adsp)(dsp) to the poly(amic acid) backbone in the presence of N,N'-dicyclohexylcarbodiimide (DCC). The reaction of Zr(adsp)(dsp) with carboxylic acid groups on the MADA moieties of the poly(amic acid) was promoted by dehydration due to the DCC. Yellow Zr(adsp)(dsp) powder, 3.546 g (4.892 mmol), along with 9.70 mL of NMP was added to the reactor flask containing the poly(amic acid) solution (160 mL). A stoichiometric amount of DCC (0.9955 g, 4.824 mmol) was first dissolved in NMP (2.70 mL) solution and then added dropwise to the polymer solution via a 5 mL syringe. Additional NMP was used to rinse the syringe and the container three times and added to the reaction flask. As DCC was added, gel formation was observed on the surface. After vigorously shaking the flask, the gel disappeared. The reaction was monitored at regular intervals by spotting the solution on a silica gel TLC plate and eluting with methylene chloride/ ethyl acetate (93:7). The Zr(adsp)(dsp) and non-pendent poly(amic acid) were used as references on the TLC plate and viewed under a UV lamp. A spot due to the free Zr complex was still observed after the addition of the DCC/NMP solution indicating that the entire amount of Zr complex

added was not attached to the polymer backbone. An additional 10 mole % of DCC / NMP solution was added and a TLC test performed again showed no spot due to the free Zr complex, which meant that the appending reaction had been completed. The viscous polymer solution was then stored in a cold room with continuous stirring. The reaction scheme is summarized in Figure 2.4.

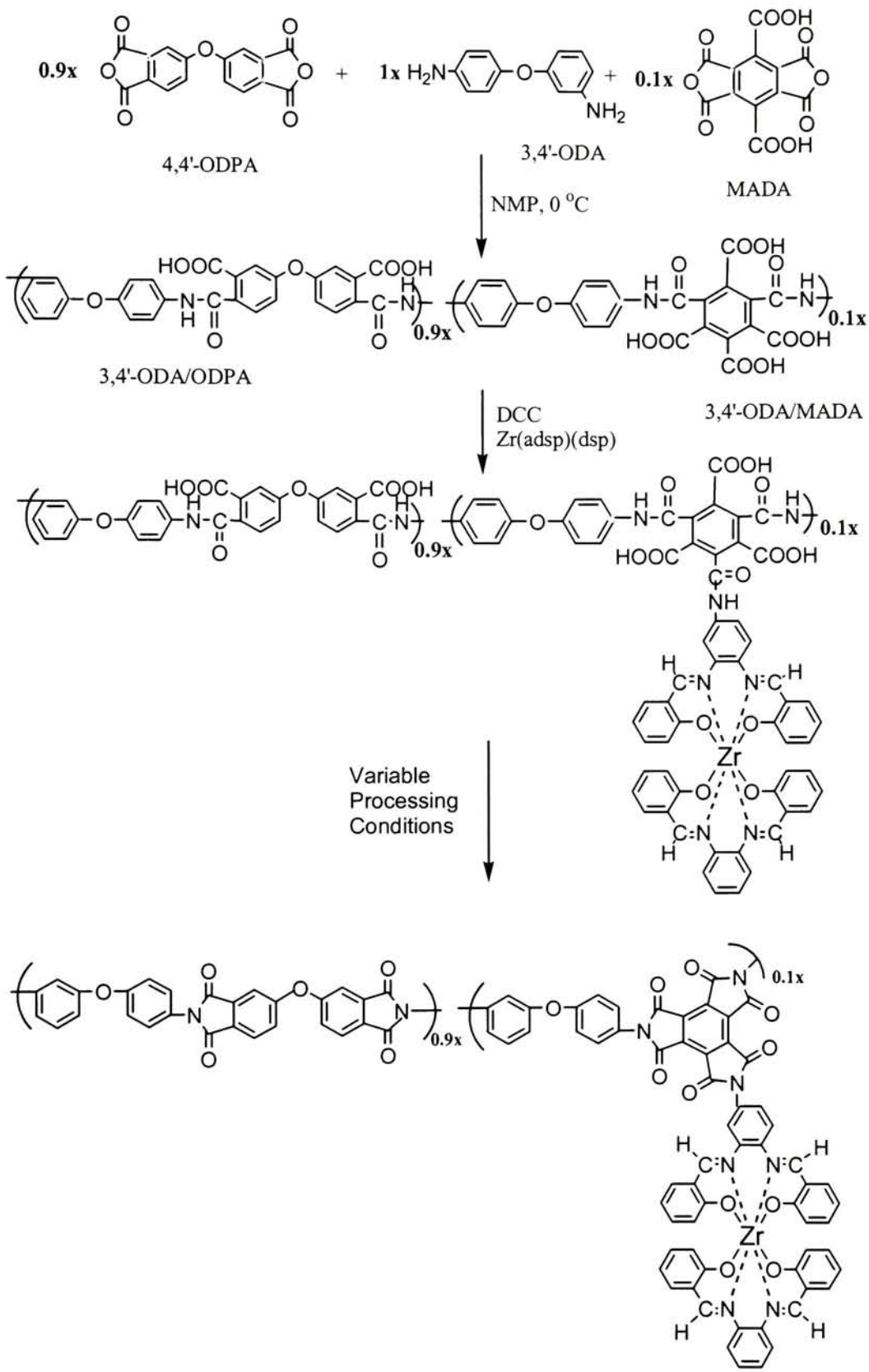

Figure 2.4. Synthesis of Zr(adsp)(dsp) Co-polyimide

2.2.5 Precipitation of Poly(amic acid) Solution

Portions of the poly(amic acid) solutions made above of 2 g each, were separated from the bulk solution for precipitation. The poly(amic acid) solution was added to a 1000 mL beaker filled with 450 mL of anhydrous ether (ethyl ether) using a dropper. The solution was continuously stirred and the poly(amic acid) precipitated in the ether. Fresh ether was added to facilitate the removal of the NMP from the polymer. For larger scale precipitations, a blender was used to break the precipitated lumps in to a finer powder in fresh ether solution. The powdered precipitate was then filtered and dried in a vacuum oven for 2 days. A mortar and pestle was used to grind the dried powder to a finer grade. Precipitation was carried out on all three polyimides for establishing the processing conditions.

2.3 Establishing Optimum Processing Conditions

2.3.1 Heating Steps

To establish the optimum processing conditions, the time and temperature settings of a programmable oven (Lindberg/Blue Model 2416) were varied. One of the most popular heating cycles in the literature for imidization consists of heating the poly(amic acid) at 100 °C for an hour, followed by 200 °C for an hour and finally at 300 °C for an hour [10]. Ten samples of each polyimide precursor (i.e. poly(amic acid), PAA) were subjected to the heating steps reflected in Table 2.2.

Table 2.2. Heating Steps for the poly(amic acid) powder

Processing Condition	Temperature (°C)	Time (Hours)	Temperature (°C)	Time (Hours)	Temperature (°C)	Time (Hours)
1	100	1	200	1	--	--
2	100	1	200	1	300	0.5
3	100	1	200	1	300	1
4	100	1	200	1	300	1.5
5	100	1	200	1	350	0.5
6	100	1	200	1	350	1
7	100	1	--	--	350	0.5
8	--	--	240	0.25	--	--
9	--	--	--	--	310	0.25
10	--	--	--	--	310	0.5

2.4 Characterization techniques

Characterization has been performed to determine which set of processing conditions is superior. If incomplete imidization or decomposition is seen, then those processing conditions have been rejected. We have characterized the 2-component, parent and Zr-pendent polymers by carrying out Fourier Transform Infrared Spectroscopy (FTIR), Thermogravimetric Analysis (TGA) and Differential Scanning Calorimetry (DSC) on each.

2.4.1 Fourier Transform Infrared Spectroscopy (FTIR)

This technique has been used to reveal the extent or degree of imidization taking place in the sample. Spectra have been analyzed by a band ratio method. Peak intensity ratio for the imide ring stretch occurring at 1779 cm^{-1} and a reference aromatic peak at 1012 cm^{-1} (ether oxygen-to-aromatic ring stretching vibration) has been calculated [16]. Degree of imidization has been calculated by normalizing a sample band ratio with one showing the maximum band ratio. For analysis, each peak was enlarged to minimize the measurement errors [17]. A Bio-Rad Excalibur Series FTS 3000 instrument was used to analyze the samples. The polymer and KBr powder (IR Grade) were grounded to obtain a good dispersion and the spectra were recorded using a diffuse reflectance cell.

2.4.2 Thermogravimetric Analysis (TGA)

TGA indicates (1) if any weight loss occurs due to incomplete imidization, or (2) for the Zr-pendent polymer, the extent of decomposition that takes place in the sample during processing, if any. The decomposition of the Zr-pendent polyimide can be calculated by:

Expected Wt of undecomposed polyimide

$$= \text{g } ZrO_2 \times \left(\frac{\text{1 mole } ZrO_2}{\text{123.2 g } ZrO_2}\right) \times \left(\frac{\text{1 mole Zr pendent group}}{\text{1 mole } ZrO_2}\right) \times \left(\frac{\text{1 mole Zr pendent mer}}{\text{1 mole Zr pendent grp}}\right) \times \left[1\left(\frac{1187.3\text{ g}}{\text{1 mole Zr pendent mer}}\right) + 9\left(\frac{474.4\text{ g}}{\text{1 mole non-pendent mer}}\right)\right]$$

....Eqn. 2.1

If the difference between the expected weight and the actual weight is ≈ 0, then the sample was completely imidized and no decomposition took place. If the difference is

>> 0, then either the sample has not been completely imidized or some ZrO_2 was lost from the TGA pan due to the airflow and if the difference between the expected weight and the actual weight is < 0, it means that the sample has decomposed at the chosen processing condition.

A TA Instruments TGA 2050 was used to perform the analysis. Samples weighed between 10 and 20 mg and were heated at 10 °C /min in air atmosphere up to 800 °C.

Molding cycles used for fabrication of the composite laminates in the autoclave have also been emulated in the TGA furnace to study decomposition taking place in the polymer, if any. The 2-component, parent and pendent poly(amic acid)s were heated up to 370 °C and held at this temperature for an hour in nitrogen atmosphere.

2.4.3 Differential Scanning Calorimetry (DSC)

This characterization technique is used to indicate the effect of processing on glass transition temperatures of the different polymers. It would also identify the presence of unimidized polymer if any. The analysis was carried out in a nitrogen atmosphere (flow rate of 80 mL/min) in a TA Instruments DSC 2010 machine. The samples were hermetically sealed and weighed between 5 and 10 mg. The following heating cycle was used:

Step 1: Ramp @ 10 °C/min to 450 °C

Step 2: Isothermal for 10 min

Step 3: Ramp @ 10 °C/min to 25 °C

Step 4: Isothermal for 10 min

Step 5: Ramp @ 10 °C/min to 450 °C

Step 6: Isothermal for 10 min

Step 7: Ramp @ 20 °C/min to 25 °C

2.5 Fabrication of Composite Laminates

A vacuum oven (National Appliance Co., Model 5831) was used for making the prepregs and the laminates were fabricated in an autoclave (Thermal Equipment Corporation). The carbon and glass reinforced composites were fabricated at the Center for Composite Materials (C.C.M.), University of Delaware.

2.5.1 Fabrication of Prepregs

Prepregs are defined as a reinforcing material impregnated with resin prior to the molding process and cured by the application of heat. The prepregs were fabricated using the conventional hand lay-up technique. The amount of resin needed for each ply was calculated by following the procedure given below:

To maintain a fiber to resin ratio of 60:40 by weight,

$$W_{resin}\ \text{needed} = W_{fiber} \times \frac{40}{60} \qquad \text{.....Eqn. 2.2}$$

For a 15 weight % solids solution, the weight of the solution needed:

$$0.15 = \frac{W_{resin}}{W_{resin} + W_{solvent}} \qquad \text{.....Eqn. 2.3}$$

Where,

W_{resin} = Weight of the resin (g),

$W_{solvent}$ = Weight of the solvent (g), and

$W_{resin} + W_{solvent}$ = Weight of the solution (g)

The procedure for making the prepregs is as follows:

1) In order to make a 4-ply laminate, a single sheet of 11" x 7" of the woven fabric was cut.
2) The sheet was weighed on a laboratory electronic balance and placed on a plastic tray covered with a release film.
3) The amount of resin and hence the amount of solution needed was then calculated to obtain the desired 60:40 fiber to resin by weight ratio using the equations shown above.
4) The weighed amount of solution was poured in a beaker, plus some extra solution was weighed to compensate for solution that would stick on the walls of the tray.
5) The brush was dipped in the solution for around 5 minutes to saturate it.
6) The resin was applied using the brush and the excess resin was squeezed out using a roller that also facilitated wetting the fabric.
7) Resin was then applied on the reverse side and the excess resin was squeezed out.
8) A release film was perforated and spread inside the vacuum oven.

9) The prepreg was placed on the film and heated at 65 °C for 30 minutes. This was done to retain some solvent facilitating the mobility of the polymer chains in the presence of the plasticizing action of the solvent.
10) The prepreg was weighed and if the ratio of fiber to resin was not reached, then more resin was applied followed by heating in the vacuum oven.
11) The above process was repeated until the desired ratio was reached.
12) The sheet was then cut into four plies each having a dimension of 7" x 2.75".
13) The prepregs were wrapped in an aluminum foil and stored in the cold room.

For single-ply laminas, sheets of 7" x 4" of the woven fabric were cut and prepregs were made using the above procedure. All the prepreg sheets (single ply and 4-ply) had a resin content of ~52 % by weight to account for the solvent losses and the loss of water during imidization taking place in the autoclave. This was done based on the following calculation / argument:

For a 2-component polyimide,

molecular weight of the repeat unit = 510.44 g/mol

Since two molecules of water are lost upon imidization,

$$\text{loss in weight due to water} = \frac{36}{510.44} \times 100 = \sim 7\%$$

It was also observed that during the vacuum oven treatment of the prepregs, there was a loss of ~ 4 weight % due to solvent evaporation. In order to achieve 40% by weight of the resin,

$$\text{resin to be applied to the fibers} = 40\ \% + 7\ \% + 4\ \% = 51\ \%$$

2.5.2 Fabrication of Laminates

For a single-ply lamina, the prepreg was laid out on the autoclave table, while for making a four-ply laminate, 4 plies were stacked on top of each other. The entire assembly was vacuum bagged and placed inside the autoclave. Composite lamination was performed using a Thermal Equipment Corporation autoclave under controlled pressure, temperature and time. Listed in Table 2.3 are the parameters used for the autoclave.

Table 2.3. Autoclave Parameters

Recipe Parameters	Units	Heating Cycle	Cooling Cycle
Target Temperature	°F	702	230
Soak Time	min	60	1
Heating Rate	°F/min	20	5
Target Pressure	psi	250	250
Target Vacuum	in. Hg	30	30

2.5.3 Resin Content of Laminates

Two methods were employed to calculate the resin content of the laminates after autoclave consolidation.

Method I: The resin content of the laminates was found according to ASTM D 2584-94, *Standard Test Method for Ignition Loss of Cured Reinforced Resins*. A 1 cm x 1 cm sample was cut from each laminate and the resin content was obtained by following the procedure described below:

An empty ceramic crucible was heated in a furnace at 560 °C for about 15 minutes. It was then cooled to room temperature in a dessicator and weighed. The sample was placed in the crucible and weighed precisely. It was burned in a furnace at 560 °C for about 1 hour. The resin burned off completely and the crucible was allowed to cool back to room temperature in the dessicator. The weight of the fibers was recorded and the resin content was calculated using the formula given below:

$$\% \text{ Resin Content} = \frac{W_{\text{laminate}} - W_{\text{fibers}}}{W_{\text{laminate}}} \qquad \text{.....Eqn. 2.4}$$

Where,

W_{laminate} = Weight of the composite sample (g),

W_{fibers} = Weight of the fibers (g), and

$W_{\text{laminate}} - W_{\text{fibers}}$ = Weight of the resin (g)

Method II: This is a very rough technique employed to determine the resin content. In this method, the weight of a comparable size sheet of fiber was recorded before the application of any resin. The laminates were then weighed on an electronic balance after fabrication, and resin content was determined using equation 2.4.

2.5.4 Machining of Composite Laminates

Various specialized techniques such as water-jet or laser cutting for machining composite laminates have been developed [13]. Prior to mechanical testing, the composite laminates were machined using a laser beam and specimen edges were smoothed using sand paper (Grade 320) to ASTM recommended dimensions.

2.6 Mechanical Properties of Composite Laminates

Various mechanical tests such as Tensile, Flexural (three-point bend), Izod Impact and Dynamic Mechanical Analysis (DMA) were conducted on the composite specimens. The tensile and DMA tests were performed on single ply laminas while the flexural and Izod impact tests were performed on four-ply laminates.

2.6.1 Tensile Testing

Tensile test is a measurement of the ability of the material to withstand forces that tend to pull it apart and to determine to what extent the material stretches before breaking. The tension test has been used to measure the tensile modulus, strength and ultimate strain to failure for composites. Tests were performed on single ply laminas on an MTS 45G Universal Testing Machine (U.T.M.) according to ASTM D3039/D3039M-95a, *Tensile Properties of Polymer Composite Materials*. The machine was computer controlled using a Test Works 4® software.

2.6.1.1 Specimen Preparation

Bonding of end tabs to tensile specimen

Conventional dog-bone specimens for tensile testing have a tendency to split in the region where the width changes. For fiber composites, uniform width (rectangular) ASTM D3039/D3039M-95a test specimen geometry with tabbed ends is most commonly

used. The end-tabs were bonded to the test specimens to minimize stress concentration at load introduction regions at the specimen ends. A Hysol 9303 grade adhesive (Dexter Adhesives, Inc.) was used to bond the end-tabs to the tensile specimen. The procedure described below was followed [13]:

1) Using a sand paper (grade 220 or 180), the regions of the panel where the end tabs are bonded were sanded in $\pm$ 45° motions.
2) Using a wire brush, the loose particles were carefully removed.
3) The surface was cleaned with acetone until all the loose fibers were removed.
4) The surface of the end tabs were sanded and cleaned according to the procedure described above for the composite.
5) After mixing the two components of the adhesive, it was applied to both bonding surfaces and cured under pressure for ~ 12 hours. A heavy wooden frame was used to apply the pressure by placing the samples beneath it.

2.6.1.2 Tensile Test Parameters

The parameters in Table 2.4 were used when conducting the tensile tests.

Table 2.4. Tensile Test Parameters (ASTM D3039/D3039 M-95a)

Specimen Size:	
With carbon reinforcements →	6" x 0.5" x 0.014" (152.4 mm x 12.7 mm x 0.355 mm)
With glass reinforcements →	6" x 0.5" x 0.012" (152.4 mm x 12.7 mm x 0.305 mm)
Strain Rate:	0.01 min^{-1}
Rate of Crosshead motion:	2 mm/min
Load Cell [a]:	10 kN (2248.09 lbf) [b]
Gage Length [c]:	102.5 mm

[a] Load Cell→ a device used for applying load to the specimen.

[b] Ref. [18]

[c] Gage Length→ the original length of that portion of the specimen over which strain or change of length is determined.

2.6.2 Flexural Testing (Three-point bending)

Flexural strength is the ability of the material to withstand bending forces applied perpendicular to its longitudinal axis. The stresses induced by the flexural loads are a

combination of compressive and tensile stresses. Flexural properties such as strength and modulus were determined by ASTM test method D790-00, *Flexural Properties of Unreinforced and Reinforced Plastics and Electrical Insulating Materials*. In this test, a composite beam specimen of rectangular cross section was loaded in a three-point bending mode. This mode is chosen for materials that break at relatively small deflections.

Beams with small span-to-depth ratio are dominated by shear failure. A span to depth ratio of 32:1 was chosen so that the failure takes place due to bending mode and not due to any shearing effects. Flexural tests were conducted on an MTS frame (Model 45G) with a three-point bending fixture. All composite specimens used for this test were four-ply laminates.

The parameters in Table 2.5 were used when conducting the flexural tests.

Table 2.5. Flexural Test Parameters (ASTM D790-00)

Diameter of loading nose and support pins:	10 mm
Span[a] to Depth Ratio:	32:1
Specimen Size:	4" x 0.5" x 0.042" (101.6 mm x 12.7 mm x 1.066 mm)
Load Cell:	10 kN (2248.09 lbf) [b]
Rate of Crosshead motion:	Based on formula [c]
Strain Rate:	0.01 mm/mm/min

[a] Span→ distance between the two support pins

[b] Ref [18]

[c] The rate of crosshead motion was calculated by using the formula:

$$R = \frac{ZL^2}{6d} \qquad \text{.....Eqn. 2.5}$$

Where,

R = rate of crosshead motion, mm/min

L = support span, mm

d = depth of beam, mm and

Z = strain rate (0.01 mm/mm/min)

2.6.3 Izod Impact Testing

The impact properties of a material represent its capacity to absorb and dissipate energies under impact or shock loading. This test was performed to evaluate the resistance of composites to failure due to impact. A Testing Machines, Inc. Impact Tester (Model 43-1) with a hammer mass of 10 lbf was used to evaluate the impact test. The specimens measured 2.5" x 0.5" x 0.04" (63.5 mm x 12.7 mm x 1.016 mm) as specified by ASTM D256-00, *Determining the Izod Pendulum Impact Resistance of Plastics* and were notched with a carbide tipped dove tail (2 x 45°) cutting tool. The notch acts as a stress concentration site to minimize the energy required for initiation of fracture. Thus, the total measured energy required for fracture is essentially the energy required for propagation of the fracture. The impact energy (or resistance) was calculated as the impact load per unit width (kJ/m) while the impact strength was calculated by dividing the impact load per unit width by the depth of the specimen under the notch (kJ/m^2).

2.6.4 Dynamic Mechanical Analysis (DMA)

DMA was performed on the single ply composite laminas according to ASTM D4065-95, *Standard Practice for Determining and Reporting Dynamic Mechanical Properties of Plastics* using Seiko Instruments SDM/5600 equipment in a three point bending mode. Samples had a dimension of 2" x 0.38" x 0.03" (50.8 mm x 9.65 mm x 0.76 mm) and were subjected to frequencies of 0.2, 2 and 20 Hz. They were heated from room temperature up to 400 °C at a constant heating rate of 2 °C/min.

In dynamic mechanical analysis, an oscillatory strain is applied to a sample and the resulting stress is measured. If the material is viscoelastic and a sinusoidal strain is applied, it will exhibit a sinusoidal stress response. This can be separated into two components, the in-phase (0°) and the out-of-phase component (90°). The in-phase component describes the elastic component of the materials and is an indication of the storage modulus G' while the out-of-phase component is proportional to the viscous component and is represented by the loss modulus G'' of the material. A ratio of the viscous to the elastic component G'' / G' is called the tan delta (δ). High tan delta values indicate a viscous material and low tan delta indicates an elastic material.

The modulus measured in DMA is, however, not exactly the same as the Young's modulus of the classic stress-strain curve. Young's modulus is the slope of a stress-strain curve in the initial linear region. In DMA, a complex modulus (E*), an elastic modulus (E') and a loss modulus (E'') are calculated from the material response to the applied sinusoidal strain. These different moduli allow better characterization of the material, because we can now examine the ability of the material to return or store energy (E'), to its ability to lose energy (E'') and the ratio of these effects (tan delta), which is called damping.

2.7 Optical & SEM Imaging

Optical images of the composite laminates were obtained before and after failure. A Nikon Eclipse E600 optical microscope was used for the analysis and the images were recorded with the analySIS® software.

A Philips SEM 525 instrument was used to obtain images of the laminates after failure. Images were recorded using a Sony digital camera attached to the instrument with a spot size of 100 nm and a high tension of 30 kV. The working distance was between 9 and 11 mm.

Chapter III

RESULTS AND DISCUSSION

3.1 Synthesis of 2-, 3- and 4-Component Poly(amic acid)s

Poly(amic acid)s were synthesized for all the three different resin systems according to techniques described in sections 2.2.1 - 2.2.4. Viscous, homogeneous solutions were obtained after the polymerization reactions and stored in a cold room for further use. A 15 % by weight solids solution was prepared for all poly(amic acid) solutions.

A clear, pale yellow colored viscous solution was obtained for the 2-component poly(amic acid). A brownish, viscous solution was obtained at the end of the reaction for the parent polymer. The purity of the Mellitic Acid Dianhydride (MADA) used for this polymer was confirmed by the TGA graph depicted in Figure 3.1.

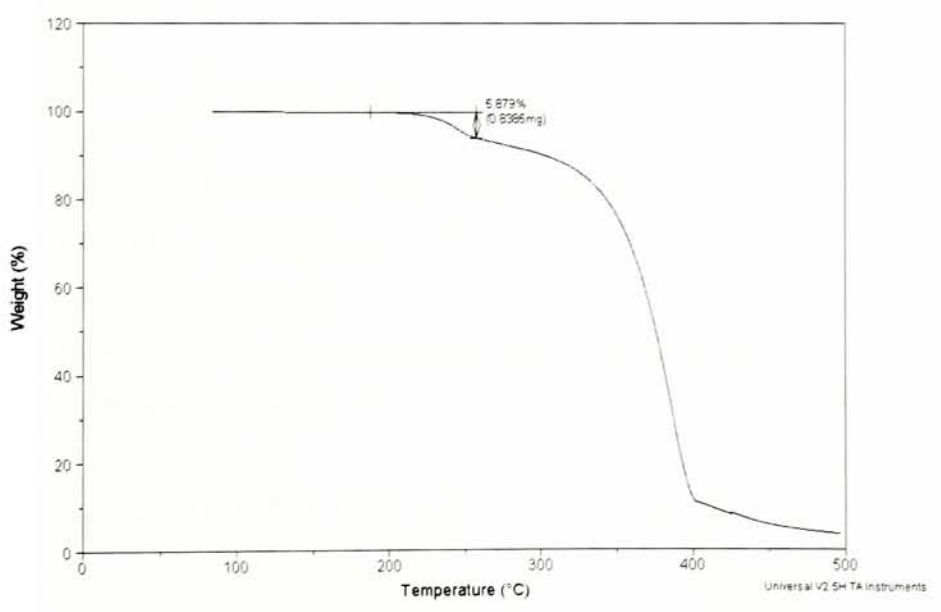

Figure 3.1. TGA graph of MADA

There was only a one-step weight loss (~ 5.88 %) seen in the TGA curve, which was the result of 1 mole of water being removed from the dianhydride to form the trianhydride.

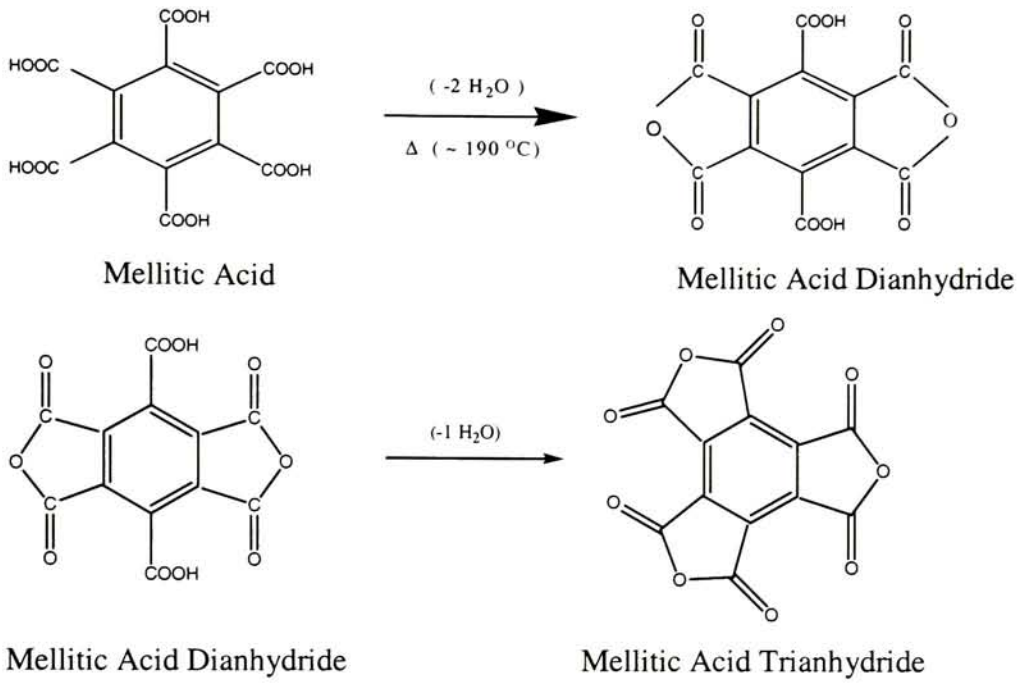

Figure 3.2. Mellitic acid and its products

This loss in weight of 5.88 % is based on the following calculation:

M.W. of Mellitic Acid Dianhydride (MADA) = 306.14 g/mol

i.e. 1 mole of MADA = 306.14 g

M.W. of Mellitic Acid Trianhydride (MATA) = 288.03 g/mol

i.e. 1 mole of MATA = 288.03 g

Hence,

$$\% \text{ Weight Loss} = \frac{306.14 - 228.03}{306.14} \times 100 = 5.88\ \%$$

Gel formation was observed while synthesizing the pendent poly(amic acid). The mixing due to the magnetic stirring bar proved ineffective and the flask was then shaken vigorously by hand till the gel dissolved again in to the solution. TLCs taken at regular

intervals helped monitor the reaction of the Zr(adsp)(dsp) attaching to the polymer backbone. A brownish orange colored solution was obtained at the end of the reaction.

The poly(amic acid) solutions prepared above were then separated in to two parts: one portion was used for evaluating the processing conditions and the other portion was used for fabricating prepregs for the composite laminates. Precipitation using anhydrous ether in a blender was successfully carried out on all the three different poly(amic acid)s, and the powders obtained were used for establishing the optimum processing conditions.

3.2 Establishing Optimum Processing Conditions

3.2.1 Visible Color Changes

When the poly(amic acid) powders were heated, varying the time and temperature, a general observation regarding its color was noted. The intensity of the color increased as the time and temperature were increased. This observation is consistent with increasing conjugation along the chain due to the formation of imide rings as the reaction progresses, which is expected for the conversion of the amic acid to polyimide.

3.2.2 Fourier Transform Infrared Spectroscopy (FTIR)

Table 3.1 presents the characteristic IR bands generally used for polyimide quantification.

Table 3.1. Infrared Absorption Bands of Imides [19]

	Absorption Band (cm^{-1})	**Origin**
Aromatic Imides	1780	C=O sym. stretch
	1720	C=O asym. stretch
	1380	C-N stretch
	725	C=O bending
Amic acids	2900-3200	COOH and NH_2
	1710	C=O (COOH)
	1660 amide I	C=O (CONH)
	1550 amide II	C-NH
Anhydrides	1820	C=O sym. stretch
	1780	C=O asym. stretch
	720	C=O bending

The IR spectra of the 2-component, parent and pendent polyimide resins cured using different processing conditions are presented in Figures 3.3-3.5, respectively. The major characteristic imide ring bands for the pendent polymer occur at 1779 cm^{-1} (C=O asym. stretch), 1720 cm^{-1}(C=O sym. stretch), 1370 cm^{-1} (C-N imide stretch) and 725 cm^{-1} (C=O bend). It was difficult to identify the bands at 2930 cm^{-1} (imino C-H vibration) and 2860 cm^{-1} (amido N-H vibration), unique to the spectra of the zirconium pendent polyimides, because at 10 mol % pendent group concentration, it is difficult to resolve these peaks.

For the parent polymer, along with the imide peaks, an anhydride band at 1850 cm^{-1} was noted. This is due to the incorporation of MADA into the 2-component polymer structure to form the parent polymer. Anhydride rings are able to form at the MADA locations. To verify that each MADA residue had reacted with the Zr complex, the pendent polymer spectra were analyzed for peaks originating near 1850 cm^{-1} representing the anhydride group. These anhydride peaks were not observed for any processing condition of the pendent polymer indicating that the pendent groups had attached themselves at the MADA sites.

3.2.2.1 Degree of imidization

Several methods have been adopted to find the degree or extent of imidization in the neat polyimide resins. The bands that have been most widely used are imide absorption bands near 1780 cm^{-1} (C=O symmetric stretch), 1380 cm^{-1} (C-N stretch) and 725 cm^{-1} (C=O bend). As internal standards, the absorptions near 1500 cm^{-1} (aromatic stretch) [20], 1012 cm^{-1} (ether oxygen-to-aromatic ring stretching vibration) and 820 cm^{-1} (C-H vibrations) have been used to find the extent of imidization [19].

Navarre [19] suggested two methods to find the degree of imidization. The first one consisted of using an external reference sample defined by its absorption bands at 1770 cm^{-1} and 720 cm^{-1} as being a fully cured polyimide. The second method consisted of measuring for each sample the absorbance observed at 1720 cm^{-1}, due to the imide carbonyl vibration, and the absorbance at 820 cm^{-1} due to the C-H vibrations. By determining the increase in the ratios 1770 cm^{-1} / 820 cm^{-1} or 720 cm^{-1} / 820 cm^{-1}, the

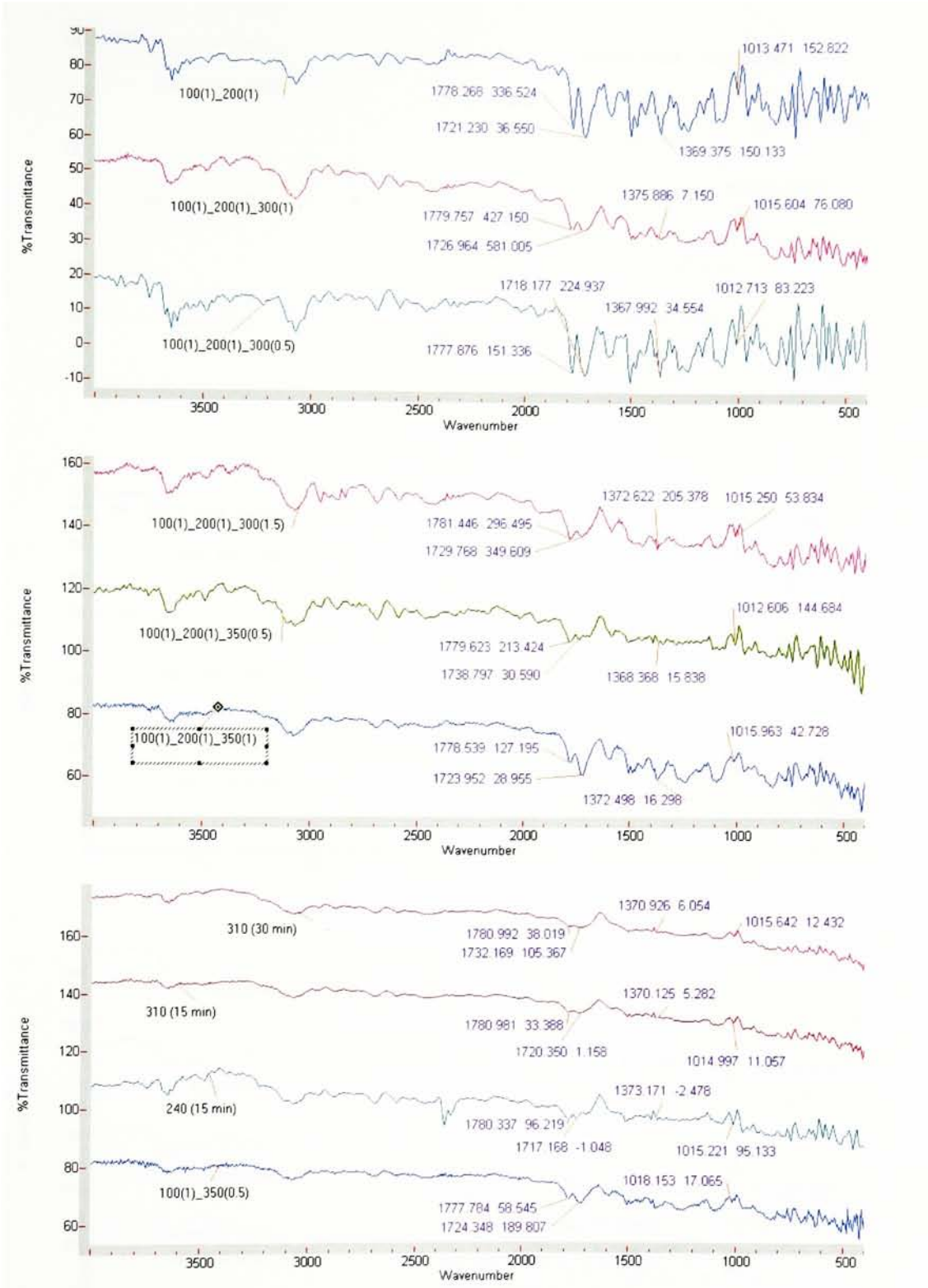

Figure 3.3. FTIR Spectra for 2-component polyimide

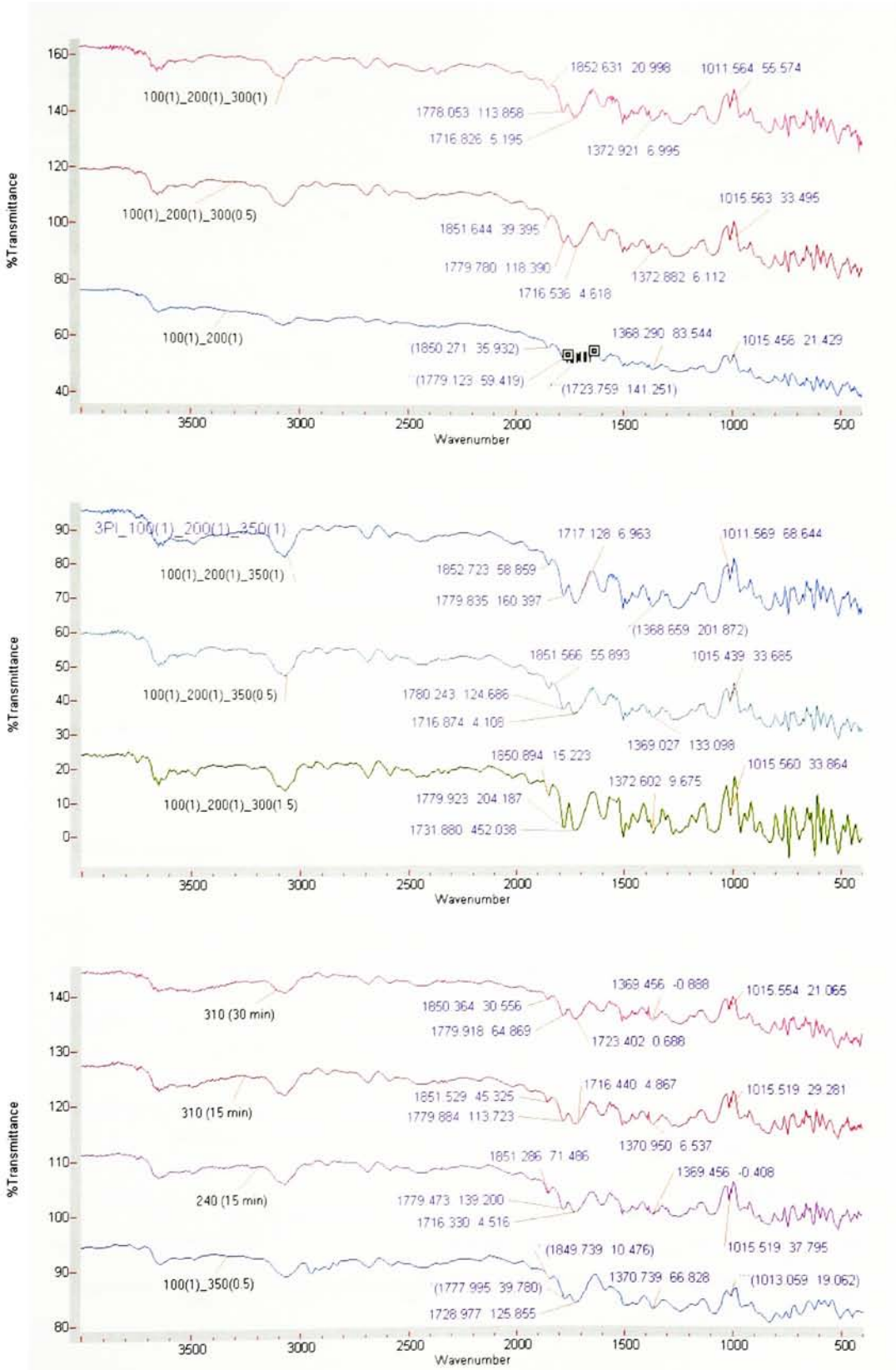

Figure 3.4. FTIR Spectra of parent polyimides

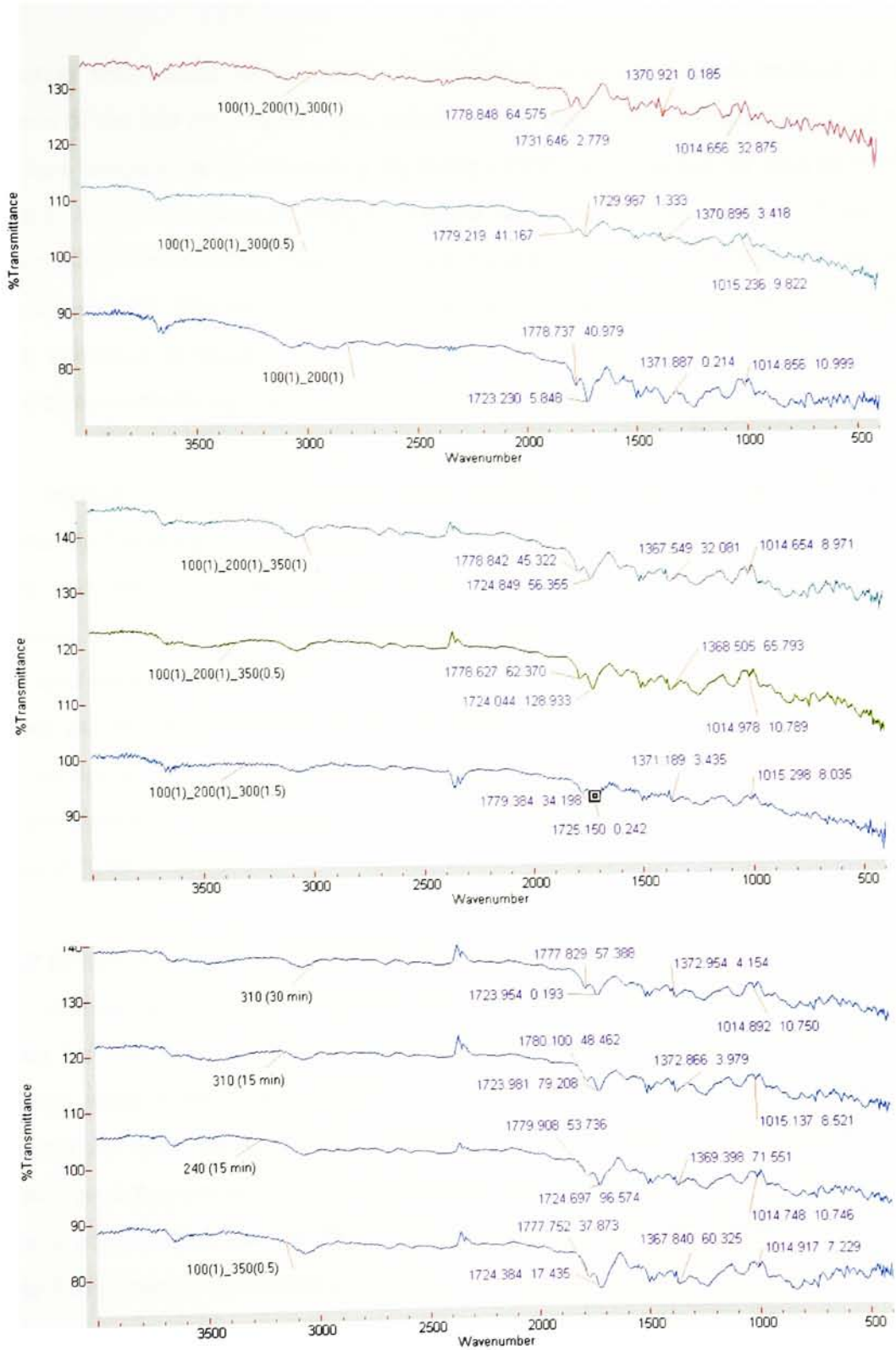

Figure 3.5. FTIR Spectra of pendent polyimides

imidization level could be evaluated. This method was less precise because of the weakness of the 820 cm^{-1} band. Pryde calculated the degree of imidization as a function of the cure temperature by comparing the imide / 1500 ratio obtained for each peak after heating to a given temperature with the highest ratio obtained for that peak in the cure sequence [20]. Ginsburg and Susko also analyzed poly(amic acid) / polyimide films by a band ratio method. The area of the symmetric carbonyl stretch at 1776 cm^{-1} was ratioed with a reference aromatic vibration at 1012 cm^{-1} and the percent imidization was calculated by normalizing the sample band ratio with that of a fully cured polyimide film [16].

Spectra for this research work were analyzed by a similar band ratio method followed by Ginsburg. Since the 1012 cm^{-1} peak was fairly isolated from the rest of the spectra and the area under the peak remained constant for the different processing conditions, this peak was chosen as an internal standard or reference peak. A band ratio of the area under the 1779 cm^{-1} (imide) peak to the area under the 1012 cm^{-1} peak was obtained and the degree of imidization was calculated as a ratio of the sample band ratio to the maximum band ratio obtained for that resin. The degree of imidization obtained for the 2-component, parent and pendent polyimide using different processing conditions can be seen in Tables 3.2 - 3.4.

3.2.2.2 Errors Associated with FTIR Analysis

A large scatter in the imidization data was however observed. One of the possible reasons for this scatter was due to the reference peak chosen. In most spectra, two reference peaks at 1012 cm^{-1} were observed: one due to the aromatic ether of the 3,4'-ODA and the other due to the aromatic ether of the 4,4'-ODPA, while in other spectra only one peak appears at 1012 cm^{-1}. The latter may have been due to the overlap of the aromatic ether peaks, leaving the instrument unable to separately analyze each peak. Figure 3.6 supports this reasoning.

Figure 3.6. Isolated reference peaks observed at 1012 cm^{-1} for the different polyimides

Attempts to analyze the spectra using other reference peaks at 1500 cm^{-1} and 820 cm^{-1} as mentioned earlier were eliminated. This was because the area under the 1500 cm^{-1} peak was not consistent with each spectra and the one at 820 cm^{-1} was reported as a weak band [19].

Table 3.2. % Degree of imidization for the 2-component polyimide resin

Processing Conditions	Area under 1779 cm^{-1}	Area under 1012 cm^{-1}	Band Ratio	% Degree of Imidization
100(1)_200(1)	336	152	2.20	39
100(1)_200(1)_300(0.5)	151	83	1.8	32
100(1)_200(1)_300(1)	427	76	5.6	100
100(1)_200(1)_300(1.5)	296	53	5.5	98
100(1)_200(1)_350(0.5)	213	144	1.47	26
100(1)_200(1)_350(1)	127	42	2.9	53
100(1)_350(0.5)	58	17	3.4	61
240(15 min)	96	95	1.0	18
310(15 min)	33	11	3.0	53
310(30 min)	38	12	3.0	54

Table 3.3. % Degree of imidization for the parent polyimide resin

Processing Conditions	Area under 1779 cm^{-1}	Area under 1012 cm^{-1}	Band Ratio	% Degree of Imidization
100(1)_200(1)	26	21	1.2	35
100(1)_200(1)_300(0.5)	86	33	2.5	75
100(1)_200(1)_300(1)	96	28	3.3	99
100(1)_200(1)_300(1.5)	109	32	3.4	100
100(1)_200(1)_350(0.5)	79	33	2.3	69
100(1)_200(1)_350(1)	112	35	3.1	93
100(1)_350(0.5)	37	25	1.4	44
240(15 min)	81	37	2.1	63
310(15 min)	76	29	2.6	77
310(30 min)	40	21	1.9	55

Table 3.4. % Degree of imidization for the pendent polyimide resin

Processing Conditions	Area under 1779 cm^{-1}	Area under 1012 cm^{-1}	Band Ratio	% Degree of Imidization
100(1)_200(1)	40	10	3.7	64
100(1)_200(1)_300(0.5)	41	9	4	70
100(1)_200(1)_300(1)	64	32	1.9	33
100(1)_200(1)_300(1.5)	34	8	4	70
100(1)_200(1)_350(0.5)	62	10	5.7	100
100(1)_200(1)_350(1)	45	8	5	90
100(1)_350(0.5)	37	7	5	90
240(15 min)	53	10	5.0	86
310(15 min)	48	8	5	100
310(30 min)	57	10	5.3	92

The observation also holds true for the 2- component and parent polyimides. This caused errors in calculating the area under the peak leading to the data scatter.

The method for spectra analysis was adopted from reference papers [15, 18] in which Kapton® was studied. Since this polyimide has only one aromatic ether linkage, only one peak can be observed at 1012 cm^{-1}. The research copolymer has two aromatic ether linkages but due to the errors shown in Figure 3.6, only one of the areas under the peak was accounted for. Since this copolymer and Kapton® have different chemical structures, the methods to determine the degree of imidization did not apply well for the polymers under study. Another possible reason may have been the sample preparation technique. It was difficult to obtain a finely grounded mixture of the KBr powder and the imidized polymer, affecting the dispersion within the sample.

3.2.3 Thermogravimetric Analysis (TGA)

TGA was performed on the imidized polymers using the processing conditions shown in Table 2.2. Figure 3.7 shows TGA curves for the poly(amic acid)s [unimidized polymer] for all three resins.

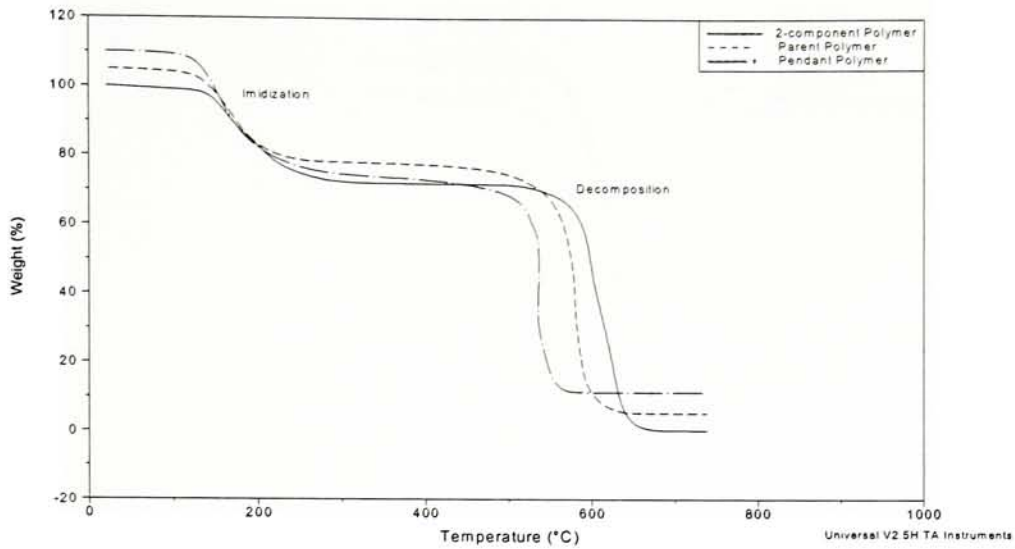

Figure 3.7. TGA curves of poly(amic acid)s of the three different resins

As seen, there are two typical weight loss events in the curves: one due to imidization of the poly(amic acid) occurring ~ 180 °C and one due to decomposition, the onset of which takes place ~ 500 °C. Figures 3.8-3.10 represent the TGA curves for the processed 2-component, parent and pendent polymers, respectively. These polymers were subjected to ten different processing conditions in the oven, and were then reheated in the TGA furnace at 10 °C / min up to 800 °C in air.

As seen from the TGA curves, incomplete imidization was observed for the three polymers when processed using conditions # 1 {100(1)_200(1)} and # 8 {240(15 min)}. A relatively flat plateau was observed near the imidization temperatures for all other conditions, indicating that imidization must have been complete using these conditions.

Decomposition in the novel polymer due to the processing conditions, if any, was estimated by calculating the theoretical weight (assuming 10 mol % Zr pendent groups) and comparing it with the actual weight used (obtained from the TGA graph). Calculation of the theoretical weight is based on the formation of ZrO_2, a white powder formed during the decomposition of the polymer. A sample calculation follows.

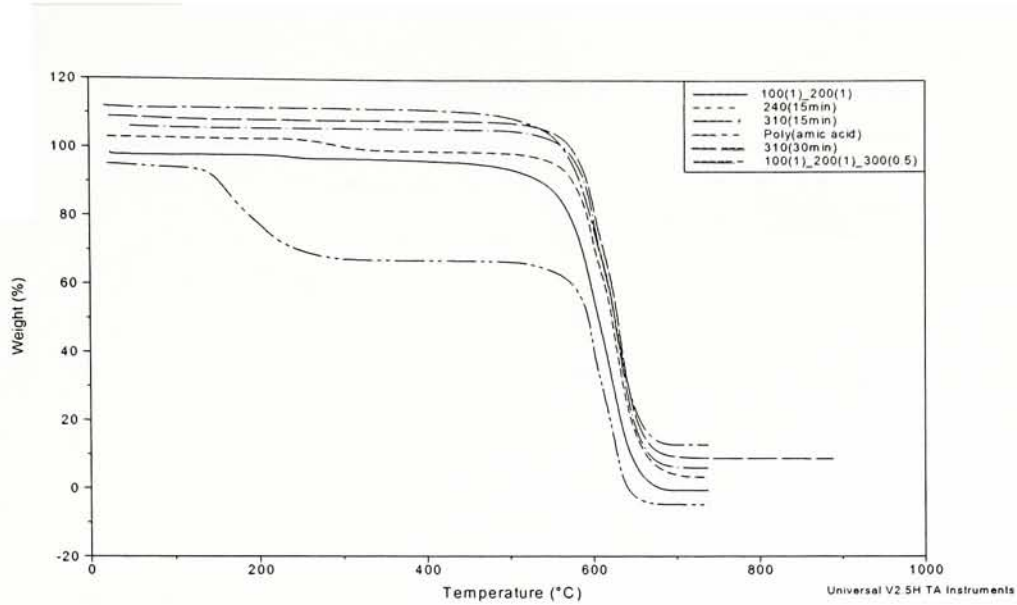

Figure 3.8a. TGA curves of 2-component polymer

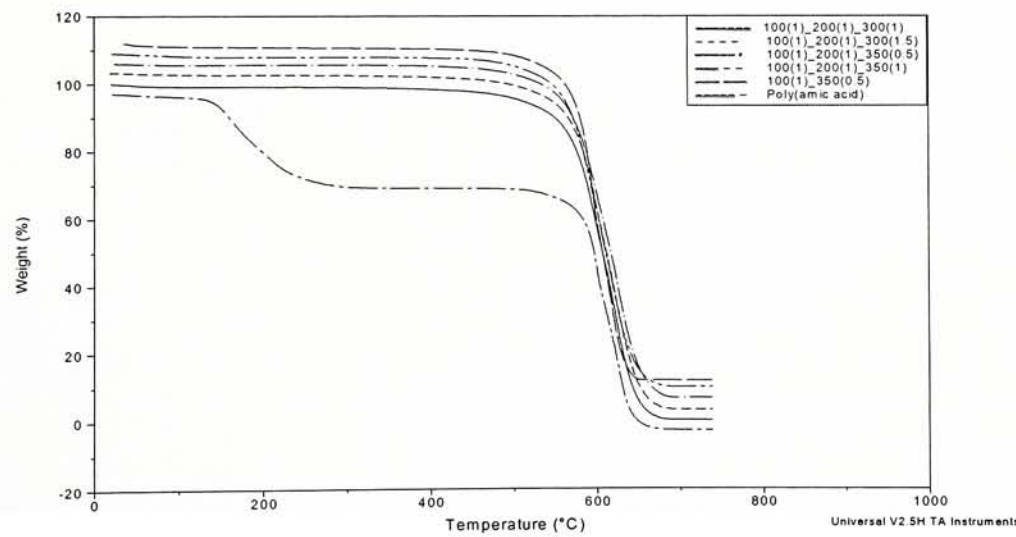

Figure 3.8b. TGA curves of 2-component polymer

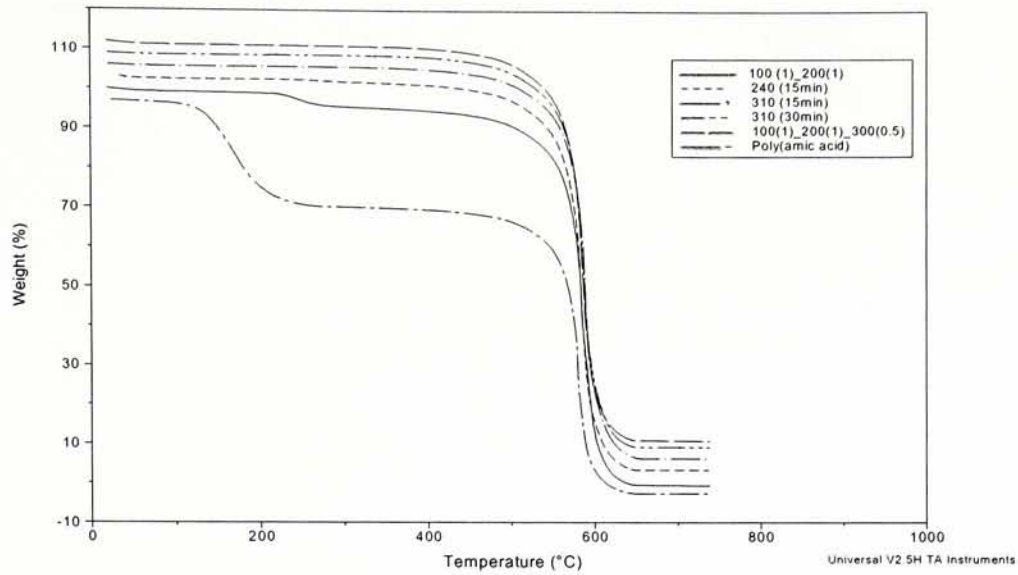

Figure 3.9a. TGA curves of the parent polymer

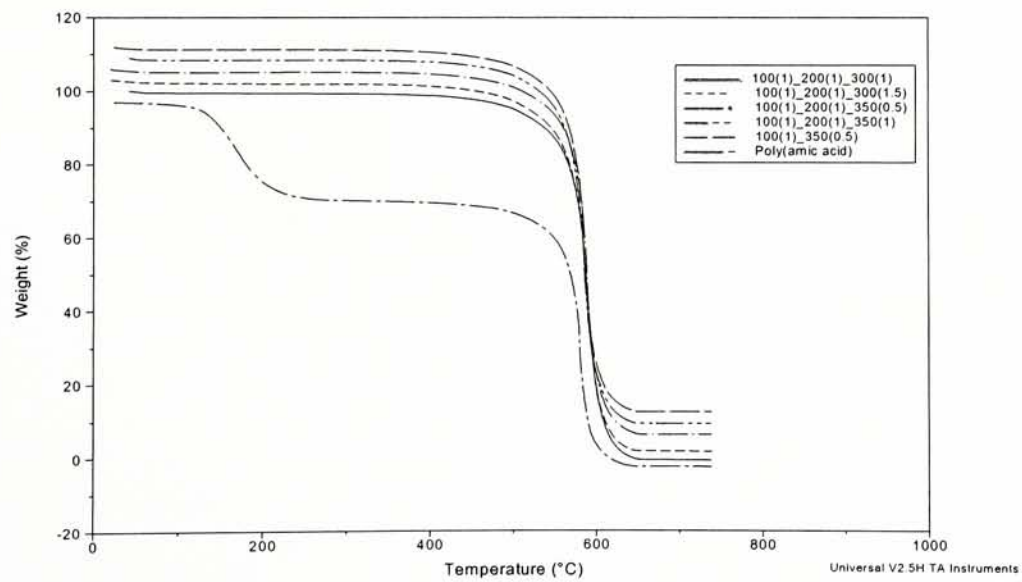

Figure 3.9b. TGA curves of the parent polymer

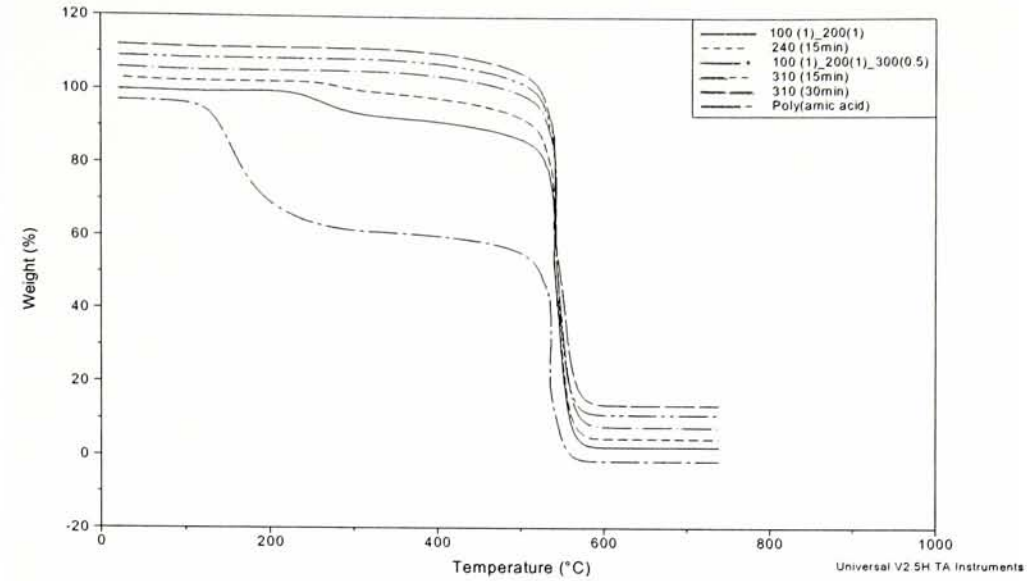

Figure 3.10a. TGA curves of the pendent polymer

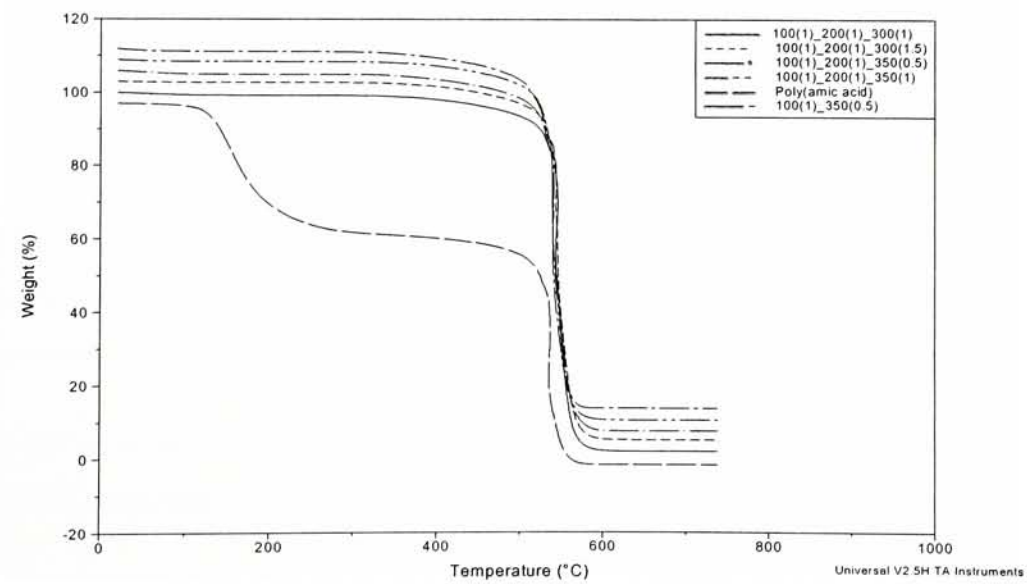

Figure 3.10b. TGA curves of the pendent polymer

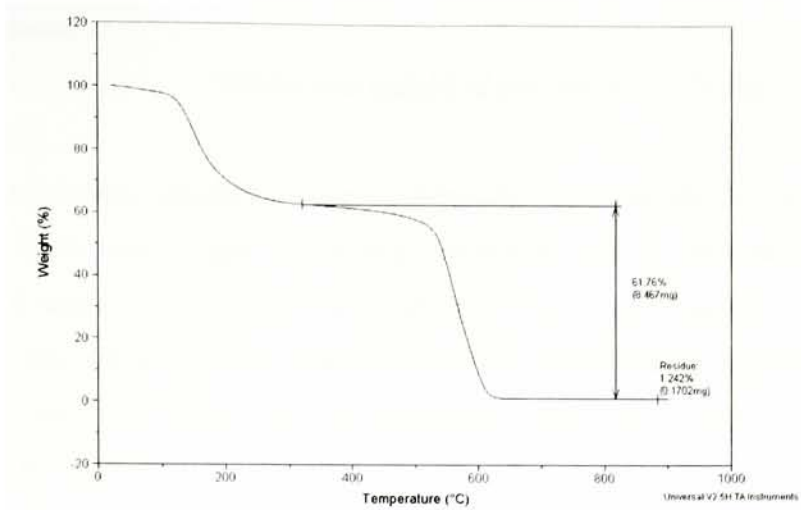

Figure 3.11. TGA graph of the pendent poly(amic acid)

The following problem was constructed to calculate the theoretical weight of the Zr pendent mer, and allow comparison to the actual weight used.

Equation:

$$\text{Theoretical Wt of PI} = \text{g } ZrO_2 \times \left(\frac{1 \text{ mole } ZrO_2}{123.2 \text{ g } ZrO_2}\right) \times \left(\frac{1 \text{ mole Zr pendent group}}{1 \text{ mole } ZrO_2}\right) \times \left(\frac{1 \text{ mole Zr pendent mer}}{1 \text{ mole Zr pendent grp}}\right) \times$$

$$\left[1 \times \left(\frac{1187.3 \text{ g}}{1 \text{ mole Zr}}\right) + 9 \times \left(\frac{474.4 \text{ g}}{1 \text{ mole non-pendent mer}}\right)\right] \quad \text{....Eqn. 3.1}$$

The equation assumes 10 mol % pendent groups, 90 mol % non-pendent groups, and reflects that 1 mole of $ZrO_2 \cong$ 1 mole of Zr pendent group $\cong$ 1 mole pendent mers (1187.3 g/mole)

Data: From Figure 3.11,

Actual Wt. of polyimide used = Wt. after imidization and solvent losses + Wt. of ZrO_2

$$= 8.467 + 0.1702 = 8.6372 \text{ mg}$$

Weight of ZrO_2 residue formed = 0.1702 mg

To find theoretical weight of polyimide:

Plug 0.1702 mg into Equation 3.1

By solving equation 3.1,

Theoretical weight of polyimide = 7.54 mg

Interpretation:

If decomposition occurs during processing, the actual weight of polyimide will be less than the theoretical weight (some mass would be lost as volatiles). Since actual weight (8.6372 mg) exceeds theoretical weight (7.54 mg), significant decomposition has not occurred. The differences in masses reflect the magnitude of experimental errors. Also, the large positive values would be expected if there were significant loss of ZrO_2 residue due to the airflow.

Table 3.5. Comparison of actual and theoretical weight using different processing conditions

Processing Condition	Imidization Temp. (°C)	Decomposition Temp. (°C)	Δ =Actual Wt – Theoretical Wt	Normalized[a] Δ (%)	Range of Error Bar
100(1)_200(1)	230.79	535.00	-0.8528	-6.50	-30.85 - 12.40
100(1)_200(1)_300(0.5)	--	540.84	2.6364	22.57	5.57 - 36.79
100(1)_200(1)_300(1)	--	535.09	1.2380	8.81	-11.36 - 25.45
100(1)_200(1)_300(1.5)	--	539.91	0.5216	4.86	-16.26 - 22.17
100(1)_200(1)_350(0.5)	--	537.59	3.3943	27.73	12.04 - 41.12
100(1)_200(1)_350(1)	--	537.11	3.5130	32.68	17.95 - 45.07
100(1)_350(0.5)	--	539.68	2.0488	20.07	2.51 - 34.74
240 (15 min)	256.13	537.33	3.3586	27.74	13.36 - 42.00
310 (15 min)	--	537.60	0.7127	6.69	-14.00 - 23.68
310 (30 min)	--	537.74	2.9770	24.63	8.09 - 38.47

[a] Normalized Δ (%) = [(Actual Wt – Theoretical Wt) / Initial Wt] x 100

As seen from Table 3.5, a negative value was indicated for processing condition # 1. This could be due to the ± 10 % error caused by machine analysis. Hence, a range had been calculated to check if the values obtained lied within this 10 % error bar. As indicated in the Table, all these values lied within the 10 % error range and that for decomposition to take place, values must lie outside this range. Thus, from this analysis, it was only possible to say that no decomposition took place or that the decomposition in the polymer was so small that the TGA was insensitive to it.

Molding cycles used for fabrication of the composite laminates were emulated in the TGA furnace to study the effects of decomposition taking place in the polymer, if any. As seen from Figure 3.12, there is a negligible decomposition of all three polymers when held at 370 °C for an hour in nitrogen atmosphere.

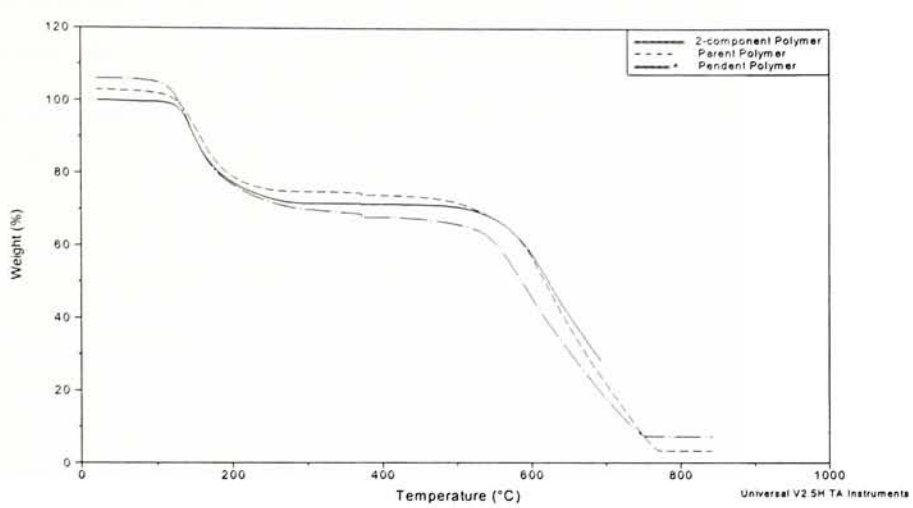

Figure 3.12. Emulation of molding cycles for the neat polymer resins. TGA of 2-, 3- and 4-component polyimides after heating at 370 °C for 1 hour under N_2 gas

The negligible decomposition could also be verified for the pendent polyimide using the method based on the formation of ZrO_2 as described in section 2.4.2. A positive delta value obtained by comparing the actual weight to its theoretical weight indicated that no decomposition took place in the polymer. The weight losses for the three polymers when held at 370 °C for an hour are shown in Table 3.6.

Table 3.6. Weight loss (%) of the three resins held at 370 °C for one hour

Resin	% Weight Loss
2-component	0.1 %
3-component	0.6 %
4-component	0.8 %

Limitations of TGA Analysis

The method of finding the decomposition in the polymer works only for the pendent polymer due to the formation of the ZrO_2 powder. Also, since the data values having $\Delta > 0$ described in Table 3.5 are attributed to the loss of ZrO_2 due to the airflow, there was always a certain degree of error associated with the data analysis using this technique. It was difficult to find the extent of decomposition for the 2-component and parent polyimides. Since the 2-component and parent polymers do not contain the Zr-pendent group, this method was not applicable. Also, since previously imidized polymers were used in the TGA, there was no reference polymer to compare the amount of decomposition taking place in the sample. Whereas imide peaks (FTIR) all appeared the same after processing using different conditions (see Figures 3.3-3.5), at least TGA showed some imidization weight loss for certain processing conditions (see Figures 3.8-3.10)

3.2.4 Differential Scanning Calorimetry (DSC)

This technique was used to study the effect of the different processing conditions on the glass transition temperatures of the polymer. Figure 3.13 shows the glass transition temperatures obtained during the first and second heating cycles for the 2-component polyimide.

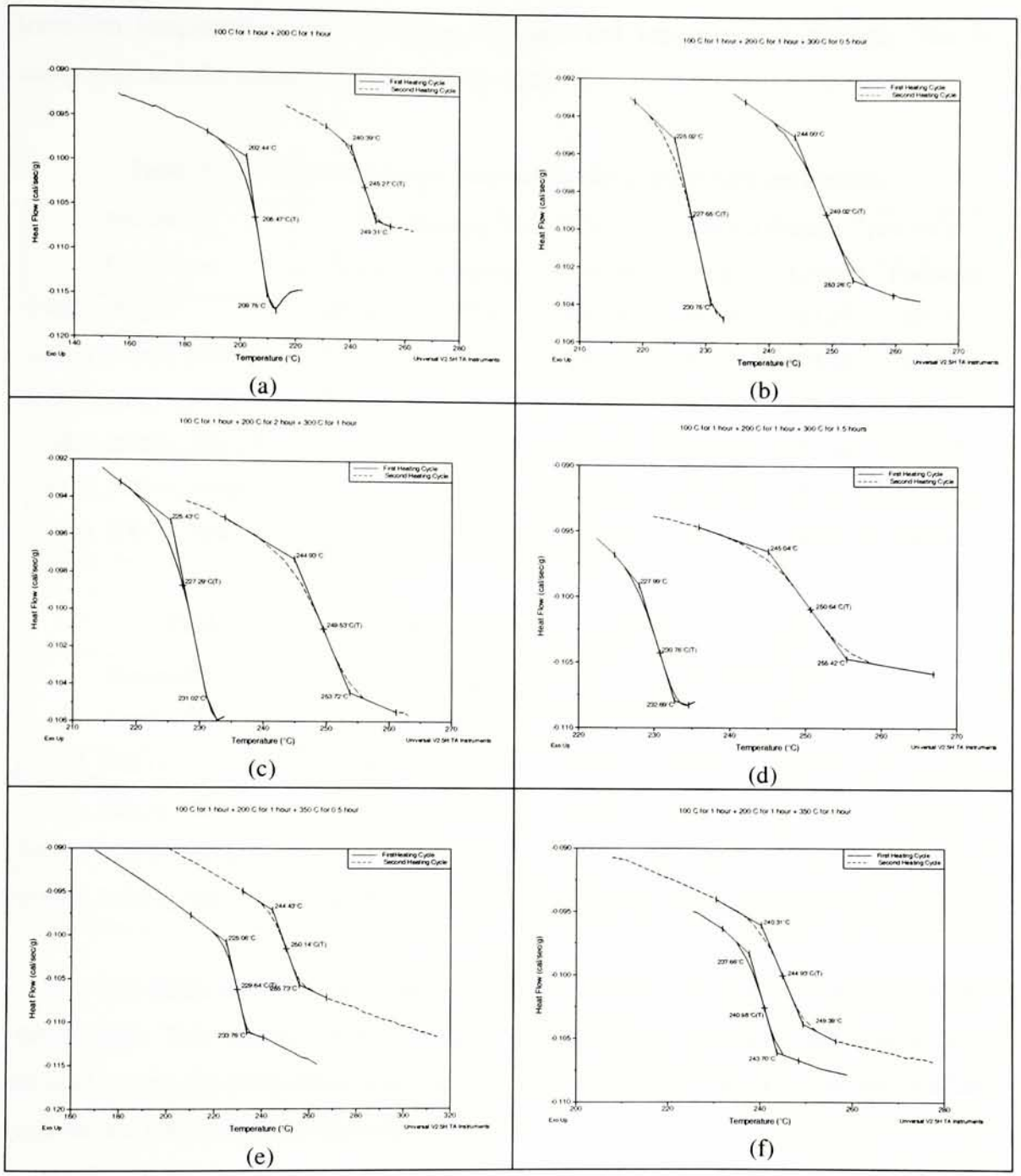

Figure 3.13 (a-f). DSC curves for the 2-component polyimide resin

The effect of the processing conditions on the glass transitions temperatures is shown in Tables 3.7 a and b. The onset of the second heating cycle was chosen as the T_g for the polymer. It could be seen that there was not a significant change in the glass

transition temperatures upon changing the time and temperature conditions. The 2-component and the parent polymers had $T_g \sim 242$ °C.

Table 3.7a. Glass transitions observed in the 2-component polyimides

Processing Conditions	First Heating Cycle (°C)			Second Heating Cycle (°C)		
	Onset	Midpoint	Endpoint	Onset	Midpoint	Endpoint
100(1)_200(1)	202.44	205.47	209.75	240.39	245.27	249.31
100(1)_200(1)_300(0.5)	225.02	227.65	230.75	244.00	249.02	253.26
100(1)_200(1)_300(1)	225.43	227.29	231.02	244.93	249.53	253.72
100(1)_200(1)_300(1.5)	227.99	230.76	232.69	245.04	250.64	255.42
100(1)_200(1)_350(0.5)	225.06	229.64	233.76	244.43	250.14	255.73
100(1)_200(1)_350(1)	237.66	240.98	243.70	240.31	244.93	249.39

Table 3.7b. Glass transitions observed in the parent polyimides

Processing Conditions	First Heating Cycle (°C)			Second Heating Cycle (°C)		
	Onset	Midpoint	Endpoint	Onset	Midpoint	Endpoint
100(1)_200(1)	202.44	205.47	209.75	240.39	245.27	249.31
100(1)_200(1)_300(0.5)	225.02	227.65	230.75	244.00	249.02	253.26
100(1)_200(1)_300(1)	225.43	227.29	231.02	244.93	249.53	253.72
100(1)_200(1)_300(1.5)	227.99	230.76	232.69	245.04	250.64	255.42

The entire set of the ten processing conditions could not be evaluated for all the three resins. This was due to the escape of volatiles from the hermetically sealed pans, formed during the imidization reaction. This caused discoloration of the furnace surface and further DSC runs were discontinued.

3.2.5 Summary: Determination of Optimum Processing Condition& Molding Cycle

In choosing the optimum processing conditions for the pendent polymer, samples indicating incomplete imidization (condition # 1 and # 8) or those showing decomposition (no conditions) were eliminated. Based on the above data, the processing condition of heating the poly(amic acid) at 310 °C for 15 minutes could be chosen as an

optimum processing condition. The sample showed complete imidization without any decomposition at the given processing temperature in the shortest amount of time. This was verified by the absence of the imidization step in the TGA and also by the absence of any anhydride peak at 1850 cm^{-1}, indicating attachment of pendent groups which prevent formation of anhydride groups at the MADA locations. The remaining conditions could also be potential processing conditions except that by eliminating the extended heating steps seen in the other conditions, it is possible to save time and hence, energy.

For fabricating composite laminates, 370 °C was chosen as the molding temperature. Since our primary reason of retaining additional solvent in the prepreg was to effect a plasticizing action on the polymer resin during fabrication thereby increasing melt flow, this would facilitate a faster reaction and hence, consolidation will be more effective at higher temperatures. The long holding time of an hour at 370 °C was essential to ensure the removal of the solvent and to obtain well-consolidated laminates. NASA scientists also used similar molding temperatures [21-25] to fabricate composite laminates. In addition, this choice seems justified because the processing conditions which employed 350 °C gave no indication of > 10 % decomposition (Table 3.5) and none of the polymers showed significant weight loss after one hour at 370 °C under N_2 gas using TGA (Table 3.6).

3.3 Composite Fabrication and Processing

3.3.1 Fabrication of Prepregs

The prepregs were made using the technique described in Section 2.4.1. To achieve a 60:40 fiber to resin ratio by weight after autoclave consolidation of the laminate, the prepregs were fabricated such that they had a resin content ~ 51 % by weight instead of the desired 40%. This calculation/argument was discussed in section 2.5.1.

3.3.2 Fabrication of Composite Laminates

The technique used most often in the fabrication of composites is the autoclave processing. Laminates were fabricated in an autoclave at the Center for Composite Materials (C.C.M.), University of Delaware. As the 2-component polyimide closely

resembles NASA's LARC-IA polyimide, their recommended pressure of 1.72 MPa (250 psi) as reported by Hou, Johnston et al [21] was used to obtain well-consolidated laminates. The molding cycle consisted of heating the prepregs directly from room temperature up to 700 °F (370 °C) at a heating rate of 5 °F/min followed by a soak time for an hour at that temperature. Pressure was applied at the beginning of the cycle along with the vacuum. This was done because it was difficult to reach this high pressure before reaching the desired processing temperature. Figure 3.14 represents the molding cycle.

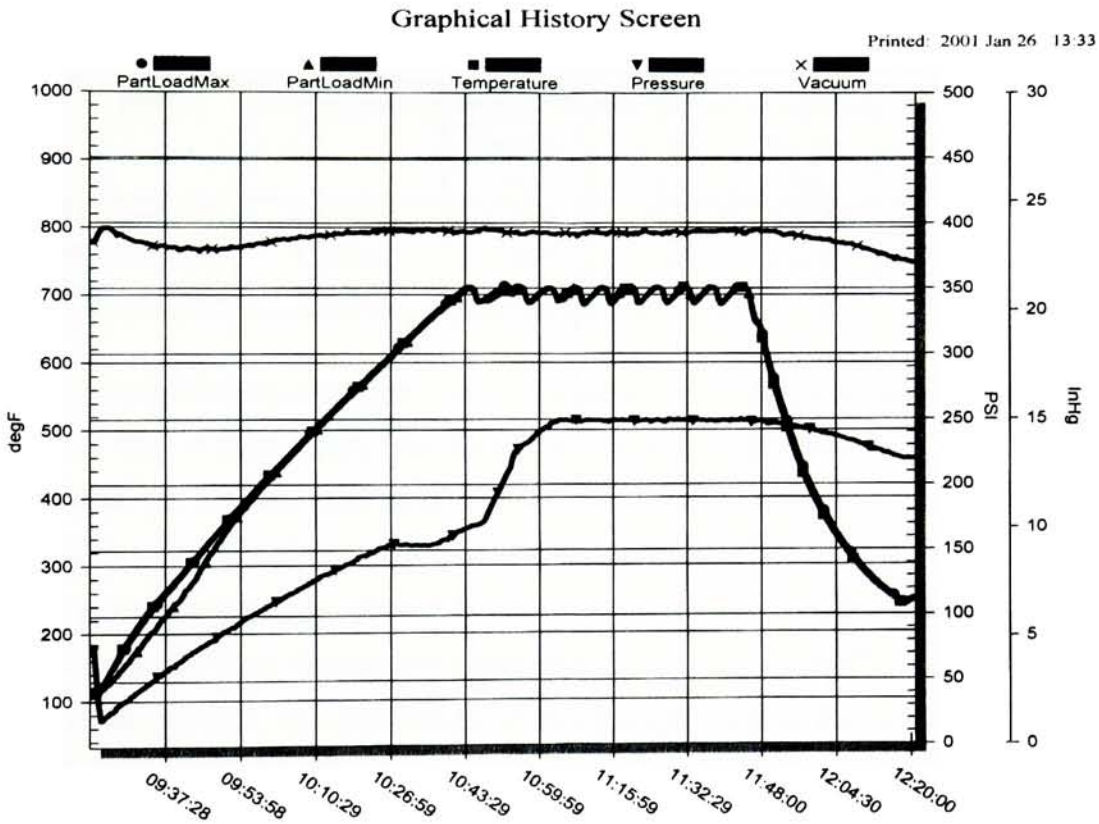

Figure 3.14. Molding Cycle for composite laminate fabrication

3.3.3 Resin Content of Fabricated Laminates

Two methods were adopted to estimate the resin content in the laminates. In the first method, the resin burn-off technique, tests were conducted on a 1cm x 1cm sample according to ASTM 2584-94. Table 3.8 reflects the values obtained.

Table 3.8. Resin content of composite laminates using Method I

Single Ply Lamina

Resin	Reinforcement	Weight of Sample (g)	Weight of Fiber (g)	Weight of Resin (g)	Resin Content (%)
2-component	Carbon	0.109	0.050	0.060	54.63
3-component	Carbon	0.134	0.063	0.070	52.73
4-component	Carbon	0.136	0.069	0.068	49.71
4-component	Glass	0.180	0.101	0.079	43.85

Four Ply Laminates

Resin	Reinforcement	Weight of Sample (g)	Weight of Fiber (g)	Weight of Resin (g)	Resin Content (%)
2-component	Carbon	0.415	0.219	0.196	47.26
3-component	Carbon	0.144	0.091	0.053	37.01
4-component	Carbon	0.112	0.074	0.038	34.08

As seen from the table, the four ply laminates have shown a closer proximity to our desired fiber to resin weight ratio with values ranging from 34-47 % by weight of the resin. Single ply laminas reinforced with carbon fibers however show a higher resin content than expected. This could be because the Kapton® film used in the vacuum bagging process may have adhered to the single plies accounting for the additional superficial weight. Even though polyimide resins, including Kapton®, decompose upon heating in the furnace, the contribution of this Kapton® film to the initial weight may have led to the higher values. Since all plies were fabricated in a single batch using identical conditions in the autoclave, the resin content of the single plies could be also approximated to be in the vicinity of 40 % by weight. The glass reinforced lamina showed a resin content of ~ 44 % by weight.

In our second method, individual sheets of the 2-, 3- and 4-component laminates were weighed after the autoclave fabrication and the resin content values were calculated by subtracting the estimated weight due to the woven fabric. Single ply lamina were obtained from a 7" x 4" sheet while for making four ply laminates, a 7" x 2.75" sheet was used. Values are shown in Table 3.9.

As seen from the Tables, this method did not work well due to the low resin content values obtained when compared with those obtained using Method I. This may be because the resin was not applied to the edges of the laminates to the same extent as elsewhere, rendering this technique not useful to make any estimation regarding the resin content.

Table 3.9. Resin content of composite laminates using Method II

Sheet Dimension: 7" x 4" (Used for single ply)

	Resin	Reinforcement	Weight of fiber (g)	Weight of composite (g)	Resin Content (%)
Sheet 1	2-component	Carbon	6.84	7.66	10.70
Sheet 2	2-component	Carbon	7.08	7.80	9.23
Sheet 3	2-component	Carbon	6.66	7.78	14.39
Sheet 1	Parent	Carbon	6.56	7.76	15.46
Sheet 2	Parent	Carbon	6.79	7.58	10.42
Sheet 1	Pendent	Carbon	7.64	7.76	1.54
Sheet 1	Pendent	Glass	14.51	16.42	11.63

Sheet Dimension: 7" x 10" (Used for four plies)

	Resin	Reinforcement	Weight of fiber (g)	Weight of composite (g)	Resin Content (%)
Sheet 1	2-component	Carbon	14.98	17.46	14.20
Sheet 2	2-component	Carbon	15.16	17.71	14.39
Sheet 3	2-component	Carbon	14.72	17.91	17.81
Sheet 1	Parent	Carbon	15.54	18.12	14.23
Sheet 2	Parent	Carbon	15.92	18.77	15.18
Sheet 1	Pendent	Carbon	14.61	18.34	20.33

3.3.4. Machining of Composite Laminates

The laminates were cut to the required specimen dimensions using a laser machine at Die Max of Rochester. While cutting the samples, it was observed that the edges of the laminate were burnt due to the heat generated from the laser. A larger

edges. The external burnt edges were then sanded with a sand paper (Grade 320) to within the tolerances specified by ASTM numbers 3039, 256, 790 and 4065.

3.4 Mechanical Properties of Laminates

The mechanical properties were determined in accordance with ASTM standards. The tests included tensile, three-point flexure, Izod impact and dynamic mechanical analysis (DMA). Comparisons of mechanical properties have been made with similar laminates processed using a different molding cycle [26] and the results of each test are discussed below.

3.4.1 Tensile Test (ASTM D3039/D3039M-95a)

The tensile test was performed on single ply lamina for the carbon and glass reinforced composites. Tables 3.10-3.13 reflect the test values obtained. It was observed that the tensile modulus for the carbon fiber reinforced 2-component and 3-component parent polyimide laminas were similar. Values ranged from 20.3 GPa to 21.4 GPa. A small decrease in the modulus (~ 18.7 GPa) was observed for the Zr-pendent polyimide. The strain at break values for all the three lamina systems were low (~ 1.4 %) and comparable with each other. Glass fiber reinforced composites of the pendent polymer showed a tensile modulus ~ 6.6 GPa, i.e., lower than for carbon, which is as expected since glass fiber itself has a lower modulus than carbon fibers.

The tensile strength however varied from resin to resin. The carbon reinforced parent polyimide showed the highest tensile strength of 300 $\pm$ 16 MPa relative to the other resins, followed by the 2-component polyimide lamina which had a tensile strength of 253 $\pm$ 63 MPa. The pendent polyimide lamina showed the lowest tensile strength of 224 $\pm$ 16 MPa. The pendent glass reinforced lamina had tensile strengths up to 100 MPa.

The principal advantage of using woven fabric laminates is that they provide properties that are more balanced in the 0° and 90° directions than unidirectional laminates. However, the tensile strength and modulus of a woven fabric laminate are, in general, lower than those of non-woven laminates. This is due to the presence of fiber undulation in woven fabrics, as the fiber yarns in the fill direction (along the fabric width)

Table 3.10. Tensile test for 2-component carbon fiber reinforced composite

Sample # 1

Specimen #	Thickness (mm)	Width (mm)	Peak Load (N)	Strain At Break (%)	Tensile Strength (MPa)	Tensile Modulus (GPa)
1	0.365	14.8	1225	1.34	226	19.7
2	0.357	14.9	1520	1.46	285	20.5
3	0.356	14.8	1336	1.39	253	20.5
Average	0.359	14.8	1361	1.40	254	20.2
Std. Dev.	0.005	0.047	149.0	0.062	29.6	0.510

Sample # 2

Specimen #	Thickness (mm)	Width (mm)	Peak Load (N)	Strain At Break (%)	Tensile Strength (MPa)	Tensile Modulus (GPa)
1	0.352	14.3	1147	1.48	227	19.2
2	0.343	14.3	1254	1.48	255	19.0
3	0.352	14.2	1152	1.30	229	18.9
Average	0.349	14.3	1184	1.42	237	19.1
Std. Dev.	0.005	0.038	60.28	0.104	15.4	0.184

Sample # 3

Specimen #	Thickness (mm)	Width (mm)	Peak Load (N)	Strain At Break (%)	Tensile Strength (MPa)	Tensile Modulus (GPa)
1	0.384	13.8	1194	1.17	224	20.5
2	0.351	13.8	1263	1.35	259	21.8
3	0.338	13.8	1480	1.42	316	22.4
Average	0.358	13.8	1312	1.31	266	21.6
Std. Dev.	0.024	0.020	149.5	0.130	46.4	0.968

Combined Average	253	20.3
Std. Deviation	14.6	1.25

Table 3.11. Tensile test for 3-component carbon fiber reinforced composite

Sample # 1

Specimen #	Thickness (mm)	Width (mm)	Peak Load (N)	Strain At Break (%)	Tensile Strength (MPa)	Tensile Modulus (GPa)
1	0.359	13.8	1492	1.41	301	21.6
2	0.363	13.8	1664	1.51	331	20.9
3	0.359	13.8	1480	1.42	298	20.7
Average	0.360	13.8	1545	1.45	310	21.1
Std. Dev.	0.002	0.020	102.7	0.060	18.1	0.470

Sample # 2

Specimen #	Thickness (mm)	Width (mm)	Peak Load (N)	Strain At Break (%)	Tensile Strength (MPa)	Tensile Modulus (GPa)
1	0.362	13.7	1426	1.39	285	20.2
2	0.365	13.7	1352	1.49	269	21.7
3	0.362	13.7	1577	1.38	316	23.0
Average	0.363	13.7	1452	1.42	290	21.6
Std. Dev.	0.002	0.008	114.4	0.059	23.8	1.41

Combined Average	300	21.4
Std. Deviation	14.0	0.390

Table 3.12. Tensile test for 4-component carbon fiber reinforced composite

Specimen #	Thickness (mm)	Width (mm)	Peak Load (N)	Strain At Break (%)	Tensile Strength (MPa)	Tensile Modulus (GPa)
1	0.356	13.7	1175	1.30	239	17.7
2	0.351	13.7	975	1.25	201	18.5
3	0.346	13.7	1114	1.45	233	19.8
Average	0.351	13.7	1088	1.35	224	18.7
Std. Dev.	0.005	0.001	102.3	0.101	20.3	1.07

Table 3.13. Tensile test for 4-component glass fiber reinforced composite

Specimen #	Thickness (mm)	Width (mm)	Peak Load (N)	Strain At Break (%)	Tensile Strength (MPa)	Tensile Modulus (GPa)
1	0.529	13.7	717	1.66	98.5	6.5
2	0.548	13.7	857	1.92	113	6.9
3	0.564	13.7	673	1.72	86.7	6.4
Average	0.547	13.7	749	1.77	99.6	6.6
Std. Dev.	0.018	0.012	96.2	0.136	13.5	0.24

cross over and under the fiber yarns in the warp direction (along the fabric length) to create an interlocked structure. Under tensile loading, these crimped fibers tend to straighten out, which creates high stresses in the matrix. As a result, micro cracks are formed in the matrix at relatively light loads.

Alignment of the specimen axis with respect to the fiber direction is an important issue in the machining of composites. Hartsmith observed that specimens cut with only 1° of misalignment could cause as much as 30 % decrease in strength [13]. The tensile specimen seemed to be slightly disoriented compared to the direction of the test. Due to this, the following observations and effects were noted:

1) The fibers were being twisted, as if trying to straighten out in the direction of the pull. This could have led to some amount of shear between the fibers and the specimen would not have failed due to a pure tensile pull, but due to a combined tensile and shear stress.

2) Due to the slight disorientation, the fibers at the edges, which were not embedded in the end tab, were being pulled out. This may have initiated the failure mechanism in some cases.

3) Most of the samples failed near the center of the gage length while some of them failed off-center within 1" from the center.

Comparison of tensile strength and moduli of the single ply laminas were made in Figures 3.15 and 3.16. Stress-strain curves were plotted for the carbon and glass fiber reinforced laminas in Figures 3.17-3.20.

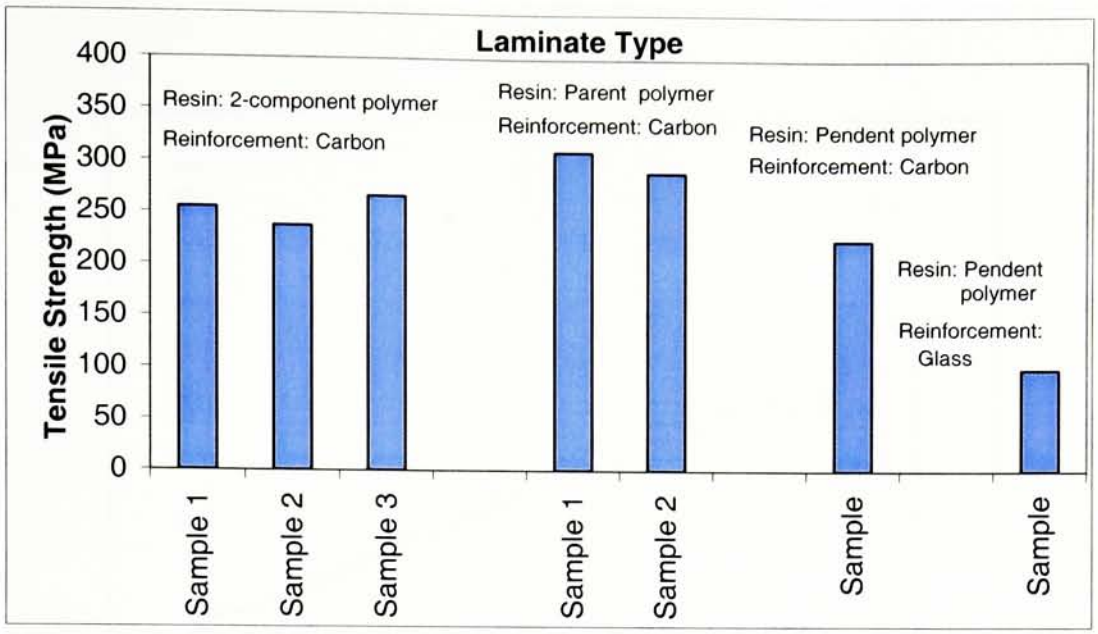

Figure 3.15. Comparison of tensile strength of laminas

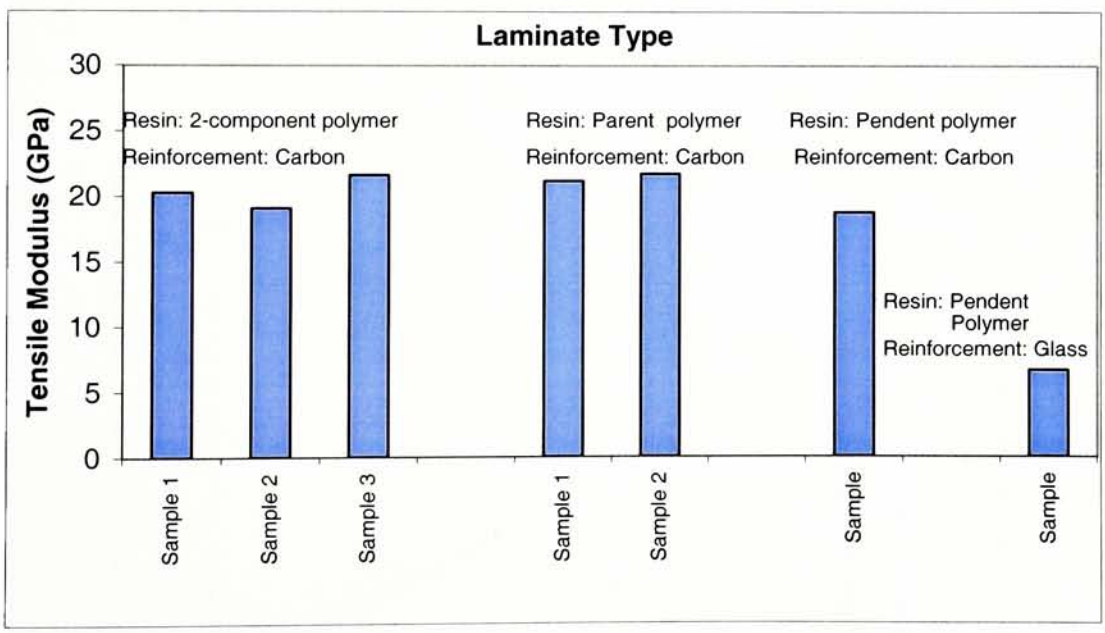

Figure 3.16. Comparison of tensile modulus of laminas

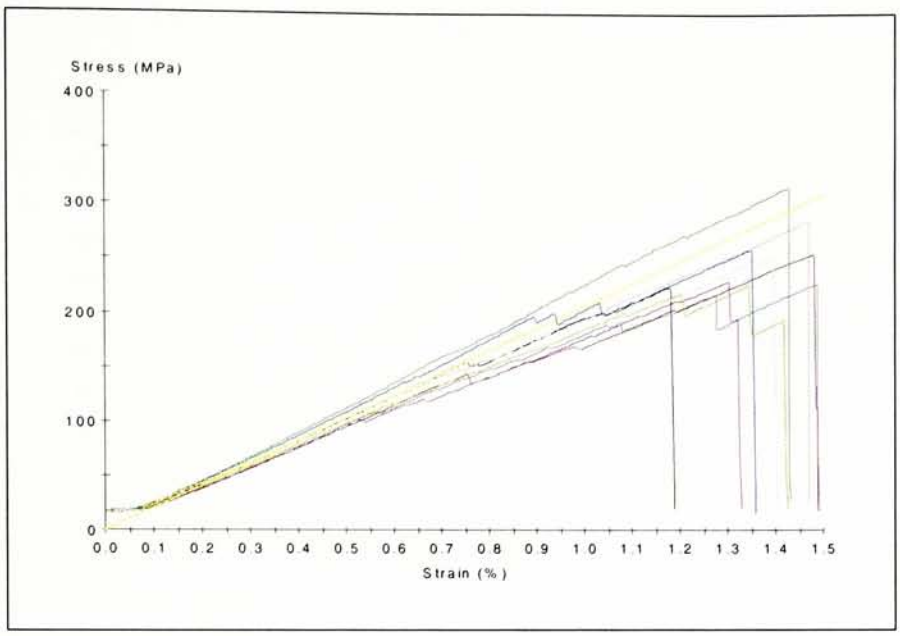

Figure 3.17. Stress-Strain curves for 2-component carbon reinforced tensile lamina

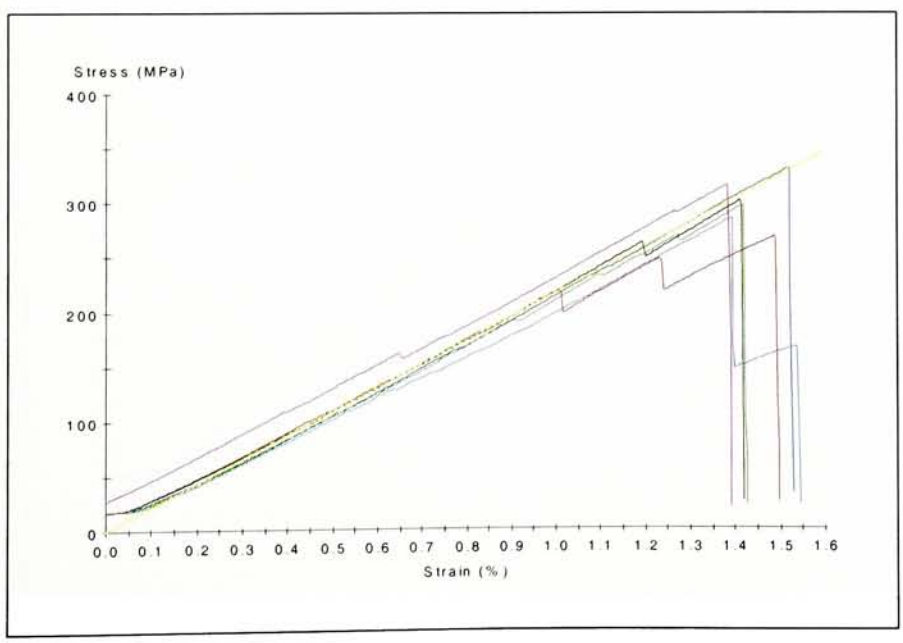

Figure 3.18. Stress-Strain curves for 3-component carbon reinforced tensile lamina

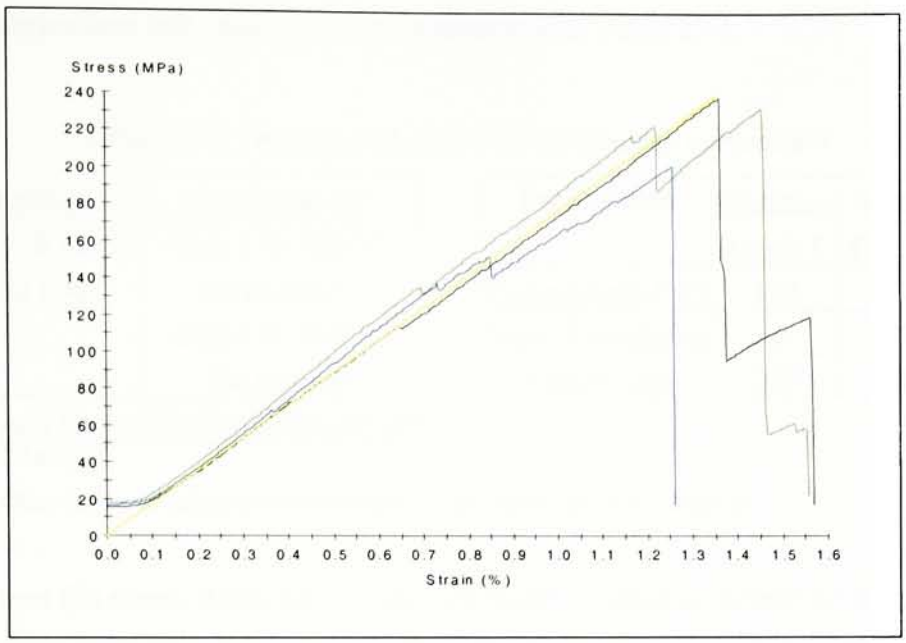

Figure 3.19. Stress-Strain curves for 4-component carbon reinforced tensile lamina

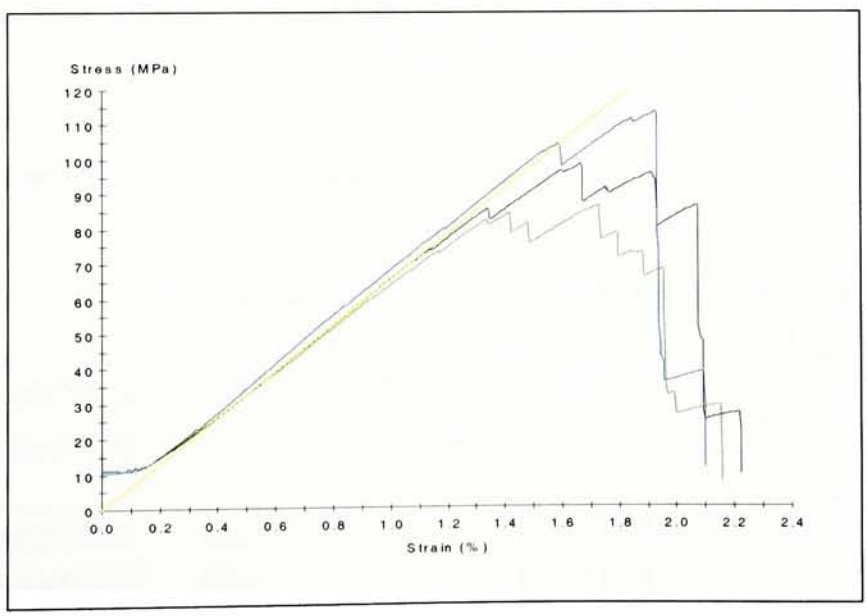

Figure 3.20. Stress-Strain curves for 4-component glass reinforced tensile lamina

A comparison of the above tensile properties with the ones using a different molding cycle [26] was made. A brief distinction between the parameters used for these prepreg fabrications and molding cycles is described in Table 3.14.

Table 3.14. Prepreg and autoclave fabrication parameters

Condition I	**Condition II** [a]
Step I → 65 °C for an hour [b] --	Step I → 100 °C for an hour [b] Step I → 160 °C for an hour
Vacuum Oven	Air-Circulating Oven

[a]: Ref [26]

Parameters	**Molding Cycle I**	**Molding Cycle II** [a]
Temperature (°C)	370	300
Soak Time (min)	60	60
Pressure (psi)	250	250

[b]: Step repeated till desired 60:40 fiber to resin by weight ratio achieved.

From the stress-strain curves, the first failures (strain at break) for the 2-, 3- and 4-component worst specimens are 0.55 %, 0.65 %, 0.66 % and 1.15 % respectively. The 4-component on glass value is higher because the carbon fabric is more brittle than the glass.

Table 3.15a – 3.15b represents a comparison of the tensile properties for the two molding cycles.

Table 3.15a. Comparison of tensile strength and moduli of 2- and 3-component composite laminates from different molding cycles

	Reinforcement	2-component system		3-component system	
		I	II [a]	I	II [a]
Tensile Strength (MPa)	Carbon	253 ± 63	483 ± 64	300 ± 15	413 ± 83
Tensile Modulus (GPa)	Carbon	20 ± 2	27 ± 4	21 ± 1	23 ± 2
Tensile Strength (MPa)	Glass	-	159 ± 55	-	267 ± 46
Tensile Modulus (GPa)	Glass	-	11 ± 1	-	9 ± 3

[a]: Ref [26]

Table 3.15b. Comparison of tensile strength and moduli of 4-component composite laminates from different molding cycles

	Reinforcement	4-component system	
		I	II [a]
Tensile Strength (MPa)	Carbon	224 ± 14	259[b] ± 10
Tensile Modulus (GPa)	Carbon	18 ± 1	11[b] ± 1
Tensile Strength (MPa)	Glass	99 ± 14	79[b] ± 14
Tensile Modulus (GPa)	Glass	6 ± 0	16[b] ± 1

[a] : Ref [26]

[b] : Corrected values, Ref [26]

From the above Tables, it was seen that the tensile properties obtained by using molding cycle I are lower than the ones using molding cycle II. Reasons for this may be due to the disparity in processing temperatures and also in the technique used for prepreg fabrication. A primary reason may be due to the processing temperatures used for the two molding cycles. This led to differences in the color observed for the laminates. Molding cycle I laminates were black while brown laminates were seen for molding cycle II. The darker color for the former laminates could be due to extensive imidization. Another reason may have been due to the differences in prepreg fabrication. As a lower temperature was used in Condition I for the prepregs, it was more likely to retain the solvent. Kreuz et al reported that the imidization process is enhanced by the presence of solvent [10]. Hence, this could be justified by the darker color observed for these conditions.

Optical and SEM images of the failed tensile test specimen of the carbon and glass fiber laminates were recorded in Figures 3.21-3.25. As seen from the images, samples mainly failed due to fiber breakage. Since the woven fabrics were made by interlacing two yarn systems orthogonal to each other, a misalignment in the orthogonality due to the tensile stretching was observed. Resin adhered to the fibers indicating no debonding taking place. However, resin rich areas were seen for the 4-component lamina. This could indicate a poor resin flow and thus affect the wettability. Since the tensile specimens were singly-ply laminas, failure due to delamination was not considered.

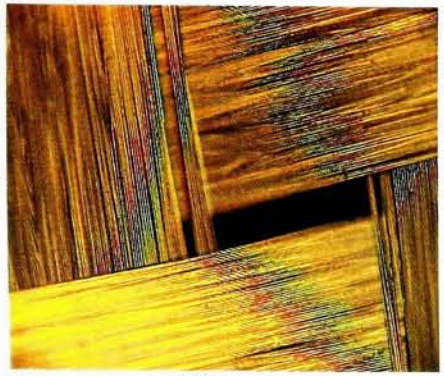

(a)

Magnification: 100x
Observation: Pure Carbon Woven Fabric

AFTER

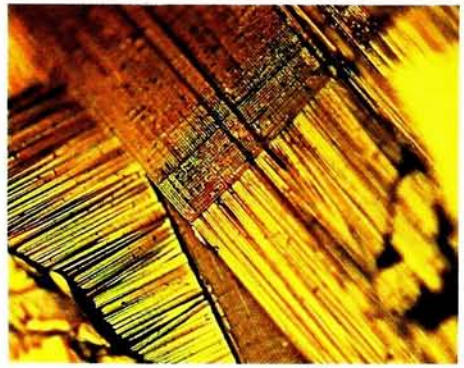

(b)

Magnification: 100x
Observation: Fiber Misalignment due to tension

AFTER

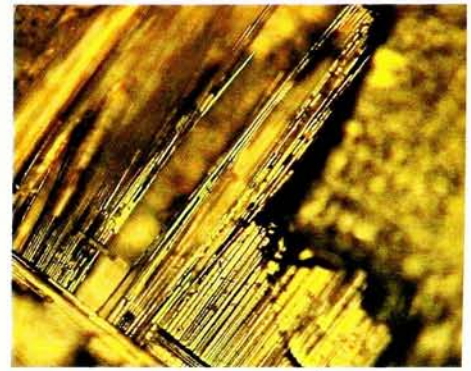

(c)

Magnification: 100x
Observation: Fiber Failure near end tab

(d)

Magnification: 500x
Observation: Pure Carbon Woven Fabric

AFTER

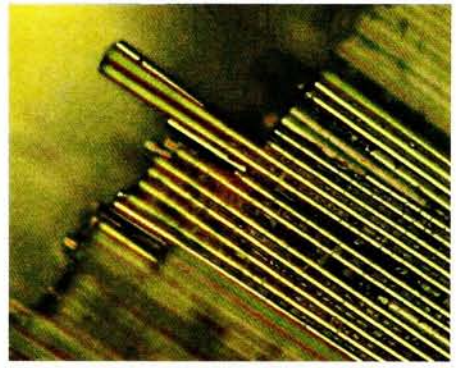

(e)

Magnification: 500x
Observation: Fiber Failure but no Debonding

Figure 3.21. Tensile test optical images of 2-component carbon fabric laminas (Magnifications: 100x & 500x)

AFTER

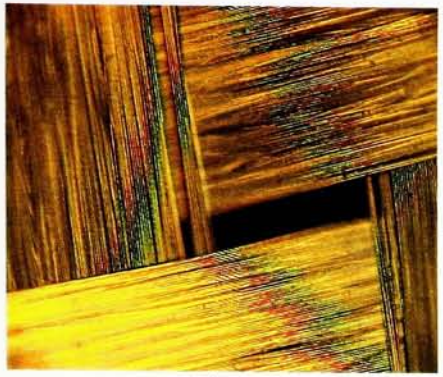

(a)

Magnification: 100x
Observation: Pure Carbon Woven Fabric

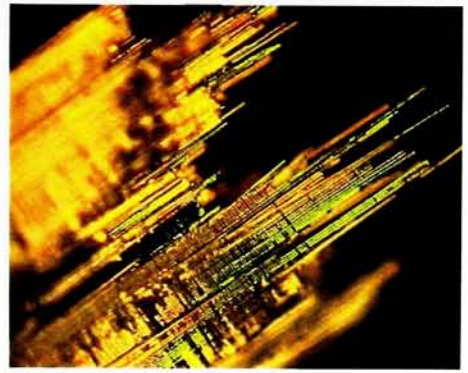

(b)

Magnification: 100x
Observation: Fiber Failure in the gage length

AFTER

(a)

Magnification: 500x
Observation: Pure Carbon Woven Fabric

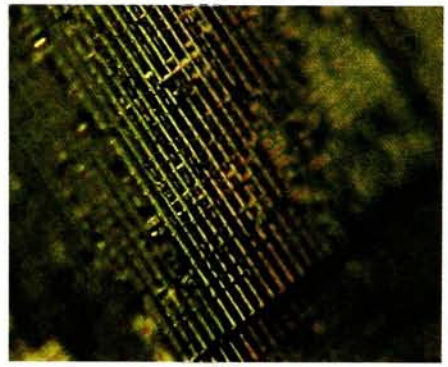

(b)

Magnification: 500x
Observation: No Debonding

Figure 3.22. Tensile test optical images of 3-component carbon fabric laminas (Magnifications: 100x & 500x)

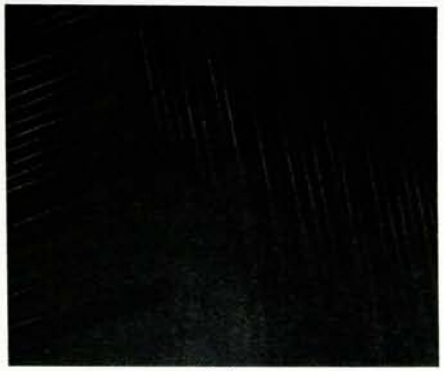

(a)

Magnification: 500x
Observation: Pure Carbon Woven Fabric

AFTER

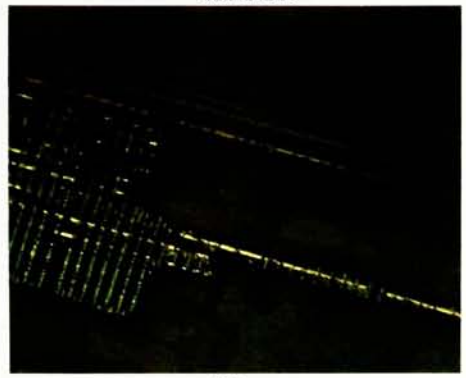

(b)

Magnification: 500x
Observation: Fiber Failure near center of the gage length

AFTER

(c)

Magnification: 500x
Observation: Resin rich areas

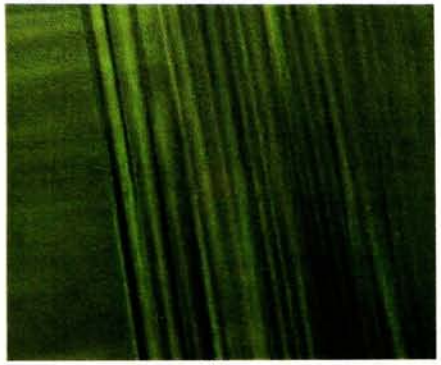

(d)

Magnification: 500x
Observation: Pure Glass Woven Fabric

AFTER

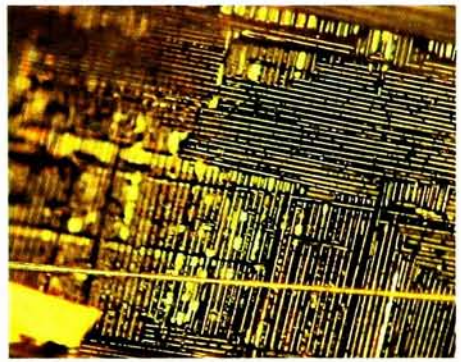

(e)

Magnification: 500x
Observation: Fiber Failure near center of the gage length

AFTER

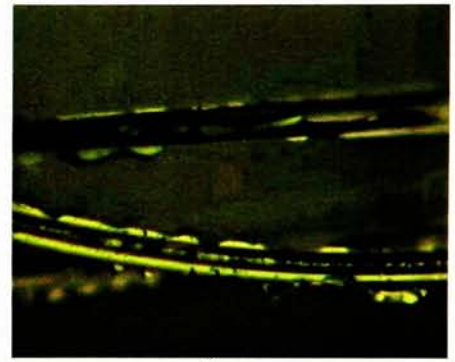

(f)

Magnification: 500x
Observation: Fiber Failure but no debonding

Figure 3.23. Tensile test optical images of 4-component carbon and glass fabric laminas (Magnifications: 500x)

(a)

Magnification: 1000x
Observation: Pure Carbon Woven Fabric

2-component system

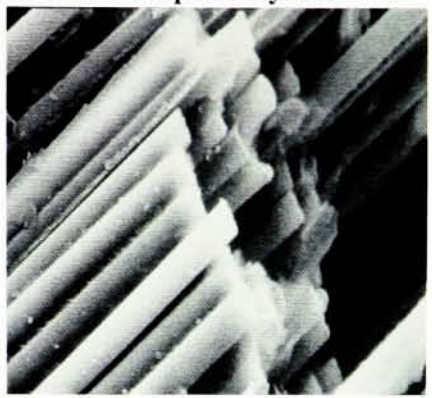

(b)

Magnification: 1000x
Observation: Fiber Failure

2-component system

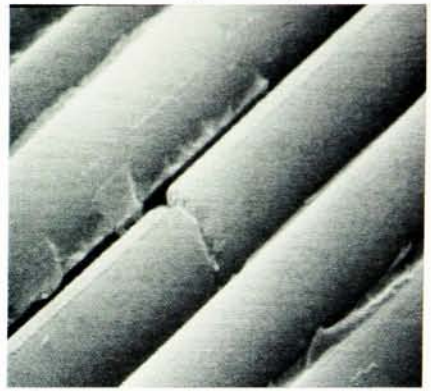

(c)

Magnification: 4000x
Observation: Fiber Breakage

(d)

Magnification: 1000x
Observation: Pure Carbon Woven Fabric

3-component system

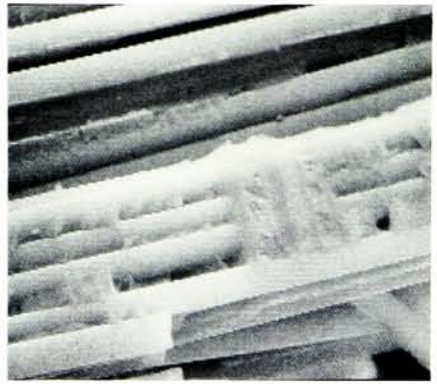

(e)

Magnification: 1000x
Observation: Fiber Failure + Resin Rich Areas

4-component system

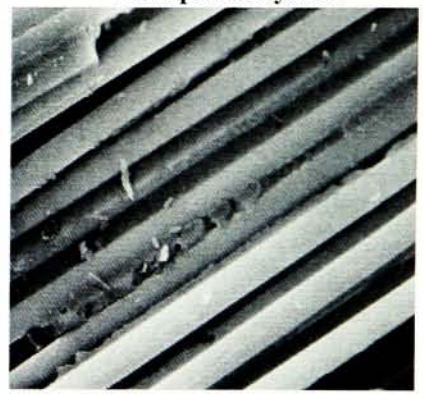

(f)

Magnification: 1000x
Observation: Resin Rich Areas

Figure 3.24. SEM images of failed tensile specimens (Magnifications: 1000x)

4-component system

(a)

Magnification: 1000x
Observation: Pure Glass Woven Fabric

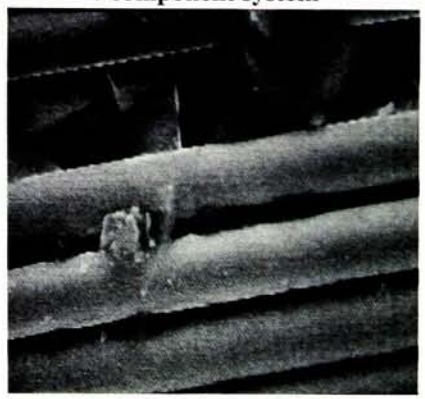

(b)

Magnification: 1000x
Observation: Fiber Failure + Resin Rich Areas

Figure 3.25. SEM images of failed tensile specimens (Magnifications → 1000x)

3.4.2 Izod Impact Test (ASTM D256-00)

Notched Izod impact testing was performed according to ASTM D256-00 and the impact energies and strengths were calculated. These tests are frequently used for comparing the impact response of isotropic materials that have different compositions or that are fabricated from different processing conditions. However, as in the case of unreinforced plastics, the impact tests do not yield basic material property data that can be used for design purposes. They are useful in comparing the failure modes and energy absorption capabilities of different materials under identical impact conditions.

The impact failure of fiber reinforced polymer composites is a very complex phenomenon. A simple rule-of-mixture law cannot predict this failure behavior. The fiber-matrix interactions, fiber orientations and the processing conditions are all important factors to consider. E-glass fiber composites have the highest impact energy because of the relatively high strain to failure of E-glass fibers. Carbon and boron fiber composites have low strains to failure that lead to low impact energies for these composites. The results of the impact tests on carbon fiber laminates are presented in Tables 3.16 – 3.18.

The impact strength observed for the 2- and 3-component system was the highest while the Zr-pendent polymer system showed the lowest impact strength. Similar strengths and energies were recorded for the 2- and the 3-component system. This indicated that modifying the polymer chain structure from a simple condensation polymer (2-component) to a co-polymer (parent polymer) did not have any effects on the properties. However, when the zirconium pendent group was attached to the parent polymer, a detrimental effect on the impact properties resulted. Delamination was observed for the pendent polymer system upon impact and all the four plies separated from each other, thus indicating a poor interfacial adhesion between each ply. There was no significant delamination for the other resin systems. As the impact energy can be absorbed by the material by two basic mechanisms: elastic and plastic deformation, the pendent polymer system being more bulky is not as effective in absorbing the load as the 2- component and parent resin systems. Since the Zr-pendent polymer has a high T_g (~ 290 °C), the processing temperature of 370 °C was not high enough to cause a considerable segmental motion of the polymer chains. This would lead to a poor flow of

Table 3.16. Impact strength and resistance for the 2-component carbon fiber composites

Sample # 1

Specimen #	Width (inches)	Thickness (inches)	Depth under notch (inches)	Impact load (ft-lbf)	Impact Resistance (ft-lbf/in.)	Impact Resistance (kJ/m)	Impact Strength (ft-lbf/in^2)	Impact Strength (kJ/m^2)
1	0.040	0.520	0.420	0.350	8.75	0.467	20.8	43.7
2	0.041	0.645	0.545	0.350	8.45	0.451	15.5	32.5
3	0.040	0.660	0.560	0.400	10.1	0.541	18.0	37.9
Average	0.040	0.608	0.508	0.367	9.11	0.486	18.1	38.1
Std. Dev.	0.001	0.077	0.077	0.029	0.893	0.048	2.66	5.59

Sample # 2

Specimen	Width (inches)	Thickness (inches)	Depth under notch (inches)	Impact load (ft-lbf)	Impact Resistance (ft-lbf/in.)	Impact Resistance (kJ/m)	Impact Strength (ft-lbf/in^2)	Impact Strength (kJ/m^2)
1	0.041	0.561	0.461	0.350	8.51	0.455	18.4	38.7
2	0.041	0.553	0.453	0.350	8.60	0.459	18.9	39.8
3	0.040	0.545	0.445	0.350	8.75	0.467	19.6	41.2
Average	0.041	0.553	0.453	0.350	8.62	0.460	19.0	39.9
Std. Dev.	0.001	0.008	0.008	0.000	0.119	0.006	0.599	1.25

Sample # 3

Specimen	Width (inches)	Thickness (inches)	Depth under notch (inches)	Impact load (ft-lbf)	Impact Resistance (ft-lbf/in.)	Impact Resistance (kJ/m)	Impact Strength (ft-lbf/in^2)	Impact Strength (kJ/m^2)
1	0.041	0.544	0.444	0.350	8.60	0.459	19.3	40.6
2	0.041	0.568	0.468	0.450	11.0	0.589	23.5	49.5
3	0.040	0.567	0.467	0.440	10.9	0.583	23.3	49.0
Average	0.041	0.560	0.460	0.413	10.1	0.544	22.1	46.4
Std. Dev.	0.000	0.013	0.013	0.055	1.37	0.073	2.37	4.99
			Combined Average		9.30	0.497	19.7	41.5
			Combined Std. Dev.		1.07	0.057	2.55	5.36

Table 3.17. Impact strengths and resistance for the 3-component carbon fiber composite

Sample # 1

Specimen #	Width (inches)	Thickness (inches)	Depth under notch (inches)	Impact load (ft-lbf)	Impact Resistance (ft-lbf/in.)	Impact Resistance (kJ/m)	Impact Strength (ft-lbf/in^2)	Impact Strength (kJ/m^2)
1	0.040	0.565	0.465	0.400	10.0	0.535	21.5	45.2
2	0.039	0.557	0.457	0.400	10.2	0.548	22.4	47.1
3	0.039	0.555	0.455	0.350	9.06	0.484	19.9	41.8
Average	0.039	0.559	0.459	0.383	9.78	0.522	21.3	44.7
Std. Dev.	0.001	0.005	0.005	0.029	0.630	0.034	1.28	2.69

Sample # 2

Specimen #	Width (inches)	Thickness (inches)	Depth under notch (inches)	Impact load (ft-lbf)	Impact Resistance (ft-lbf/in.)	Impact Resistance (kJ/m)	Impact Strength (ft-lbf/in^2)	Impact Strength (kJ/m^2)
1	0.039	0.557	0.457	0.350	9.04	0.483	19.7	41.5
2	0.040	0.570	0.470	0.400	10.1	0.541	21.5	45.2
3	0.039	0.563	0.463	0.400	10.1	0.543	21.9	46.1
Average	0.039	0.563	0.463	0.383	9.78	0.522	21.1	44.3
Std. Dev.	0.000	0.006	0.006	0.029	0.640	0.034	1.16	2.45
			Combined	**Average**	9.42	0.503	20.5	43.0
			Combined	**Std. Dev.**	0.500	0.027	1.01	2.12

Table 3.18. Impact strengths and resistance for the 4-component carbon fiber composite

Specimen #	Width (inches)	Thickness (inches)	Depth under notch (inches)	Impact load (ft-lbf)	Impact Resistance (ft-lbf/in.)	Impact Resistance (kJ/m)	Impact Strength (ft-lbf/in^2)	Impact Strength (kJ/m^2)
1	0.040	0.549	0.449	0.200	5.05	0.270	11.2	23.6
2	0.041	0.539	0.439	0.200	4.93	0.264	11.2	23.6
3	0.041	0.533	0.433	0.200	4.92	0.263	11.3	23.8
Average	0.040	0.540	0.440	0.200	4.97	0.265	11.2	23.7
Std. Dev.	0.001	0.008	0.008	0.000	0.069	0.004	0.068	0.143

the polymer and hence poor intermingling at the laminar interfaces between the resin and the fiber, a major factor for delamination. This can also be confirmed through the optical and SEM images (vide infra) of the failed specimen where resin rich areas were observed. It was also observed by Numata et al [27] that as temperature increases, imide rings are formed in the molecular chains causing an increase in the molecular chain rigidity and the transition temperature of the polymer shifts towards a higher temperature. The fabrication time of one hour at 370 °C may also have not been sufficient to cause adequate resin flow between the plies.

A comparison was made of the impact strengths and energies for each laminate system as shown in Figures 3.26 and 3.27.

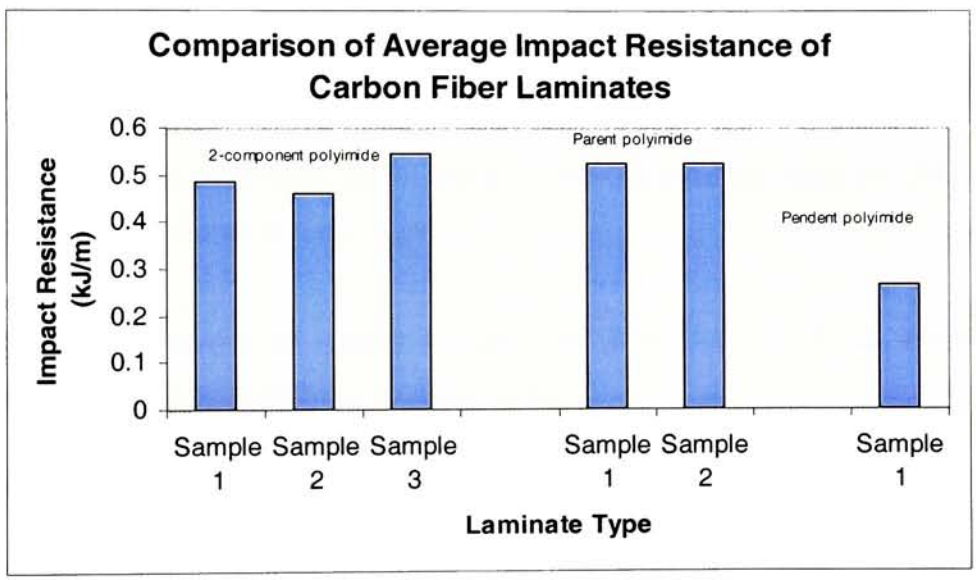

Figure 3.26. Comparison of average impact resistance (energy) of carbon fiber laminates

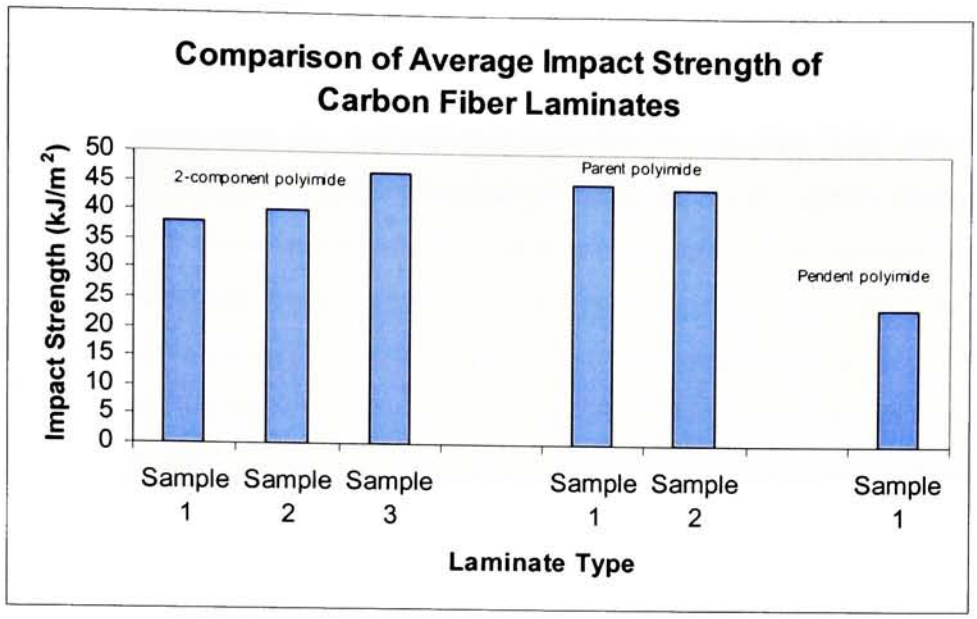

Figure 3.27. Comparison of average impact strengths of carbon fiber laminates

Comparisons made between the impact properties obtained using the different molding cycles are shown in Table 3.19.

Table 3.19. Comparison of impact strength and Moduli of 2-, 3- & 4-component composite laminates from different molding cycles

	Reinforcement	2-component system		3-component system	
		I	II [a]	I	II [a]
Impact Resistance (kJ/m)	Carbon	0.50 ± 0.09	1.1 ± 0.18	0.52 ± 0.03	0.93 ± 0.19
Impact Strength (kJ/m^2)	Carbon	41 ± 0.02	95 ± 14	44 ± 2.6	91 ± 1.5

	Reinforcement	4-component system	
		I	II [a]
Impact Resistance (kJ/m)	Carbon	0.27 ± 0.00	-
Impact Strength (kJ/m^2)	Carbon	23 ± 0.17	-

[a] : Ref [26]

Upon comparison, it was seen that the impact properties were higher for the laminates fabricated from molding cycle II. The general trend observed for both the molding cycles was that the 2-component and parent polymer laminates showed comparable values while the pendent laminates showed the lowest impact strength. This was consistent with observations for the tensile data interpreted in section 3.4.1. The larger degree of imidization using molding cycle I will also make the matrix more rigid, which would result in a lower impact strength and energy for the laminates.

Since delamination, debonding and fiber pullout energies depend on fiber-matrix interfacial shear strength, study of the resin matrix was important as it could influence the impact damage mechanism. Images of the test specimen before and after impact shown in Figures 3.28-3.32 were obtained by placing them with the notched edge facing upwards. The most common types of failure observed were inter and intra laminar fracture, delamination, fiber breakage and micro cracking of the resin matrix. There was no debonding observed between the resin and the fibers. Fibers with adherent matrix debris were seen, indicating a considerable adhesion to the matrix. However, regions rich in resin indicated a poor resin flow. These failure modes were identified for all the three resin systems except that for the four-component resin, delamination was the most predominant type of failure observed. For the 2- and 3-component resins, delamination was concentrated at the point of impact and observed microscopically while for the Zr-pendent resin, all the four plies separated from each other upon impact and could be visually observed. In an investigation of the single impact response of laminated composites, Cheng et al concluded that matrix cracking was the initial failure mode, which was caused predominantly by the inter-laminar shear stresses and the in-plane tensile stresses [9]. The impact performance of woven carbon fiber reinforced laminates with [0°, 90°], [$\pm$ 45°] and mixed woven [0, $\pm$ 45°] lay-ups were evaluated by Bishop and Curtis [9]. They found that the damage was principally in the form of delamination between the layers. The energy absorbing capability or toughness of a material can be enhanced by increasing the total area of new surfaces created or by increasing the fiber volume fraction [9].

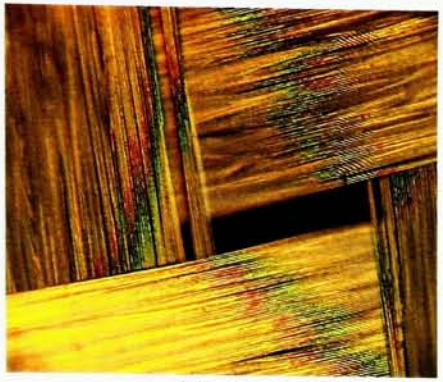

(a)

Magnification: 100x
Observation: Pure Carbon Woven Fabric

BEFORE

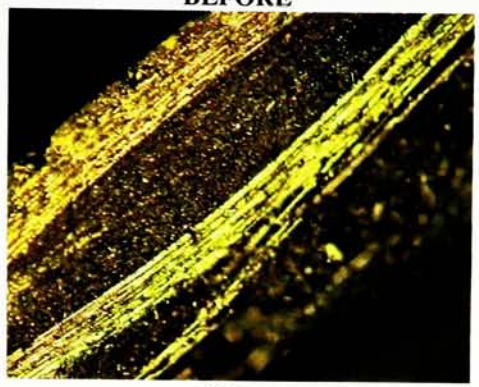

(b)

Magnification: 100x
Observation: Good Resin Consolidation

AFTER

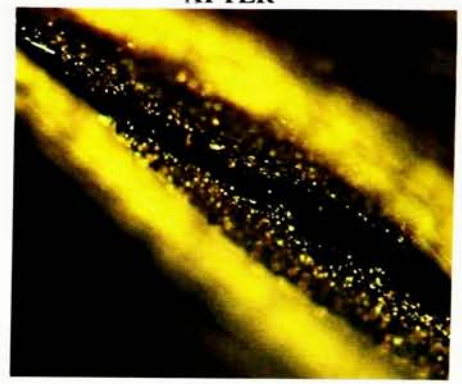

(c)

Magnification: 100x
Observation: Matrix Cracking

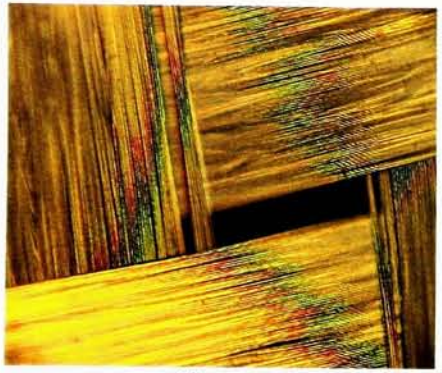

(d)

Magnification: 100x
Observation: Pure Carbon Woven Fabric

BEFORE

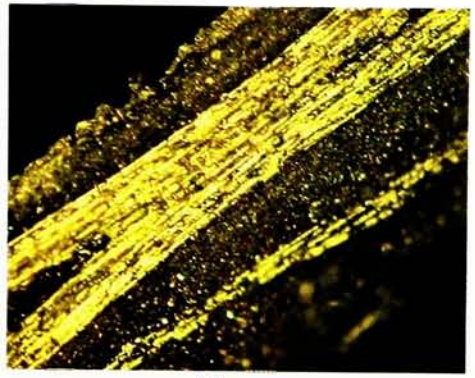

(e)

Magnification: 100x (Opposite side of notch)
Observation: Good Resin Consolidation

AFTER

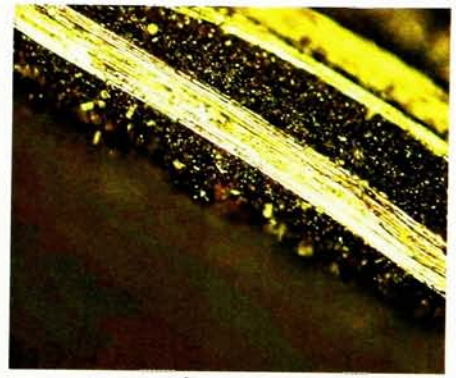

(f)

Magnification: 100x (Opposite side of notch)
Observation: No effect observed after impact

Figure 3.28. Izod Impact optical images of 2-component carbon fabric laminates (Magnifications: 100x)

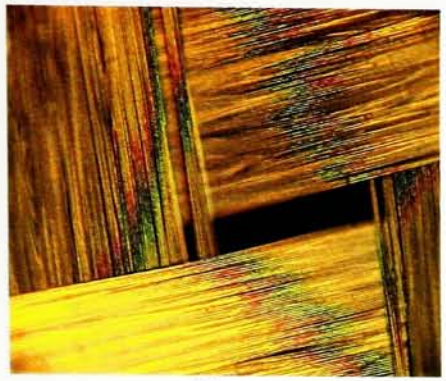

(a)

Magnification: 100x
Observation: Pure Carbon Woven Fabric

BEFORE

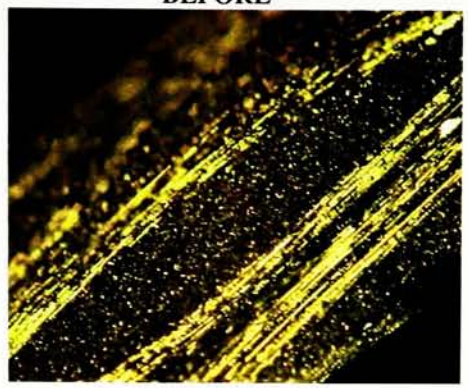

(b)

Magnification: 100x
Observation: Good Resin Consolidation

AFTER

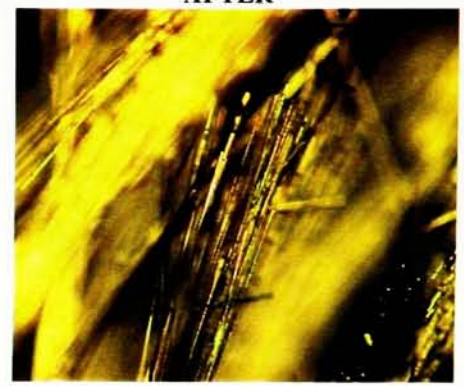

(c)

Magnification: 100x
Observation: Fiber Failure

(d)

Magnification: 500x
Observation: Pure Carbon Woven Fabric

BEFORE

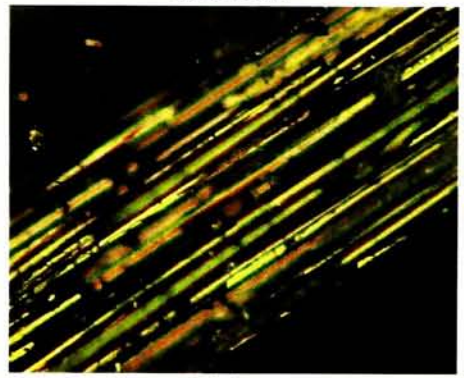

(e)

Magnification: 500x
Observation: Good Resin Adhesion

AFTER

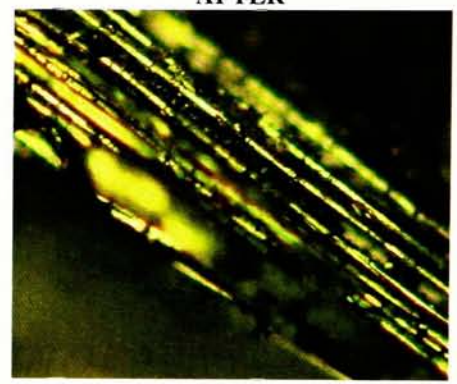

(f)

Magnification: 500x
Observation: No Debonding

Figure 3.29. Izod Impact optical images of 3-component carbon fabric laminates (Magnifications: 100x & 500x)

BEFORE

AFTER

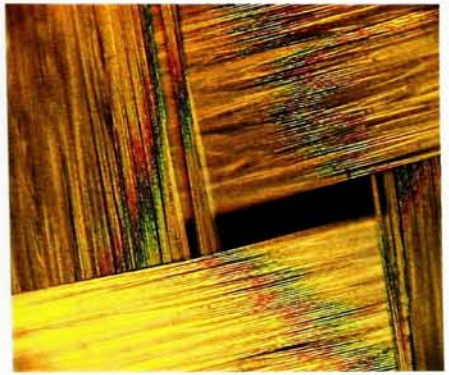

(a)

Magnification: 100x
Observation: Pure Carbon Woven Fabric

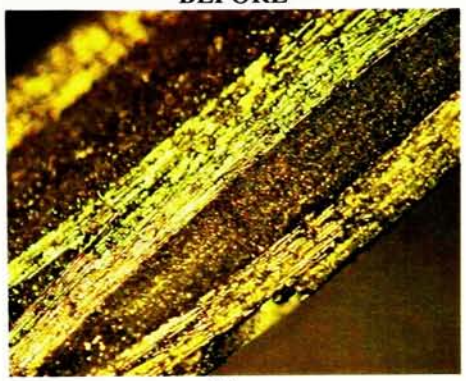

(b)

Magnification: 100x
Observation: Good Resin Fiber Consolidation

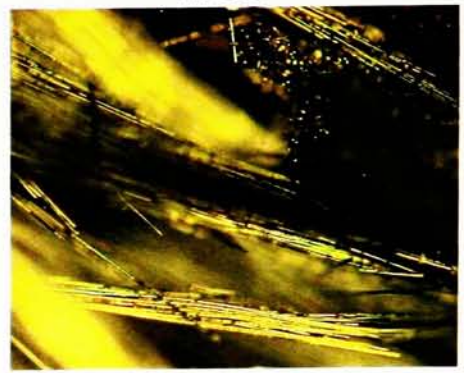

(c)

Magnification: 100x
Observation: Fiber Failure

BEFORE

AFTER

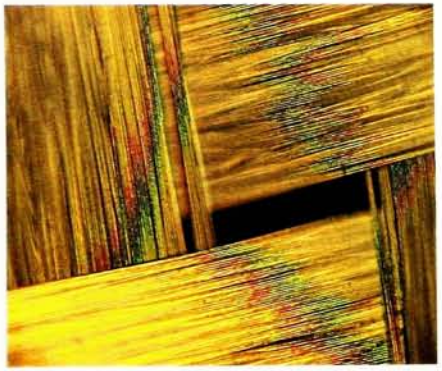

(d)

Magnification: 100x
Observation: Pure Carbon Woven Fabric

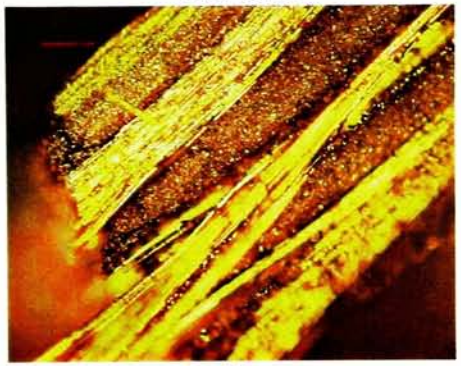

(e)

Magnification: 100x (At Notch)
Observation: Good Resin Consolidation

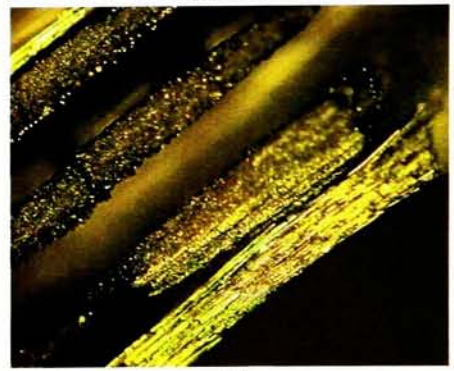

(f)

Magnification: 100x (At Notch)
Observation: Inter and Intra Laminar Fracture

Figure 3.30. Izod Impact optical images of 4-component carbon fabric laminates (Magnifications: 100x)

(a)

Magnification: 500x
Observation: Pure Carbon Woven Fabric

BEFORE

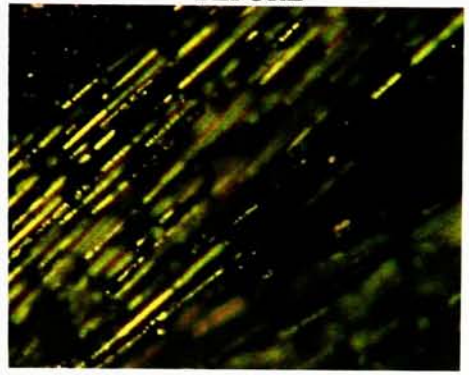

(b)

Magnification: 500x
Observation: Good Resin Adhesion

AFTER

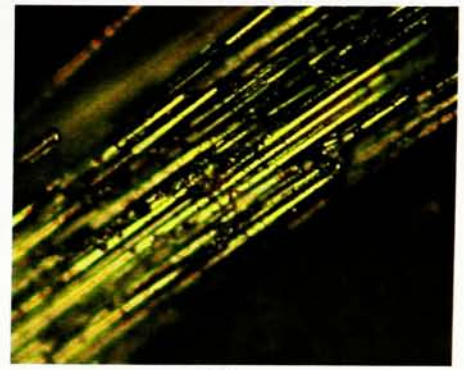

(c)

Magnification: 500x
Observation: No Debonding

(d)

Magnification: 500x
Observation: Pure Carbon Woven Fabric

BEFORE

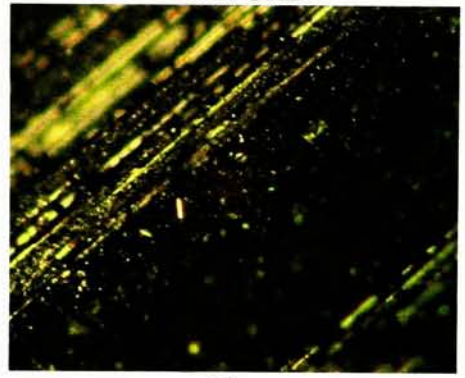

(e)

Magnification: 500x
Observation: Good Resin Consolidation

AFTER

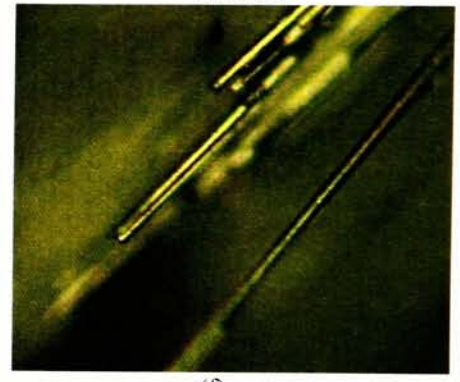

(f)

Magnification: 500x
Observation: Resin Adhesion on separated fibers

Figure 3.31. Izod Impact optical images of 4-component carbon fabric laminates (Magnifications: 500x)

(a)

Magnification: 1000x
Observation: Pure Carbon Woven Fabric

2-component system

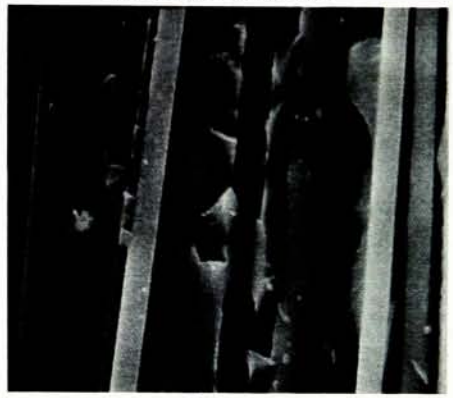

(b)

Magnification: 1000x
Observation: Resin Rich Areas

3-component system

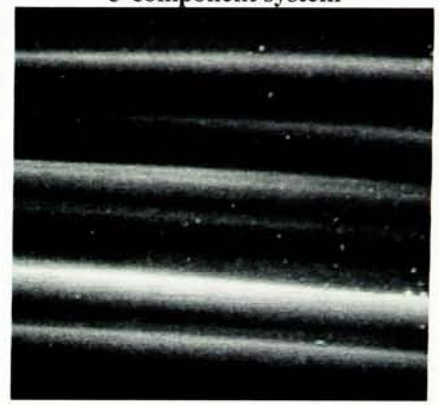

(c)

Magnification: 1000x
Observation: Good resin consolidation

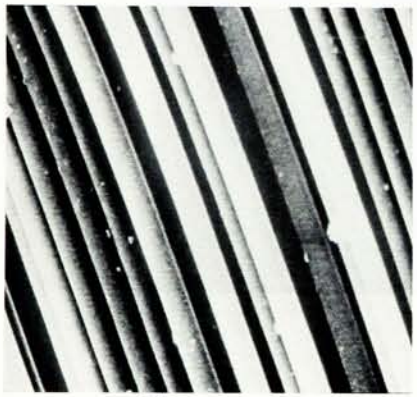

(d)

Magnification: 1000x
Observation: Pure Carbon Woven Fabric

4-component system

(e)

Magnification: 1000x
Observation: Resin Rich Areas

Figure 3.32. SEM images of failed impact specimen

3.4.3 Flexural Test (Three-point bending) (ASTM D790-00)

Flexural properties were determined for the carbon reinforced four-ply laminates using a three-point bending mode. The span-to-depth was very close to the targeted 32:1 (32.7 $\pm$ 0.00) ratio. Flexural properties showed a similar trend as observed for the tensile and impact tests. The parent polyimides exhibited the highest strengths while the Zr-pendent polyimide laminates showed the lowest flexural strengths relative to the other resin laminates.

The 2-component laminate had strengths between those of the parent and the pendent polyimide laminates. Values for all the different resin laminates ranged from 74 MPa to 174 MPa. A disparity in the strength values between the two laminates was observed for the 2-component laminates preventing us from obtaining a correct average strength. This was due to the following reasons: firstly, when the fractured surface of a specimen from sample # 1 was analyzed under the SEM (see Figure 3.33), a small piece of aluminum foil was observed on the surface of one of the inner plies. Since the prepregs were tacky and wrapped in aluminum foil during storage, some of it adhered to these prepregs and after removing them, there was a possibility of overlooking the presence of smaller pieces of this foil. This would lead to poor adhesion in this area leading to sample failure. Secondly, it was noticed that during prepreg fabrication in the vacuum oven, some of the prepregs had a raised curvature around the periphery of the laminate. During the stacking sequence of the prepregs, this may lead to a slight mismatch in the alignment in the fiber direction and thus affecting the final properties.

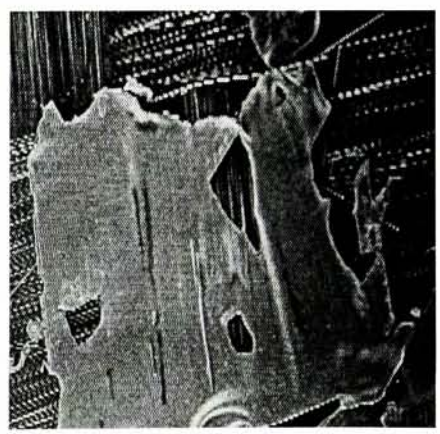

Figure 3.33. SEM image of an aluminum foil on a ply surface

The modulus values for all the laminates ranged from 22.9 GPa to 24.0 GPa. The flexural strengths and moduli are summarized in Tables 3.20 to 3.22.

Table 3.20. Flexural strengths and modulus of the 2-component carbon fiber composites

Sample # 1

Specimen	Thickness (mm)	Width (mm)	Span-Depth Ratio	Rate of Crosshead Motion (mm/min)	Peak Load (kgf)	Strain at Peak (mm/mm)	Flexural Strength (MPa)	Flexural Modulus (GPa)
1	1.075	14.150	32.00	1.835	3.446	0.011	114.8	20.46
2	1.050	13.950	32.76	1.878	3.120	0.007	103.9	21.91
3	1.075	14.300	32.00	1.835	4.239	0.012	135.2	22.27
Average	1.067	14.133	32.25	1.849	3.602	0.010	117.9	21.55
Std. Dev.	0.014	0.176	0.44	0.025	0.576	0.003	15.8	0.95

Sample # 2

Specimen	Thickness (mm)	Width (mm)	Span-Depth Ratio	Rate of Crosshead Motion (mm/min)	Peak Load (kgf)	Strain at Peak (mm/mm)	Flexural Strength (MPa)	Flexural Modulus (GPa)
1	1.050	13.775	32.76	1.878	4.735	0.012	171.5	23.73
2	1.050	13.900	32.76	1.878	4.939	0.011	175.3	23.90
3	1.050	13.600	32.76	1.878	4.938	0.013	170.6	25.16
Average	1.050	13.758	32.76	1.878	4.871	0.012	172.4	24.26
Std. Dev.	0.000	0.151	0.00	0.000	0.117	0.001	2.4	0.78

Combined Average	145.2	22.91
Std. Deviation	38.5	1.9

Table 3.21. Flexural strengths and modulus of the 3-component carbon composites

Sample # 1

Specimen	Thickness (mm)	Width (mm)	Span-Depth Ratio	Rate of Crosshead Motion (mm/min)	Peak Load (kgf)	Strain at Peak (mm/mm)	Flexural Strength (MPa)	Flexural Modulus (GPa)
1	1.050	13.600	32.76	1.878	5.235	0.015	188.1	23.74
2	1.050	13.675	32.76	1.878	4.996	0.011	174.2	23.05
3	1.050	13.816	32.76	1.878	4.860	0.011	171.0	24.23
Average	1.050	13.697	32.76	1.878	5.030	0.012	177.7	23.67
Std. Dev.	0.000	0.110	0.000	0.000	0.190	0.002	9.0	0.59

Sample # 2

Specimen	Thickness (mm)	Width (mm)	Span-Depth Ratio	Rate of Crosshead Motion (mm/min)	Peak Load (kgf)	Strain at Peak (mm/mm)	Flexural Strength (MPa)	Flexural Modulus (GPa)
1	1.050	14.050	32.76	1.878	4.744	0.015	175.4	25.18
2	1.050	14.010	32.76	1.878	4.487	0.012	153.1	24.90
3	1.075	13.850	32.00	1.835	4.944	0.013	183.6	22.86
Average	1.058	13.970	32.50	1.864	4.725	0.013	170.7	24.32
Std. Dev.	0.014	0.106	0.44	0.025	0.229	0.002	15.7	1.26

Combined Average	174.2	23.99
Std. Deviation	4.9	0.45

Table 3.22. Flexural strengths and modulus of the 4-component carbon composites

Specimen	Thickness (mm)	Width (mm)	Span-Depth Ratio	Rate of Crosshead Motion (mm/min)	Peak Load (kgf)	Strain at Peak (mm/mm)	Flexural Strength (MPa)	Flexural Modulus (GPa)
1	1.025	13.830	33.56	1.924	2.310	0.004	80.5	24.21
2	1.050	13.716	32.76	1.878	1.918	0.003	64.2	21.86
3	1.050	13.750	32.76	1.878	2.372	0.004	79.3	23.38
Average	1.042	13.765	33.02	1.878	2.200	0.004	74.6	23.15
Std. Dev.	0.014	0.059	0.46	0.000	0.246	0.001	9.0	1.19

The low strengths for the Zr-pendent polymer carbon composite could be explained as follows. The resin had a higher molecular weight due to the heavy groups attached to the chain. For achieving the desired 60:40 fiber to resin weight ratio, the weight and hence the amount of resin needed was much lesser compared to the 2-component and parent polymers. Since the role of the resin matrix is to transfer the load effectively amongst the fibers, lesser resin would lead to inadequate transfer of this load. Bar graphs indicating the strengths and moduli were plotted in Figures 3.34 and 3.35.

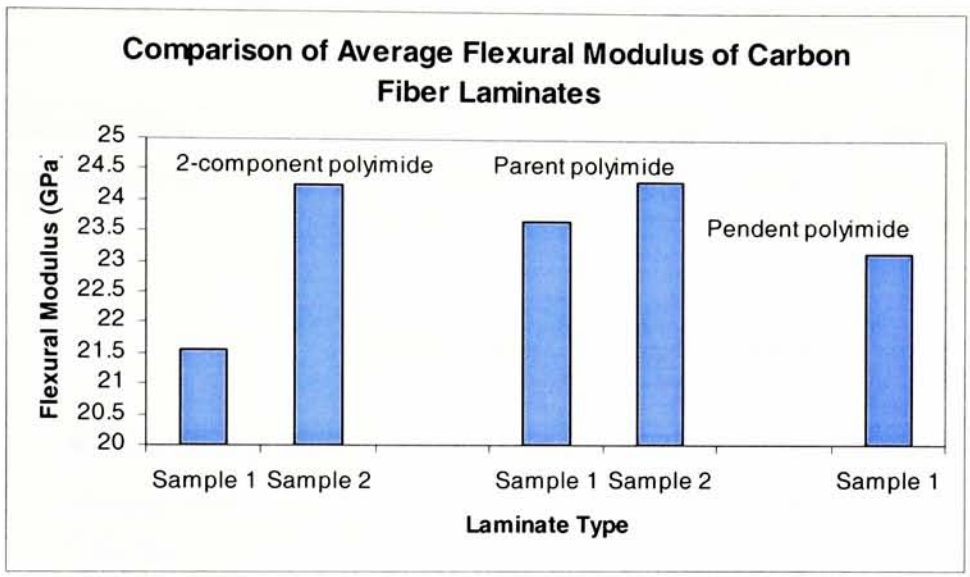

Figure 3.34. Comparison of average flexural modulus of carbon fiber laminates

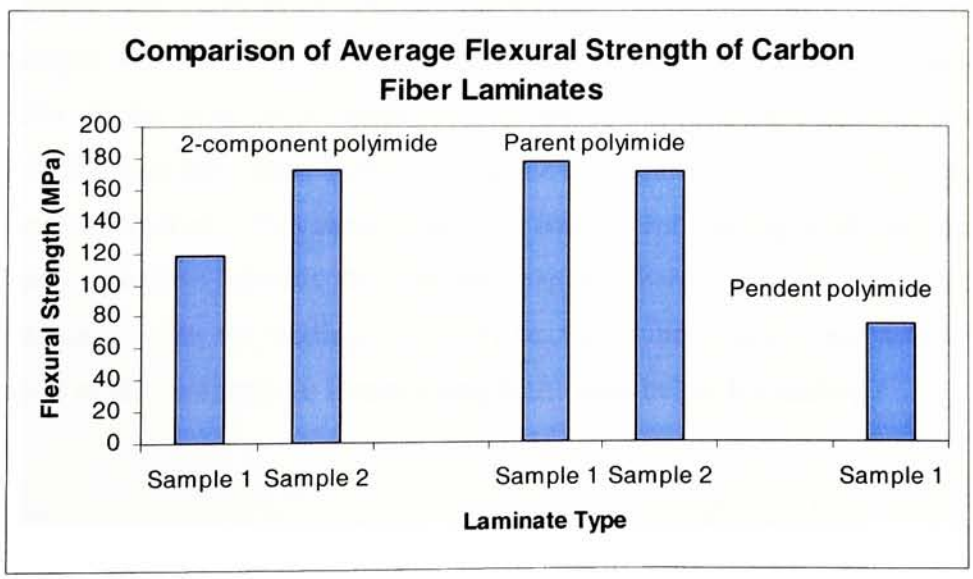

Figure 3.35. Comparison of average flexural strengths of carbon fiber laminates

Based on the unreliability of the flexural data for the 2-component laminates, it was not possible to make a comparison with the different molding cycle. A numerical comparison has been made in Table 3.23 for reference.

Table 3.23. Comparison of flexural strength and moduli of 2-, 3- & 4-component composite laminates from different molding cycles

	Reinforcement	2-component system		3-component system	
		I	II [a]	I	II [a]
Flexural Strength (MPa)	Carbon	145 ± 38	854 ± 108	174 ± 4	464 ± 173
Flexural Modulus (GPa)	Carbon	22 ± 1	47 ± 5	23 ± 0	37 ± 12

	Reinforcement	4-component system	
		I	II [a]
Flexural Strength (MPa)	Carbon	74 ± 9	163 ± 57
Flexural Modulus (GPa)	Carbon	23 ± 1	17 ± 8

[a] : Ref [26]

Figures 3.36 - 3.40 show optical images of the flexure specimen before and after failure. Images were taken of the zones under (compressive) and opposite (tensile) the loading. For all the three resin systems, delamination between each ply was primarily observed in the specimen upon loading. Areas rich in resin were seen between the plies during the SEM analysis. This could arise from insufficient wetting of all the fibers and result in poor adhesion between the fiber and matrix. Fiber breakage was also observed on the side opposite to the loading. This may be due to the tensile forces acting in this zone relative to the compressive forces acting in the zone below the loading.

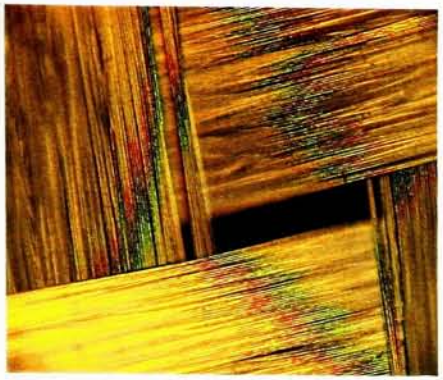

(a)

Magnification: 100x
Observation: Pure Carbon Woven Fabric

BEFORE

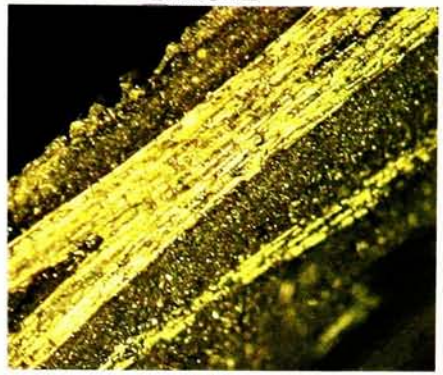

(b)

Magnification: 100x
Observation: Good Resin Consolidation

AFTER

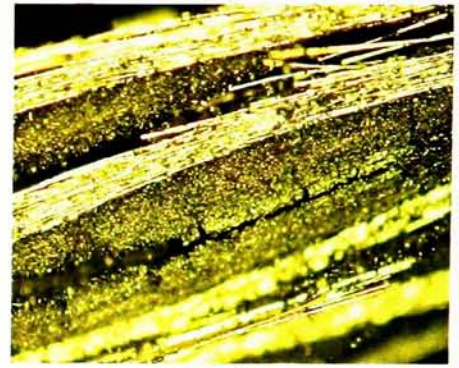

(c)

Magnification: 100x
Observation: Delamination, Fiber Breakage and Matrix Cracking

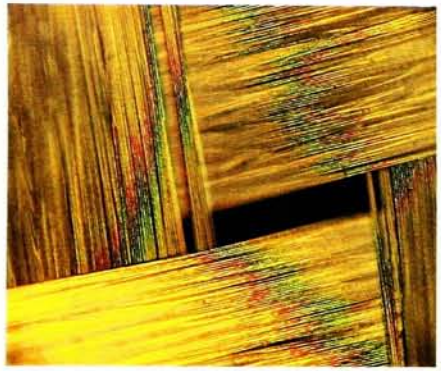

(d)

Magnification: 100x
Observation: Pure Carbon Woven Fabric

BEFORE

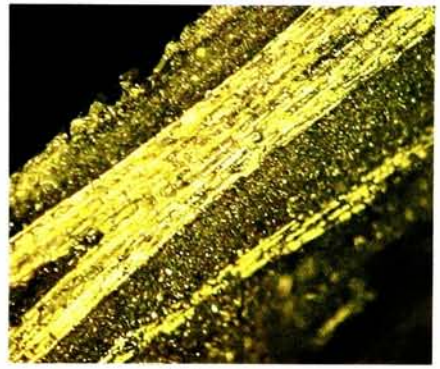

(e)

Magnification: 100x
Observation: Good Resin Consolidation

AFTER

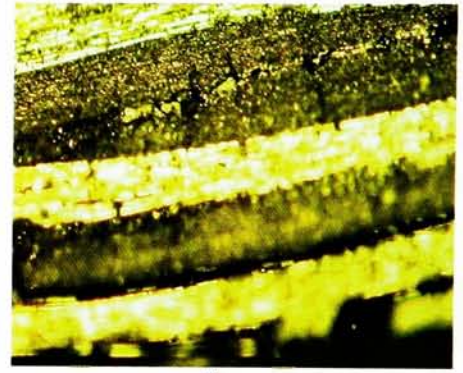

(f)

Magnification: 100x
Observation: Delamination and Matrix Micro Cracking

Figure 3.36. Flexural Test optical images of 2-component carbon fabric laminates (Magnifications: 100x)

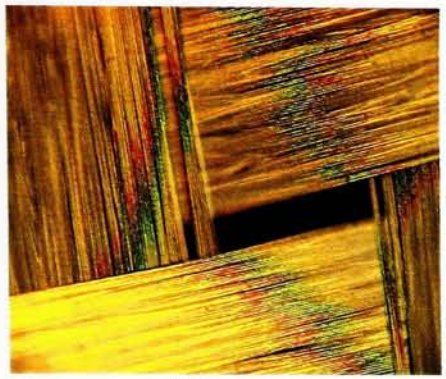

(a)

Magnification: 100x
Observation: Pure Carbon Woven Fabric

BEFORE

(b)

Magnification: 100x
Observation: Good Resin Consolidation

AFTER

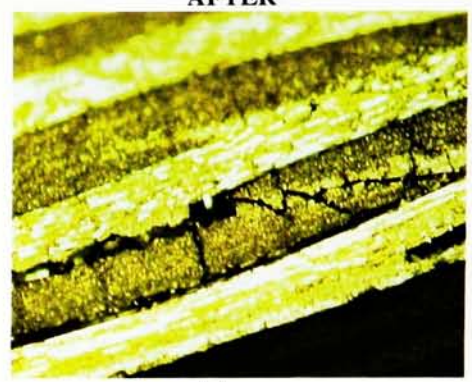

(c)

Magnification: 100x
Observation: Delamination and Matrix Micro Cracking

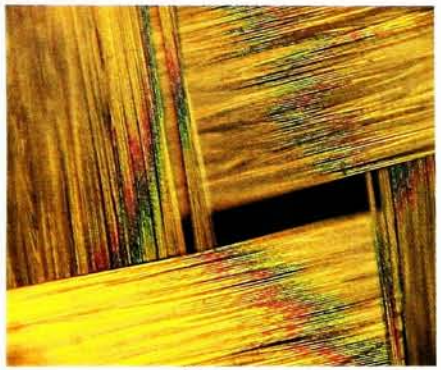

(d)

Magnification: 100x
Observation: Pure Carbon Woven Fabric

BEFORE

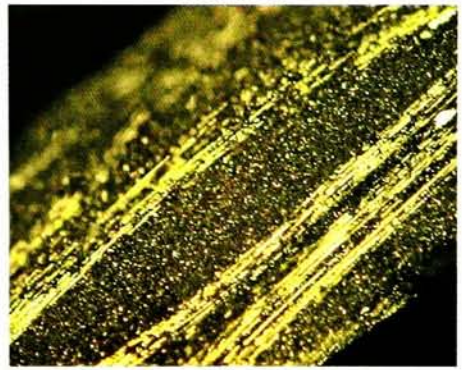

(e)

Magnification: 100x
Observation: Good Resin Consolidation

AFTER

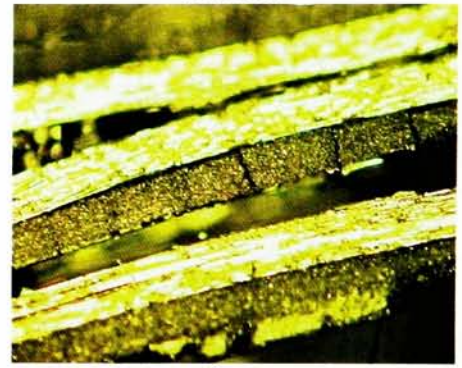

(f)

Magnification: 100x
Observation: Inter and Intra Laminar Fracture

Figure 3.37. Flexural Test optical images of 3-component carbon fabric laminates (Magnifications: 100x)

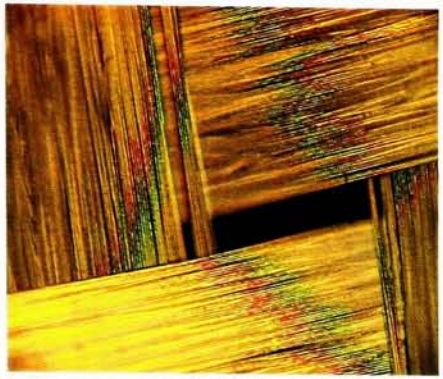

(a)

Magnification: 100x
Observation: Pure Carbon Woven Fabric

BEFORE

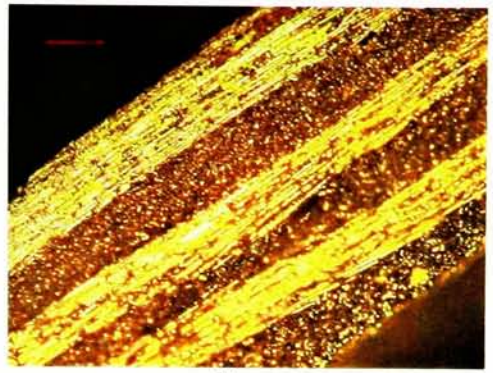

(b)

Magnification: 100x
Observation: Good Resin Consolidation

AFTER

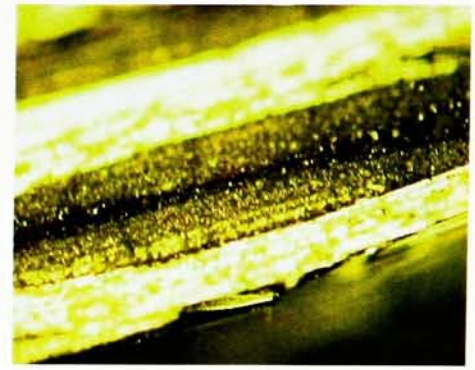

(c)

Magnification: 100x
Observation: Matrix Cracking

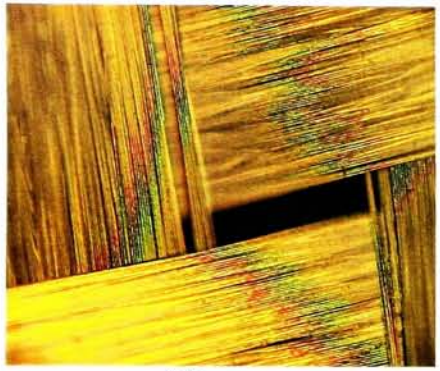

(d)

Magnification: 100x
Observation: Pure Carbon Woven Fabric

BEFORE

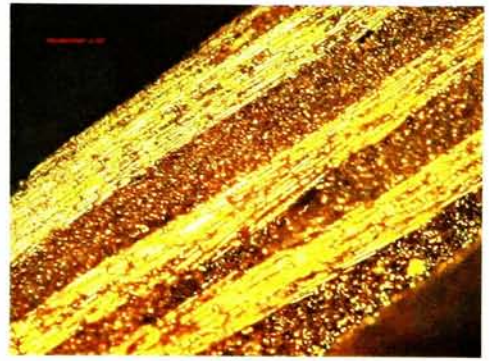

(e)

Magnification: 100x (Side opposite to loading)
Observation: Good Resin Consolidation

AFTER

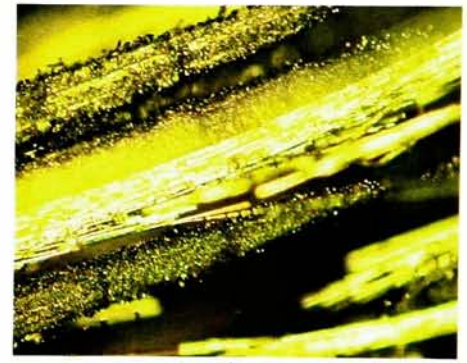

(f)

Magnification: 100x (Side opposite to loading)
Observation: Delamination and Fiber Breakage

Figure 3.38. Flexural Test optical images of 4-component carbon fabric laminates (Magnifications: 100x)

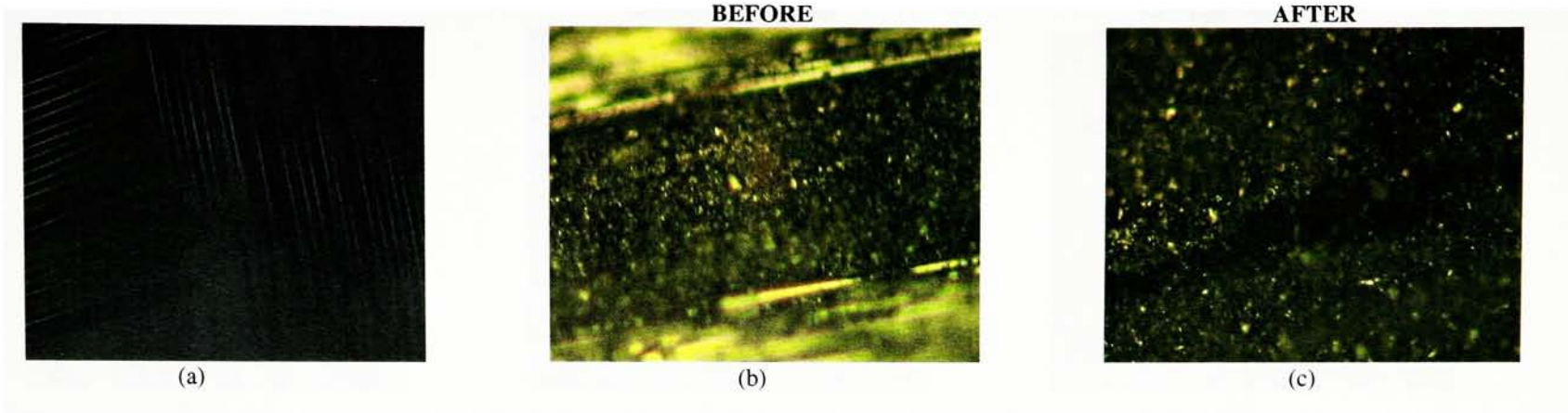

Figure 3.39. Flexural Test optical images of 4-component carbon fabric laminates (Magnifications: 500x)

(a)

Magnification: 1000x
Observation: Pure Carbon Woven Fabric

2-component system

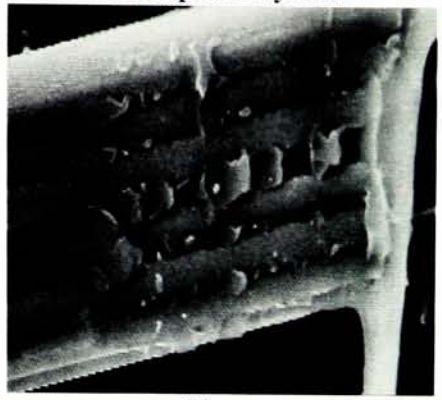

(b)

Magnification: 1000x
Observation: Fiber Failure

3-component system

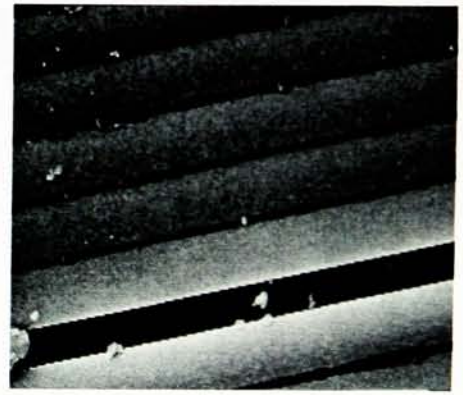

(c)

Magnification: 1000x
Observation: Resin between fibers

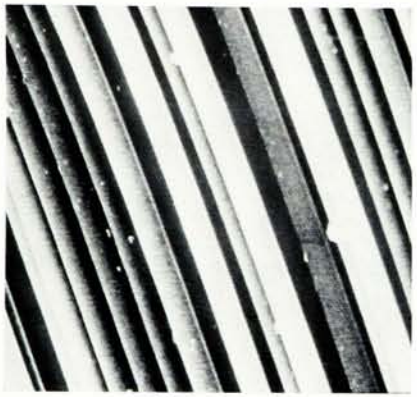

(d)

Magnification: 1000x
Observation: Pure Carbon Woven Fabric

3-component system

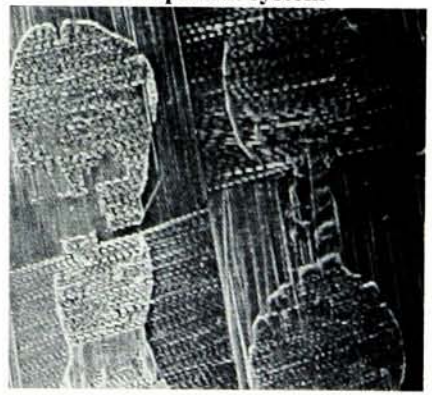

(e)

Magnification: 30x
Observation: Resin rich areas between the plies

4-component system

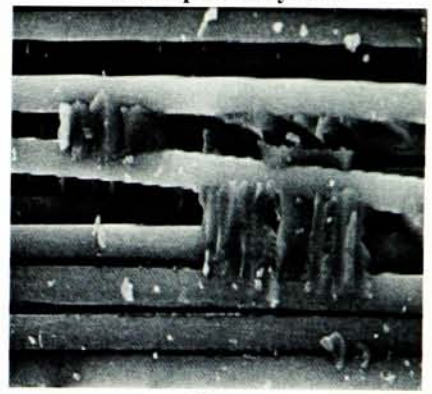

(f)

Magnification: 1000x
Observation: Resin rich areas

Figure 3.40. SEM images of failed flexural specimen

3.4.4 Dynamic Mechanical Analysis (DMA) (ASTM D4065-95)

DMA is a very powerful technique capable of providing information on the thermal mechanical behavior of a polymer due to the temperature dependence of the storage modulus, loss modulus and tan delta [4]. The DMA technique has been widely used to explore the thermal mechanical behavior of viscoelastic materials, blends and polymer composites.

DMA was performed on single ply carbon and glass fiber reinforced laminas at three different frequencies: 0.2 Hz, 2 Hz and 20 Hz. Three specimens were cut from each lamina and tested for their viscoelastic properties. Figures 3.41-3.44 represent one specimen from each lamina for the three different resin composites.

From the storage modulus curves, a nearly linear behavior of the modulus was seen with increasing temperature. This behavior could be due to two reasons:

1) There was crosslinking taking place in the resin and this would increase the modulus of the composite. The composite specimen was reheated to examine the effect of this crosslinking. A similar linearly increasing modulus was observed.
2) Differences in the thermal expansion coefficients between the matrix and the fibers could give rise to internal stresses in the composite. Since in practically all cases, the matrix has a greater expansion than the fiber, it subjects the fiber to compressive stresses [28], better transmitting the load on to them and thus resulting in higher moduli.

From the loss modulus graphs, there was no viscous component observed for the samples. No glass transition peaks were seen in these curves, indicating that the resins were highly crosslinked during composite fabrication. Therefore, reason 1 does not apply.

Tan delta values observed for these laminas were very low. Values ranged from 0.004 – 0.018. Since a material behaves elastic if tan $\delta < 1$, values obtained indicate a highly elastic material which also is consistent with a high degree of crosslinking. Tan delta would not be affected by the differences in the thermal expansion coefficients. This is because the crosslink density is not changing, so the tan delta is not changing.

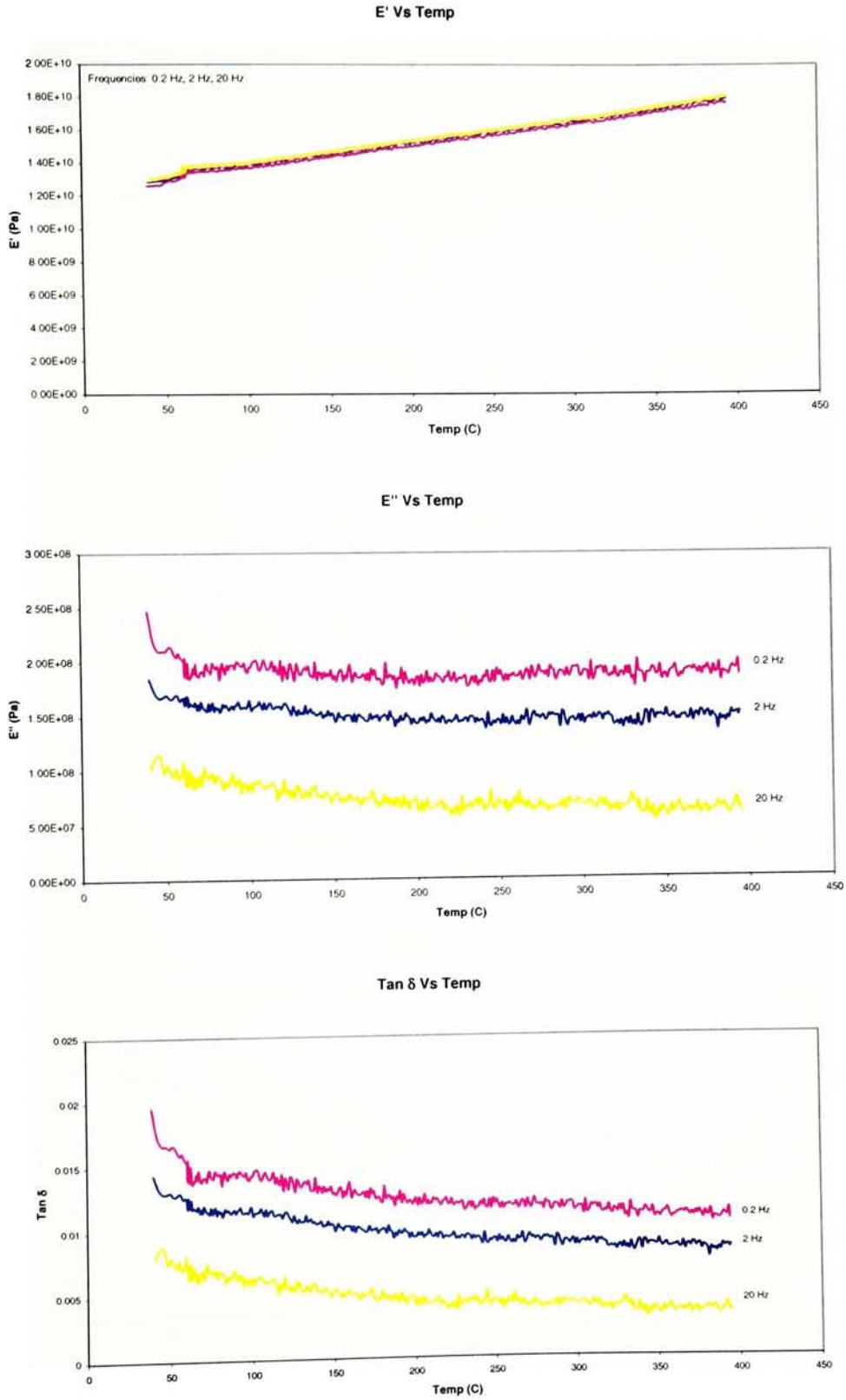

Figure 3.41. DMA curves for 2-component polyimide carbon fiber laminas

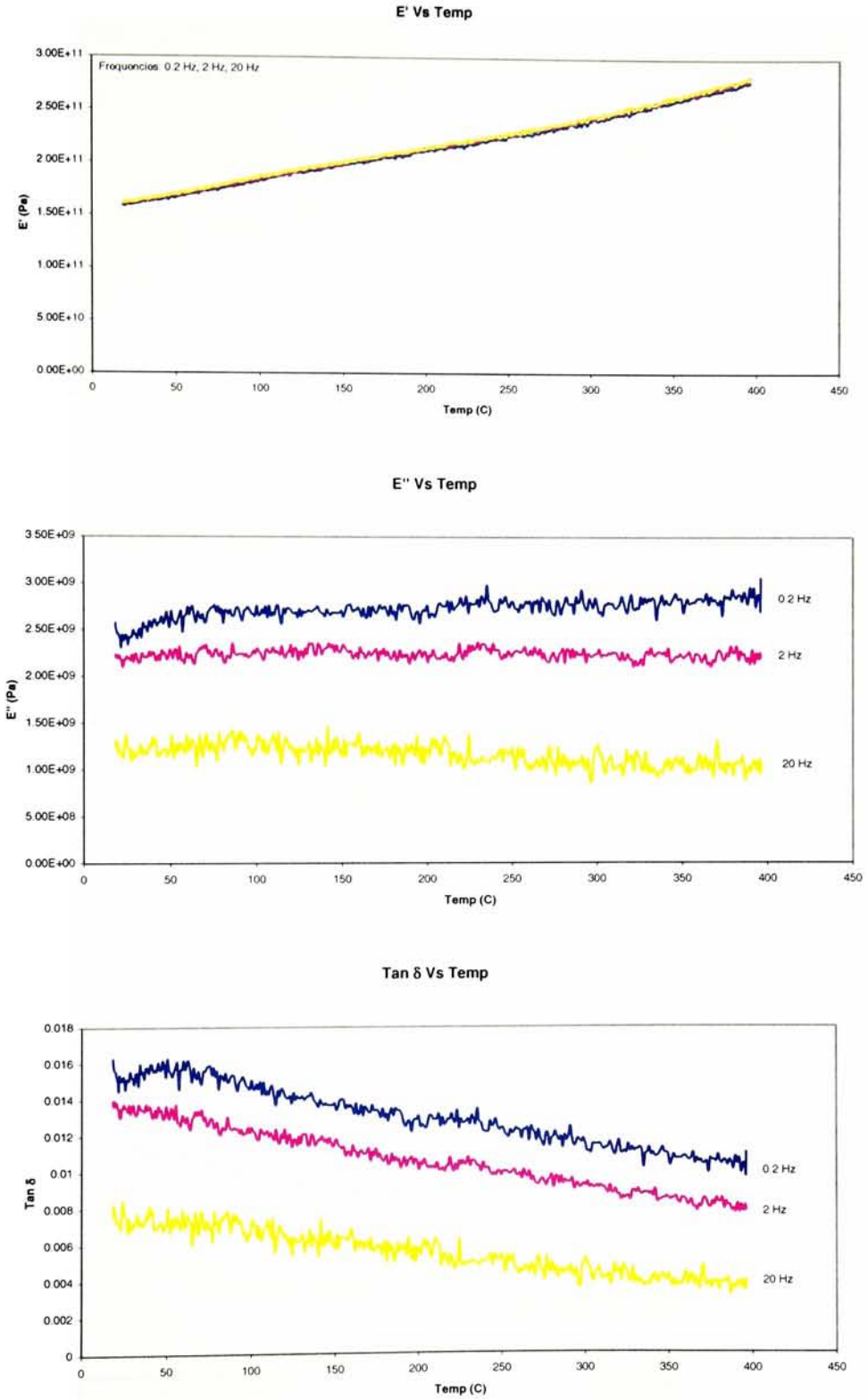

Figure 3.42. DMA curves for parent polyimide carbon fiber laminas

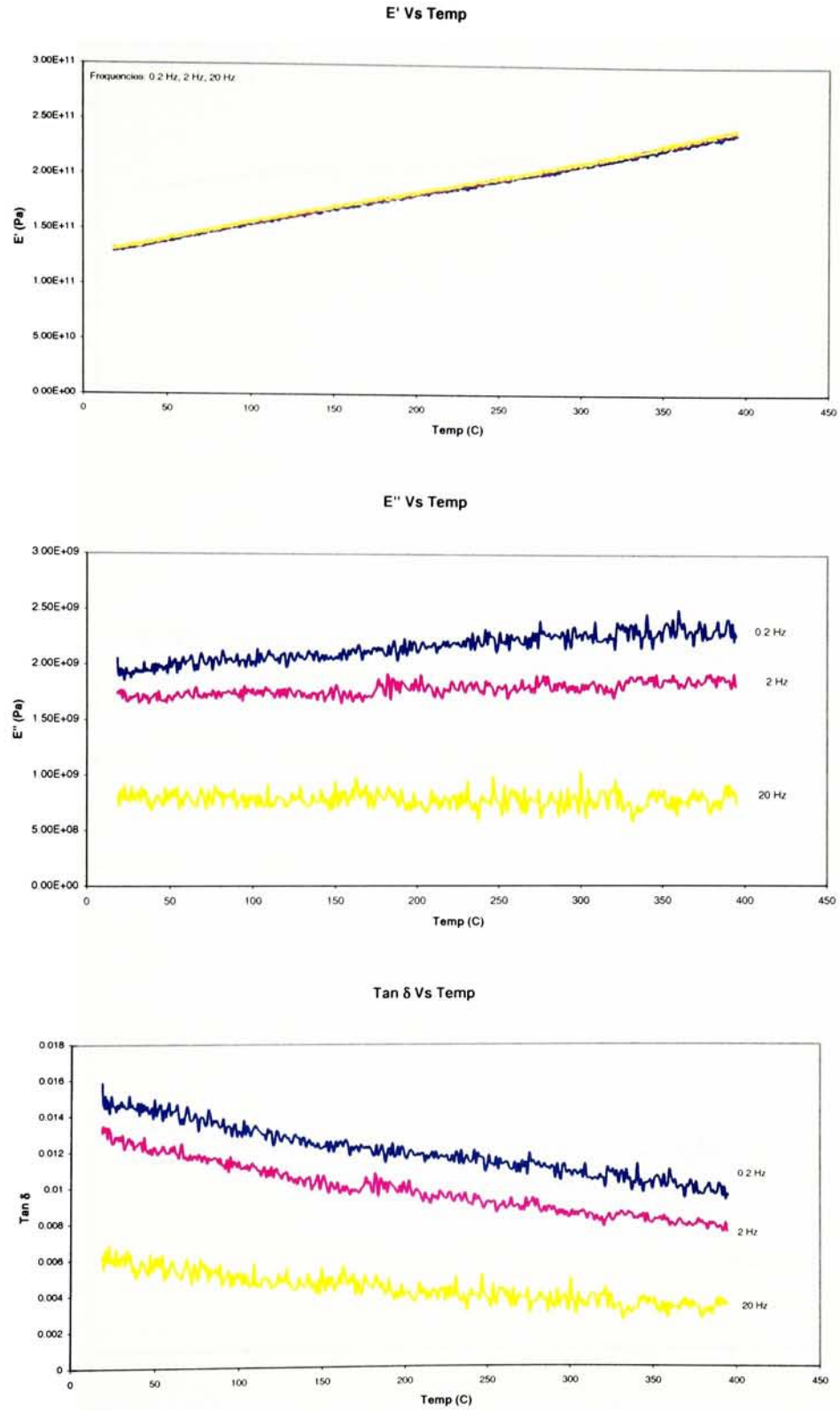

Figure 3.43. DMA curves for pendent polyimide carbon fiber laminas

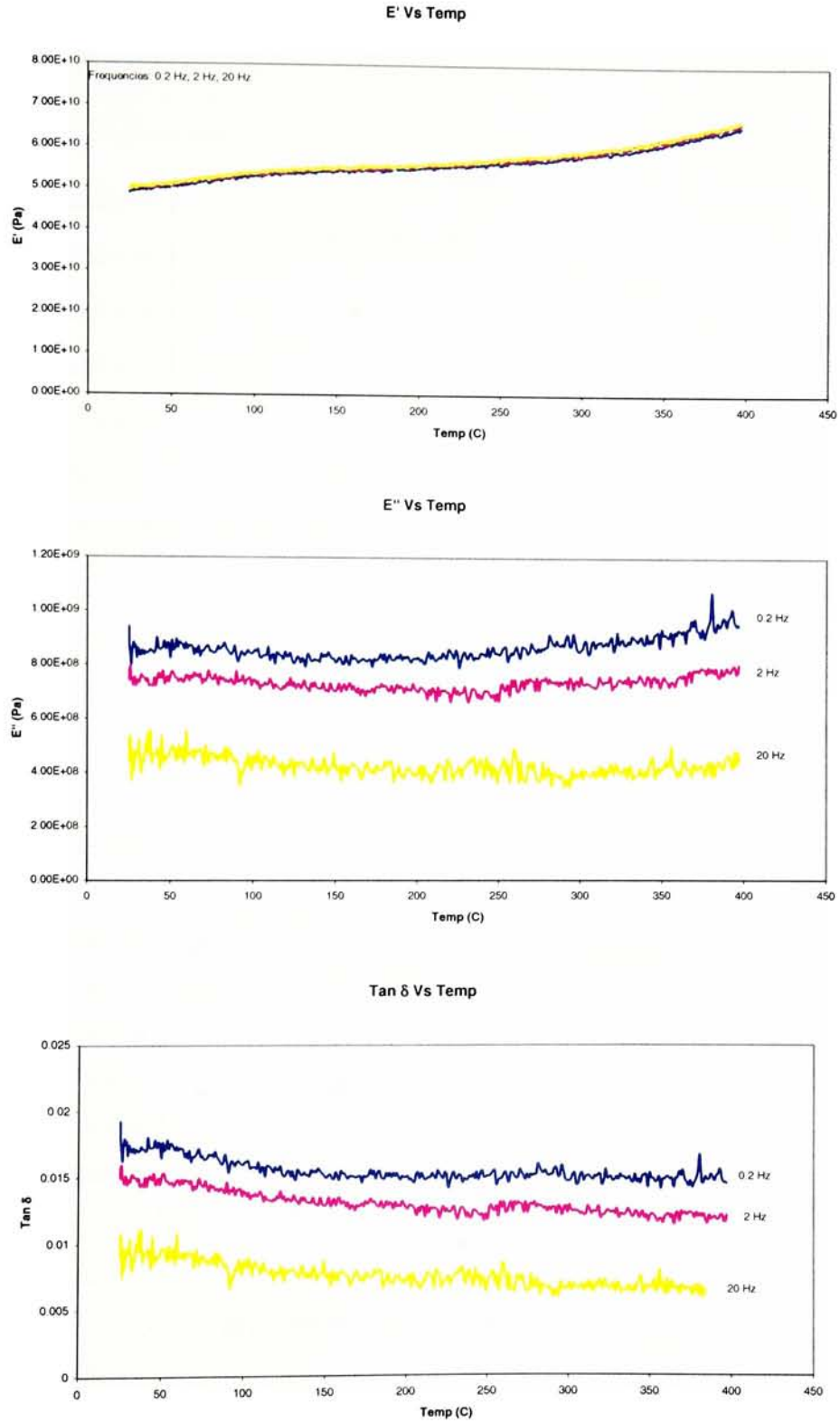

Figure 3.44. DMA curves for pendent polyimide glass fiber laminas

Figure 3.45 summarizes the values obtained for the different composite laminas at 0.2 Hz.

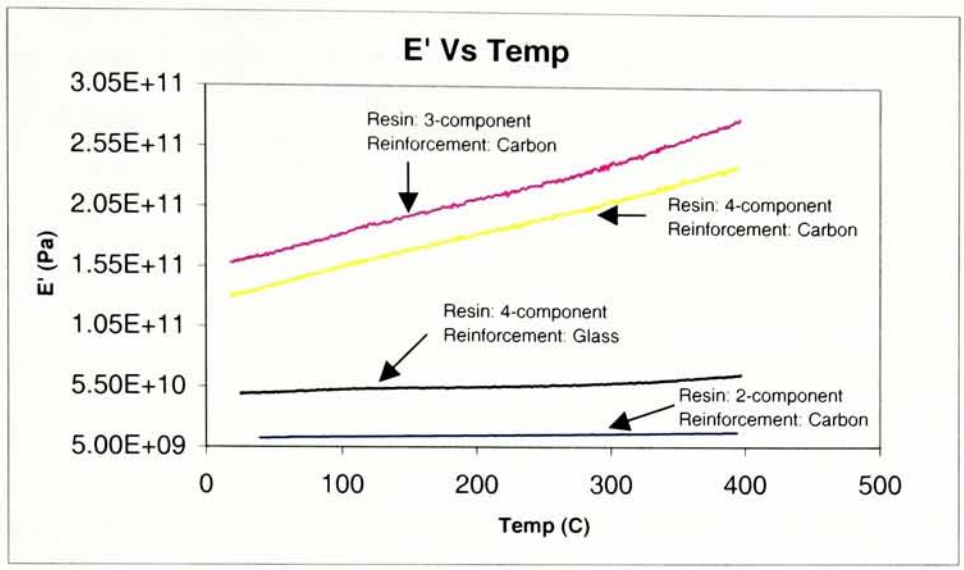

(a) Storage Modulus Vs Temperature

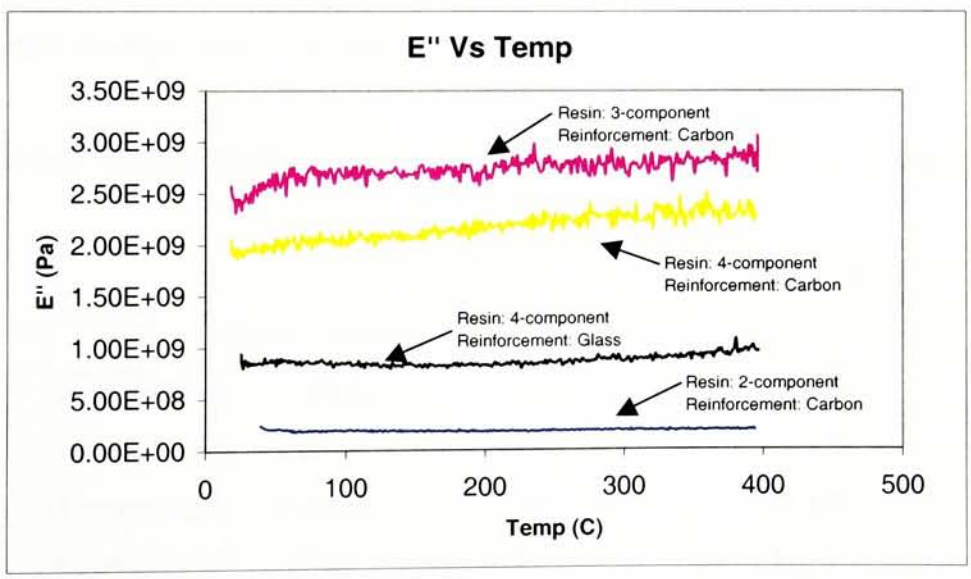

(b) Loss Modulus Vs Temperature

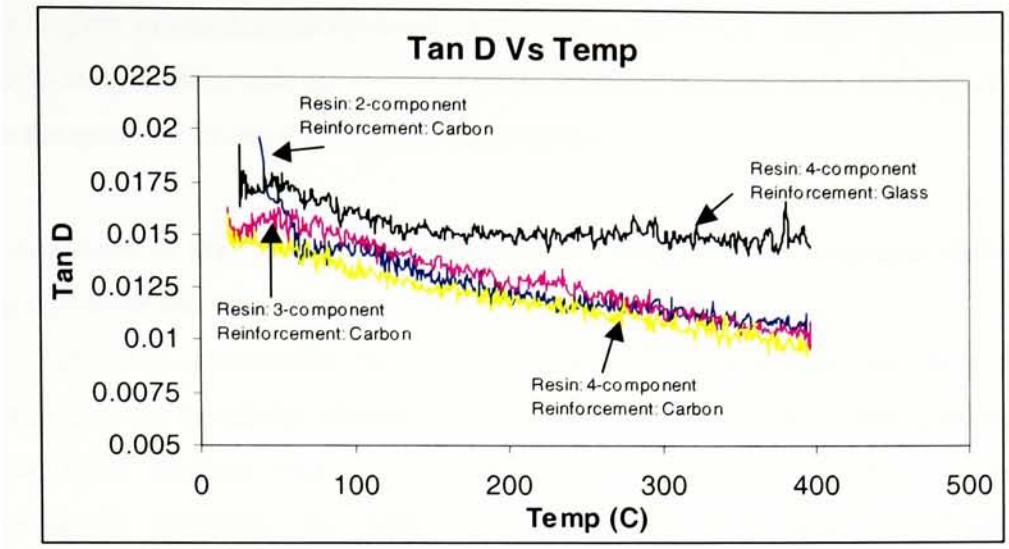

(c) Tan δ Vs Temperature

Figure 3.45. Summary of the DMA analysis for the different composite laminas

Table 3.24 shows a comparison of the storage modulus values (E') obtained from the two molding cycles. Comparisons have been made at 300 °C, a typical service temperature for high temperature applications.

Table 3.24. Storage Modulus (E') comparison at 300 °C for different molding cycles

		Storage Modulus (E'), GPa at 300 °C	
Resin	Reinforcement	I	II [a]
2-component	Carbon	15 ± 1	39 ± 6
3-component	Carbon	244 ± 16	23 ± 5
4-component	Carbon	234 ± 20	34 ± 4
4-component	Glass	52 ± 5	8 ± 1

[a] : Ref [26]

As seen from the above table, the 3- and 4-component composite systems using molding cycle I show a higher storage modulus at 300 °C, which is consistent with the

higher degrees of imidization obtained for this cycle. However, a lower storage modulus for the 2-component composite system is obtained using molding cycle I, which could be due to the retention of some solvent by this polymer.

3.4.5 Summary of the Comparison of Mechanical Properties of Laminates Fabricated Using Different Molding Cycles

Table 3.25 summarizes the results of mechanical testing from this study. It was observed that the properties obtained using molding cycle II were superior to the ones obtained using molding cycle I. Even though identical fibers and resin were used for fabricating the laminates, the different temperatures used for prepreg and autoclave fabrication may have led to different extents of imidization and cure of the resin, which ultimately affected the way in which the laminates behaved and failed under various mechanical conditions.

Also, the application of vacuum in prepreg fabrication I caused different evaporation rates, resulting in some curvature of the lamina. This curvature may have affected the extent of interaction between lamina, causing excessive scatter in these flexural test data. Similar curvature did not result from prepreg fabrication II (using ambient pressure).

Table 3.25. Comparison of mechanical properties of laminates fabricated using different molding cycles

	Reinforcement	2-component system		3-component system		4-component system	
		I	II [a]	I	II [a]	I	II [a]
Tensile Strength (MPa)	Carbon	253 ± 63	483 ± 64	300 ± 15	413 ± 83	224 ± 14	259[b] ± 10
Tensile Modulus (GPa)	Carbon	20 ± 2	27 ± 4	21 ± 1	23 ± 2	18 ± 1	11[b] ± 1
Tensile Strength (MPa)	Glass	-	159 ± 55	-	267 ± 46	99 ± 14	79[b] ± 14
Tensile Modulus (GPa)	Glass	-	11 ± 1	-	9 ± 3	6 ± 0	16[b] ± 1
Flexural Strength (MPa)	Carbon	145 ± 38	854 ± 108	174 ± 4	464 ± 173	74 ± 9	163 ± 57
Flexural Modulus (GPa)	Carbon	22 ± 1	47 ± 5	23 ± 0	37 ± 12	23 ± 1	17 ± 8
Impact Resistance (kJ/m)	Carbon	0.5 ± 0.0	1 ± 0	0.5 ± 0.0	0.9 ± 0.1	0.2 ± 0.0	-
Impact Strength (kJ/m^2)	Carbon	41 ± 0	95 ± 14	44 ± 2	91 ± 1	23 ± 0	-

[a]: Ref [26]

[b]: Ref [26], Corrected Values

3.4.6 Summary (Global Discussion)

The Zr-pendent polyimide composites showed lower mechanical properties as compared to the 2-component and parent polyimide composites. Fiber failure, matrix cracking and delamination were the most commonly observed failure modes for all the three resins. For the Zr-pendent polymer, however, delamination was the most predominant failure observed. Samples tested for impact and flexural showed extensive delamination. Since both these mechanical tests were independently performed and revealed the behavior of the material under load, similar types of failure were observed. Optical and SEM images revealed resin rich areas in pendent polyimide composites indicating poor resin flow.

Curvature in the lamina induced by prepreg fabrication I is thought to be responsible for the excessive scatter in the flexural test data.

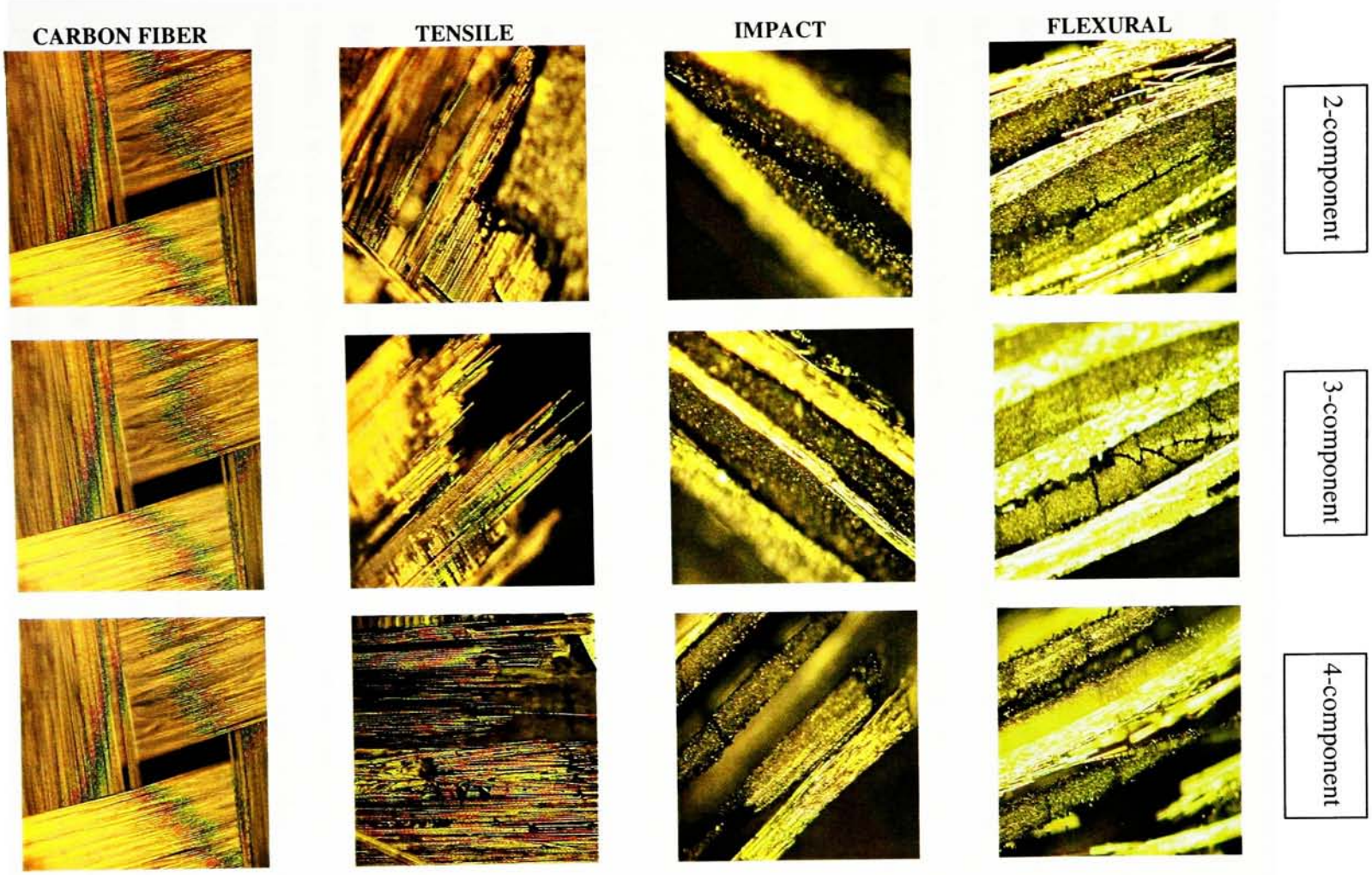

Figure 3.46. Summary of commonly observed failure mechanisms for the carbon reinforced composite specimens (Magnifications: 100x)

CHAPTER IV

CONCLUSIONS

2-component, parent and 10 mol % pendent poly(amic acid)s were synthesized with a 15 weight % solids content and investigated for optimum processing conditions. The processing condition of heating the poly(amic acid) powder at 310 °C for 15 minutes was chosen as an optimum processing condition and can be used for industrial processes using polyimide molding powders. The sample showed complete imidization without any decomposition at the given processing temperature. This was verified by the absence of the imidization step in the TGA and also by the absence of any anhydride peak at 1850 cm^{-1}, indicating a very high degree of attachment of pendent groups to MADA residues.

Carbon and glass fiber reinforced composite laminates were fabricated at 370 °C and 1.72 MPa (250 psi) pressure for an hour in the autoclave. This molding cycle however resulted in inadequate resin flow for the Zr-pendent polymer leading to poor wettability. Resin rich areas were observed under the optical and scanning electron microscope.

A 60:40 fiber to resin by weight ratio was chosen for fabricating the laminates. This ratio however did not work well for the pendent polyimide. Since its molecular weight is high, the molar amount of resin needed to achieve this ratio was much lesser compared to the 2- and 3-component polymers. This decreased number of polymer molecules resulted in less desirable mechanical properties.

Resin content of the laminates was estimated using two different methods. Method II, however, did not work well since the resin was not applied to the edges of the laminates to the same effect as elsewhere, rendering this technique to be not useful. For this reason, Method I should be chosen as the preferred way to determine the resin content.

Engineering properties were generated for carbon fiber reinforced composites for the three resin systems and glass fiber reinforced composites for the pendent polyimide. The data indicated that the Zr-pendent carbon fiber composite exhibited low mechanical properties as compared to the 2-component and parent polyimide composites. Upon

comparing mechanical test results for the 2-component and parent carbon composites, it was noted that there was no significant effect of the MADA moiety. Fiber failure, matrix cracking and delamination were the most commonly observed failure modes for the carbon and glass fiber composites. Delamination was the most predominant failure observed for the Zr-pendent polymer.

Hence, the hypothesis that the mechanical properties of the composites with pendent polymer as the resin matrix would be lower as compared to the parent (without pendent groups) polymer is justified.

Regarding the practical objectives of this work, NASA or other end user will have to decide if the enhanced atomic oxygen resistance of the Zr-pendent polyimide, and its composites, justifies the apparent trade offs in mechanical properties which have resulted from the molding cycles employed thus far. Use of revised molding conditions may result in smaller trade offs in the future.

CHAPTER V

FUTURE WORK

Although the infrared spectroscopy and TGA were used to estimate the degree of imidization in this study, an improved method for accurately determining the degree of imidization is needed. Differential scanning calorimetry was used to study the effects of processing conditions on the glass transition temperatures of the polymer. Since this study could not be completed due to evolution of volatiles, it would be worthwhile to identify sample pans that would remain hermetically sealed at elevated temperatures.

Composite material scientists aiming to improve the performance of resin matrices for, say, aerospace applications can try to enhance the established matrix systems by modifying resin chemistry. Much more work needs to be done for us to consider the Zr-pendent polyimide as a resin matrix for high performance composite materials. Recommendations to improve the mechanical properties would be to change: prepreg fabrication by using a fixture with variable tension for better alignment of fibers prior to application of resin solution and the molding cycle parameters, e.g. different temperature profiles, lower heating rates and different pressure cycles to enhance resin flow. Fiber-to-resin weight ratio for the composite should also be modified to enhance its properties.

In this study, the mechanical properties of the resin alone were not investigated. The comparison between the neat resin and the composite laminates would help us to better understand the contribution of the resin to composite performance.

REFERENCES

1) Sidney, Goodman, *Handbook of Thermoset Plastics*, 2nd Edition, Noyes Publications (1998).
2) Illingsworth, M.L.; Banks, B.A.; Smith, J.W.; Jayne, D; Garlick, R.G.; Rutledge, S.K.; deGroh, K.K., *Plasma and Beam Atomic Oxygen Erosion of a Transition Metal Complex*, Plasma Chem. and Plasma Proc., 16 (1996), 209-225.
3) Wang, W, *Synthesis and Characterization of Functionalized Zirconium Pendant Poly (amic acids) and Polyimides based on 3,4'-ODA and ODPA*, M.S. Thesis, R.I.T. Dec 2000.
4) Cho, Donghwan; Choi, Yusong; Drzal, Lawrence, *Simultaneous Monitoring of the Imidization and Cure Reactions of LARC PETI-5 Sized on a Braided Glass Fabric Substrate by DMA*, Polymer, 42 (2001), 4611-4618.
5) Kirby, A.J., *Polyimides: Materials, Processing and Application*, Rapra Technology Ltd., 1992.
6) Cano, Roberto; Hou T.H.; Weiser, Erik; Terry St. Clair, *Polyimide Composites from Salt like Solution Precursors*, High Performance Polymers, 13 (2001), 235-250.
7) Mark; Bikales; Overberger; Menges, *Encyclopedia of Polymer Science and Engineering*, 2nd Edition, 12, 364-381.
8) Lewis Research Center, *More About V-CAP Polyimides*, NASA Tech Briefs, 18 (1994), 24.
9) Jang, Bor, *Advanced Polymer Composites: Principles and Applications*, ASM International, 1994.
10) *Polyimides*, edited by D. Wilson; H.D. Stenzenberger and P.M. Hergenrother, Chapman and Hall, 1990.
11) Strong, Brent, *Fundamentals of Composites Manufacturing: Materials, Methods and Applications*, Society of Manufacturing Engineers, 1989, 107.
12) Industrial Polymers Handbook: Products, Processes, Applications, Edited by Edward Wilks, 1, 366.
13) Pipes, Byron; Carlsson Leif, *Experimental Characterization of Advanced Composite Materials*, Technomic Publishing, 2nd Edition, 1997.

14) Hou T.H.; Belvin H.L., Johnston N.J., *Automated Tow Placed LARC-PETI-5 Composites*, High Performance Polymers, 13 (2001), 323-336.

15) Scheirs, John, *Compositional and Failure Analysis in Polymers: A Practical Approach*, Wiley and Sons, 2000, 458.

16) Ginsburg R., Susko, J.R., *Polyimides: Synthesis and Characterization*, Vol. 1 (ed. K.Mittal), Plenum, NY (1984), 237-246.

17) V.L. Bell, B.L. Stump; H. Gager, *Polyimide Structure-Property Relationships II. Polymers from Isomeric Diamines*, J. Polym.Sci., Poly.Chem.Ed., 14 (1976) 2275-2292.

18) Semioli, W; Schubert, P., *Conversion Tables for SI Metrication*, Industrial Press Inc., 1974.

19) M. Navvare, *Polyimides: Synthesis and Characterization*, Vol. 1 (ed. K.Mittal), Plenum, NY (1984), 429-442.

20) Pryde, C.A., *IR Studies of Polyimides I. Effects of Chemical and Physical Changes During Cure*, Journal of Polymer Science: Part A: Polymer Chemistry, 27 (1989), 711-724.

21) Hou T.H., Johnston N.J., Terry St. Clair, *IM7/LARC-IA Polyimide Composites*, High Performance Polymers, 7 (1995), 105-124.

22) Hou, T.H.; Terry St. Clair, *IM7/LARC-IAX-3 Polyimide Composites*, High Performance Polymers, 10 (1998), 193-206.

23) Connell J; Joseph Smith Jr.; Hergenrother P; Rommel M, *Neat Resin, Adhesive and Composite Properties of Reactive/PETI-5 Blends*, High Performance Polymers, 12 (2000), 323-333.

24) Hou, T.H.; Chang, A.C.; Johnston N. J.; Terry St. Clair, *Processing and Properties of IM7/LARC-IAX2 Polyimide Composites*, J. of Advanced Materials, 27 (1996), 11-18.

25) Hou, T.H.; Cano, R.J.; Jensen B.J., *IM7/LARC MPEI-1 Polyimide Composites*, High Performance Polymers, 10 (1998), 181-192.

26) Nangia S., *Zr-pendent Polyimide Carbon/glass Composites and Their Property Comparisons with the Corresponding Non-pendent Polyimide Composites*, M.S. Project, R.I.T., 2002.

27) Numata, Shun-ichi; Fujisaki, Koji; Kinjo, Noriyuki, *Polyimides: Synthesis and Characterization*, Vol. 1(ed. K.Mittal), Plenum, NY (1984), 259-271.

28) Agarwal, B.; Broutman, L, *Analysis and Performance of Fiber Composites*, Wiley and Sons, 2nd Edition, 1990, 235.